Veröffentlichungen der Schweizerischen Meteorologischen Anstalt
Publications de l'Institut suisse de météorologie
Pubblicazioni dell'Istituto svizzero di meteorologia

1992

51

Aspects of precipitation simulation in numerical weather prediction

Towards an operational mesoscale NWP model

by P. Binder

Veröffentlichungen der Schweizerischen Meteorologischen Anstalt
Publications de l'Institut suisse de météorologie
Pubblicazioni dell'Istituto svizzero di meteorologia

1992

51

Aspects of precipitation simulation in numerical weather prediction

Towards an operational mesoscale NWP model

by P. Binder

The present text is equivalent to Ph.D. dissertation No. 9908 of the Swiss Federal Institute of Technology Zurich.

Contents

Abstract

A study is made of the impact of enhanced horizontal resolution and cumulus parameterization on the simulation of precipitation by a numerical weather prediction (NWP) model. In particular theoretical, observational and modelling aspects related to a meso-β-scale NWP model are considered. In models of this scale precipitation is formally separated into an unresolved convective part and a grid-resolvable part, and there is a need for an appropriate method to parameterize the unresolved component. The study falls into three distinct, but related parts.

In the first part the concept of convective adjustment parameterization is investigated in detail. Here the basic assumption is that a quasi-equilibrium thermodynamic structure – the convectively adjusted atmospheric state – exists and that this can be represented by a so-called deep-convection reference profile. In this context the thermodynamic structure related to mid-latitude continental summer convection is examined for a set of upper air ascents of the sounding station Payerne in Switzerland and examined in relation to the convective adjustment scheme proposed by Betts (1986) (– which was based primarily on tropical data). It is shown that, given a proper set for the adjustable parameters derived from the observations, the deep-convection reference profile of Betts characterizes well the convectively adjusted atmosphere of the extra-tropical continental environment exemplified by the Payerne data. In comparison with the reference profile determined by Betts and Miller (1986) the derived temperature structure is found to be even more unstable below melting level. Also the humidity profile exhibits some distinctive physical characteristics. Given these characteristic features, the standard reference profiles available for numerical experimentation are not entirely satisfactory. In addition the convective adjustment scheme is shown to be fundamentally different from the alternative so-called mass flux approach. In general there is no mass flux that can produce the equivalent vertical heat and moisture transports and it is also impossible to determine condensation rates associated with the adjustment process.

In the second part the dependency of precipitation simulation on horizontal resolution and on the specification of the deep-convection reference profile and the adjustment time scale is systematically investigated. The original mesh width (~60km) of an existing hydrostatic meso-α-scale limited area model is successively reduced by a factor two and four. It is demonstrated that the resulting fine-mesh model versions can improve the simulation of precipitation events, particularly their temporal and spatial structure. The capability of the high-resolution models to better represent external forcing (e.g. orography) is a crucial factor. In convectively dominated weather situations the simulation results are extremely sensitive to the choice of the cumulus parameterization scheme with the precipitation amounts and intensities systematically increasing with decreasing mesh width. Enhanced grid-scale precipitation due to intensified vertical grid-scale circulation is identified as a cause. A second result is that convective precipitation increases as a consequence of the required reduction of the adjustment time scale. However, due to interactions the two contributions can not in general be linearly combined. The parameterization of convection proves to be important for a timely initiation of precipitation events and furthermore it counteracts the occurrence of grid point storms. Weather radar data are utilized to provide a first qualitative comparison of simulated and observed horizontal precipitation field pat-

terns. Thereafter quantitative assessment of model results is made by means of radar data and measurements of the automatic surface network. The two types of observations can yield substantially differing estimates and it is appropriate to use both sources of observational data for model verification. Partitioning of precipitation into its parameterized convective and grid-scale parts and consideration of their horizontal structures and time variation provide valuable insights into the life cycle of simulated convective precipitation events.

In the third part a diagnostic tool is developed to evaluate the contributions to the evolution of the model atmosphere made by all processes represented in the model. The standard formalism for heat and moisture budgets, frequently used for diagnostic studies of observations, is carefully adapted to the governing equations of NWP models. One difficulty is that in the particular model considered condensation rates are never explicitly calculated. The condensation is treated as an internal process, since the prognostic thermodynamic and moisture variables are total enthalpy and total specific water content. These predicted values are inserted into temperature and water vapour equations and the condensation rates appear as residuals. Diagnosis of a simulated convective precipitation event reveals the predominance of the convective tendencies in the early stage of development. In the mature stage grid-scale condensation and precipitation-forming processes provide the strongest forcing for the development of the model atmosphere. Since convective adjustment schemes take only static properties of the atmosphere into account the amplitudes of the associated tendencies primarily depend on the adjustment time scale. In contrast, grid-scale condensation and precipitation are largely determined by grid-scale vertical moisture transport and therefore corresponding tendencies strongly depend on the mesh size. Furthermore, a pronounced dependency is diagnosed of the vertical structure of the apparent heat source and the apparent moisture sink on the deep-convection reference profile.

Zusammenfassung

In dieser Studie wird der Einfluss von erhöhter horizontaler Auflösung und des Parametrisierungsverfahrens für die Konvektion auf die Niederschlagssimulation mit einem numerischen Wettervorhersage (NWV) Modell untersucht. Insbesondere werden Aspekte der Theorie, der Beobachtung und der Modellierung im Zusammenhang mit einem meso-β-skaligen NWV Modell betrachtet. In Modellen von dieser Auflösung wird der Niederschlag formal in einen subskaligen konvektiven und einen vom Modellgitter auflösbaren Anteil aufgetrennt. Eine geeignete Methode zur Parametrisierung des nicht aufgelösten Anteils ist notwendig. Die Arbeit ist in drei eigenständige, aber miteinander in Beziehung stehende Teile gegliedert.

Im ersten Teil wird das Konzept der konvektiven Anpassung als Verfahren zur Parametrisierung der Konvektion eingehend untersucht. Hier wird die grundlegende Annahme gemacht, dass ein Quasi-Gleichgewichtszustand der thermodynamischen Struktur der Atmosphäre existiert, nämlich der konvektiv angepasste Zustand der Atmosphäre, der durch ein sogenanntes Referenzprofil für hochreichende Konvektion dargestellt werden kann. Die thermodynamische Struktur der Atmosphäre im Zusammenhang mit sommerlicher Konvektion in kontinentalen Verhältnissen der mittleren Breiten wird mittels einer Reihe von Radiosondenaufstiegen der Station Payerne in der Schweiz untersucht, und es wird die Beziehung zu dem von Betts (1986) vorgeschlagenen Anpassungsverfahren, das vorwiegend auf tropischen Daten gründet, überprüft. Wenn ein geeigneter aus Beobachtungen abgeleiteter Satz von Werten für die freien Parameter verwendet wird, zeigt es sich, dass das Referenzprofil für hochreichende Konvektion nach Betts die extra-tropische, kontinentale, konvektiv angepasste Atmosphäre, hier am Beispiel der Payerne Daten, gut charakterisiert. Im Vergleich zu dem von Betts und Miller (1986) bestimmten Referenzprofil erweist sich die aus dem vorliegenden Datensatz abgeleitete Temperaturstruktur unterhalb der Nullgradgrenze als feuchtlabiler. Ausserdem zeigt das Feuchteprofil einige Besonderheiten von physikalischer Bedeutung. In Anbetracht dieser Charakteristika vermögen die für die numerischen Simulationen zur Verfügung stehenden Referenzprofile nicht vollständig zu befriedigen. Zusätzlich wird gezeigt, dass sich Anpassungsverfahren zur Parametrisierung der Konvektion fundamental vom alternativen, sogenannten Massenflussansatz unterscheiden. Im allgemeinen existiert kein Massenfluss, der gleichwertige vertikale Wärme- und Feuchtetransporte bewirken kann. Ebenso ist es unmöglich, durch die konvektive Anpassung verursachte Kondensationsraten zu bestimmen.

Im zweiten Teil wird die Abhängigkeit der Niederschlagssimulation von der Maschenweite und von der Spezifikation des Referenzprofils für die hochreichende Konvektion und der Anpassungszeit systematisch untersucht. Die ursprüngliche Maschenweite (~60km) eines existierenden hydrostatischen, meso-α-skaligen Ausschnittmodells wird schrittweise um einen Faktor zwei und vier verkleinert. Es wird gezeigt, dass die feinmaschigen Modellversionen die Simulation von Niederschlagsereignissen, besonders deren räumliche und zeitliche Struktur, verbessern können. Die Möglichkeit der hochauflösenden Modelle zur detaillierteren Darstellung der externen Antriebe, zum Beispiel der Orographie, ist ein ausschlaggebender Faktor. In konvektiven Wetterlagen erweisen sich die Simulationsergebnisse als äusserst empfindlich auf die Wahl der Konvektionsparametrisierung, wobei Niederschlagsmenge und -intensität mit kleiner werdender Maschenweite

systematisch zunehmen. Verstärkte skalige Niederschlagsproduktion durch die Intensivierung der skaligen Vertikalzirkulation lässt sich als eine Ursache feststellen. Zweitens nimmt der konvektive Niederschlag durch die notwendige Verkürzung der Anpassungszeit zu, wobei sich die beiden Beiträge aufgrund der bestehenden Wechselwirkungen im allgemeinen nicht additiv verhalten. Die Parametrisierung der Konvektion erweist sich als wichtig im Hinblick auf die zeitlich korrekte Auslösung eines Niederschlagsereignisses, ausserdem dämmt sie das Auftreten von Gitterpunktstürmen ein. Wetterradardaten werden benützt für einen ersten qualitativen Vergleich von simulierten und beobachteten Strukturen von Niederschlagsfeldern. Eine quantitative Einschätzung der Modellresultate wird mit Hilfe von Radardaten und Beobachtungen des automatischen Bodenmessnetzes gemacht. Die beiden Beobachtungsarten können stark divergierende Resultate liefern und es ist deshalb angezeigt, für die Verifikation von Modellresultaten beide Messdatenquellen beizuziehen. Die Betrachtung der horizontalen Strukturen und der zeitlichen Entwicklung von konvektiven und skaligen Modellniederschlagsanteilen liefert wertvolle Einsichten in den Lebenszyklus von simulierten konvektiven Niederschlagsereignissen.

Im dritten Teil wird ein diagnostisches Werkzeug entwickelt, das die eingehende Untersuchung der Beiträge zur Entwicklung der Modellatmosphäre aller im Modell dargestellten Prozesse ermöglicht. Der übliche Budgetformalismus für Wärme und Feuchte, der häufig für diagnostische Studien mit Beobachtungsdaten angewendet wird, wird sorgfältig auf die allgemeinen Grundgleichungen numerischer Wettervorhersagemodelle angepasst. Eine Schwierigkeit mit dem speziell betrachteten Modell besteht darin, dass die Kondensationsrate nie explizit berechnet wird. Die Kondensation wird als interner Prozess behandelt, da die prognostischen thermodynamischen und Feuchtegrössen die Enthalpie und der totale spezifische Wassergehalt sind. Diese vorhergesagten Werte werden in Gleichungen für die Temperatur und den spezifischen Wasserdampfgehalt eingesetzt, in denen die Kondensationsrate als Residuum erscheint. Die Diagnose eines simulierten konvektiven Niederschlagsereignisses zeigt die Dominanz der konvektiven Tendenzen im frühen Stadium der Entwicklung auf. Im voll entwickelten Stadium liefern die skaligen Niederschlagsprozesse und die Kondensation die stärksten Antriebe für die Entwicklung der Modellatmosphäre. Da das konvektive Anpassungsverfahren nur die statischen Eigenschaften der Atmosphäre berücksichtigt, hängen die Amplituden der Quellterme vorwiegend von der gesetzten Anpassungszeit ab. Dagegen werden die Kondensation und die skaligen Niederschlagsprozesse wesentlich vom vertikalen Feuchtetransport bestimmt, woraus die vorwiegende Abhängigkeit der Tendenzen von der Maschenweite folgt. Zudem zeigt sich, dass die vertikale Struktur der konvektiven Wärme- und Feuchtequellen stark vom gewählten Referenzprofil für die hochreichende Konvektion abhängt.

Résumé

Une étude de l'impact d'une augmentation de la résolution horizontale et de la paramétrisation de la convection sur la simulation des précipitations par un modèle numérique de prévision du temps est réalisée dans ce travail. En particulier des aspects liés à la théorie, à l'observation et à la modélisation en relation avec un modèle d'échelle méso-β sont étudiés. Pour un tel modèle, les précipitations sont formellement décomposées en une partie convective dont l'échelle caractéristique est inférieure à celle de la maille du modèle, et une partie résoluble sur cette même grille; une méthode appropriée pour paramétriser la composante non résoluble est alors nécessaire. L'étude ici présentée est structurée en trois parties distinctes, mais reliées entre elles.

Dans la première partie le concept d'ajustement convectif appliqué à la paramétrisation de la convection est examiné en détail. L'hypothèse fondamentale faite ici est celle de l'existence d'un état en quasi-équilibre de la structure thermodynamique de l'atmosphère, appelé état convectivement ajusté, qui peut être représenté par un "profil de référence de convection profonde". Dans ce contexte, la structure thermodynamique de l'atmosphère aux latitudes moyennes pour des situations de convection estivales continentales est examinée à partir d'un ensemble de sondages aérologiques de la station de Payerne en Suisse; au vu de ces sondages, le schéma d'ajustement convectif proposé par Betts (1986), basé avant tout sur des données tropicales, est alors contrôlé. Pour autant que les paramètres libres du modèle soient ajustés convenablement à partir des observations, on montre que le profil de référence de convection profonde de Betts caractérise bien l'état convectivement ajusté de l'atmosphère extra-tropicale continentale, tel que représenté par les données de Payerne. En comparaison avec le profil de référence déterminé par Betts et Miller (1986), il apparait cependant que la structure de la température déterminée à partir de ces données est encore plus instable en dessous de la limite du zéro degré. En outre le profil d'humidité présente quelques particularités physiques remarquables. En considération de ces caractéristiques, les profils de référence à disposition pour les expériences numériques ne sont pas entièrement satisfaisants. En outre on montre que le schéma d'ajustement convectif est fondamentalement différent de l'approche basée sur le schéma du flux de masse. En général il n'y a pas de flux de masse qui puisse reproduire des transports verticaux de chaleur et d'humidité équivalents. D'autre part il est impossible de déterminer les taux de condensation associés au schéma d'ajustement convectif.

Dans la deuxième partie on étudie de manière systématique la dépendance des précipitations simulées par rapport à la dimension horizontale de la maille du modèle et par rapport au choix du profil de référence de convection profonde et du temps d'ajustement. On considère un modèle hydrostatique existant à aire limitée et d'échelle méso-α, dont la maille (~60km) est successivement réduite par un facteur deux, puis par un facteur quatre. On montre que les versions du modèle ayant une maille plus fine peuvent améliorer la simulation des événements "précipitation", particulièrement leurs structures temporelles et spatiales. Le fait que les modèles à haute résolution ont la capacité de mieux représenter les contraintes extérieures (p.ex. orographie) est un facteur crucial. Lors de situations météorologiques convectives les résultats de la simulation sont extrêmement sensibles au choix de la paramétrisation de la convection, la quantité et l'intensité des précipitations augmentant systématiquement avec la diminution de la maille du modèle. Une première cause à ce

comportement est l'augmentation des précipitations à l'échelle de la maille due à une intensification de la circulation verticale à cette même échelle. Deuxièmement, du fait de la nécessaire diminution du temps d'ajustement, les précipitations convectives croissent. Notons que ces deux contributions ne peuvent en général pas être combinées linéairement de par l'existence d'interactions entre ces phénomènes. La paramétrisation de la convection se révèle être importante par rapport à l'horaire du déclenchement des événements "précipitation", en outre elle diminue le déclenchement de tempêtes liées à un point de grille. Des données provenant d'un radar météorologique sont utilisées pour faire une première comparaison qualitative entre la structure simulée et la structure observée du champ de précipitation. Une évaluation quantitative des résultats du modèle est en suite obtenue à l'aide des données provenant du radar et du réseau automatique d'observations au sol. Comme ces deux méthodes d'observation peuvent fournir des estimations substantiellement différentes, il est judicieux de les utiliser parallélement lors de la vérification du modèle. La partition d'un événement "précipitation" en une composante convective et une composante dont l'échelle est la maille du modèle, puis l'étude de la structure horizontale et du développement temporel de chacune de ces deux composantes fournissent des informations de valeur sur le cycle de vie des précipitations convectives simulées.

Dans la troisième partie un outil diagnostique permettant d'évaluer la contribution de chacun des processus du modèle à l'évolution de l'atmosphère simulée est développé. Le formalisme standard associé à l'étude du budget du modèle pour la chaleur et l'humidité, fréquemment utilisé lors d'études diagnostiques des observations, est soigneusement adapté aux équations gouvernant les modèles de prévision numérique du temps. Une difficulté rencontrée est que le taux de condensation n'est jamais explicitement calculé dans le modèle particulier utilisé ici. En effet, la condensation est traitée comme un processus interne, les variables prévisionnelles pour les processus thermodynamiques et humides étant l'enthalpie et le contenu spécifique total en eau; ces valeurs prévues sont insérées dans les équations gouvernant la température et le contenu en vapeur d'eau, le taux de condensation apparaissant alors comme résidu. Le diagnostique d'un événement simulé "précipitation convective" révèle la prédominance de la tendance convective durant la phase initiale du développement de la précipitation; par la suite les précipitations à l'échelle de la maille et les processus de condensation sont les facteurs dominant l'évolution de l'atmosphère. Comme le modèle d'ajustement convectif ne prend en considération que les propriétés statiques de l'atmosphère, l'amplitude des tendances associées dépend principalement du temps d'ajustement. Par contre, les précipitations à l'échelle de la maille et les processus de condensation sont principalement déterminés par le transport vertical d'humidité à cette échelle, et, par conséquent, les tendances correspondantes dépendent fortement de la taille de la maille du modèle. Enfin, une forte dépendance de la structure verticale des sources apparentes de chaleur et d'humidité par rapport au profil de référence de convection profonde est mise en évidence.

Riassunto

La presente ricerca analizza l'influsso che una maggiore risoluzione orizzontale e un processo di parametrizzazione della convezione hanno sulla simulazione delle precipitazioni per mezzo di un modello di previsione numerica (NWP). In particolare vengono considerati gli aspetti teorici, dell'osservazione e della modellizzazione in relazione a un modello numerico a mesoscala-β. Nei modelli di questa risoluzione le precipitazioni vengono formalmente divise in una componente convettiva non risolta a subscala e in una parte risolvibile dalla maglia del modello. È così necessario un appropriato metodo di parametrizzazione della componente non risolta. Il lavoro è suddiviso in tre parti distinte, ma in relazione tra di loro.

Nella prima parte viene analizzato in dettaglio il concetto dell'adattamento convettivo come processo di parametrizzazione della convezione. A questo punto viene fatto il presupposto fondamentale che esiste uno stato di quasi-equilibrio della struttura termodinamica dell'atmosfera, cioè lo stato dell'atmosfera adattato convettivamente, che può essere rappresentato da un cosiddetto profilo di referenza di convezione profonda. Viene poi analizzata la struttura termodinamica dell'atmosfera in relazione con la convezione estiva in condizioni continentali a medie latitudini, con l'aiuto di una serie di radiosondaggi della stazione aerologica svizzera di Payerne e verificata la relazione con la procedura di adattamento proposta da Betts (1986), la quale essenzialmente si basa su dati rilevati nei tropici. Sull'esempio dei dati di Payerne si è potuto dimostrare che, quando viene usata una serie adeguata di valori derivati da osservazioni per i parametri variabili, il profilo di referenza di convezione profonda secondo Betts caratterizza bene l'atmosfera extra-tropicale, continentale e adattata convettivamente. Paragonato al profilo di referenza determinato da Betts e Miller (1986), l'andamento della temperatura derivato dalla serie di dati a disposizione è risultato di labilità satura al di sotto dell'isoterma di zero gradi. Inoltre l'andamento dell'umidità presenta alcune particolarità di importanza fisica. Considerando queste caratteristiche, i profili di referenza a disposizione per le simulazioni numeriche non sembrano soddisfare completamente. Viene inoltre mostrato che la procedura di aggiustamento per la parametrizzazione della convezione differisce fondamentalmente dall'approccio alternativo con il cosiddetto flusso di massa. In generale non esiste nessun flusso di massa che può produrre un trasporto verticale di calore e umidità dello stesso tenore ed è pure impossibile determinare i tassi di condensazione provocati dall'adattamento della convezione.

Nella seconda parte viene analizzata sistematicamente la dipendenza della simulazione delle precipitazioni dalla distanza orizzontale dei punti di griglia, dalle specificazioni del profilo di referenza per la convezione profonda e dal tempo di adattamento. La distanza originale dei punti di griglia (60km) di un modello idrostatico a mesoscala-α ad area limitata già esistente viene ridotta progressivamente di un fattore due e poi di quattro. Viene così mostrato che la versione del modello a maglie ravvicinate può migliorare la simulazione degli eventi di precipitazione, soprattutto per quanto concerne la loro distribuzione spaziale e temporale. La possibilità del modello ad alta risoluzione di riprodurre in modo dettagliato i propulsori esterni, come per esempio l'orografia, è un fattore determinante. In situazioni meteorologiche convettive, i risultati delle simulazioni si sono dimostrati estremamente sensibili rispetto alla scelta della parametrizzazione della convezione, con la quantità e l'intensità delle precipitazioni in sistematico aumento con la riduzione della di-

stanza dei punti di griglia. Un primo motivo per l'aumento della produzione delle precipitazioni a livello della griglia può essere attribuito all'intensificazione della circolazione verticale a scala della griglia. Inoltre le precipitazioni convettive aumentano a causa dell'inevitabile riduzione del tempo di adattamento, anche se in generale i due contributi, a causa delle interazioni esistenti, non si sommano. La parametrizzazione della convezione si è dimostrata importante nell'ottica di un corretto inizio nel tempo degli eventi di precipitazione, oltre a mitigare la manifestazione di tempeste sui punti di griglia. I dati dei radar meteorologici vengono utilizzati per un primo paragone qualitativo della struttura dei campi di precipitazioni simulati e osservati. Una valutazione quantitativa dei risultati del modello viene invece fatta, oltre che con i dati dei radar, con i dati forniti dalle stazioni di rilevamento al suolo della rete automatica. Dato che due sistemi di rilevamento possono fornire risultati molto differenti tra di loro, per la verifica dei risultati del modello è perciò appropriato considerare entrambe le fonti di misure. L'esame della struttura orizzontale e lo sviluppo temporale delle componenti convettive a livello dei punti di griglia delle precipitazioni fornisce una preziosa visione del ciclo di vita degli eventi di precipitazione simulati.

Nella terza parte viene sviluppato uno strumento diagnostico che permette di analizzare in dettaglio i contributi all'evoluzione del modello dell'atmosfera di tutti i processi rappresentati nel modello. Il normale formalismo del bilancio del calore e dell'umidità, che spesso viene applicato negli studi diagnostici con dati misurati, viene adattato accuratamente alle equazioni di base generali del modello numerico di previsioni meteorologiche. Una difficoltà del particolare modello considerato consiste nel fatto che il tasso di condensazione non viene mai esplicitamente calcolato. La condensazione viene trattata come un processo interno, in quanto le grandezze termodinamiche e di umidità sono rappresentate dall'entalpia e dal contenuto totale di umidità specifica. Questi valori previsti vengono inseriti nelle equazioni della temperatura e dell'umidità specifica, nelle quali il tasso di condensazione appare come residuo. La diagnosi di un evento di precipitazioni convettive simulate mostra una predominanza della tendenza convettiva negli stadi iniziali dello sviluppo. Nello stadio di pieno sviluppo, i processi di precipitazione a livello dei punti di griglia e la condensazione forniscono gli impulsi più forti per l'evoluzione dell'atmosfera modellata. Dal momento che la procedura di adattamento convettivo considera solo le proprietà statiche dell'atmosfera, l'amplitudine delle sorgenti termiche dipende essenzialmente dai tempi di adattamento stabiliti. La condensazione e le precipitazioni a livello dei punti di griglia vengono invece per lo più determinati dal trasporto verticale di umidità, per cui la prevalente dipendenza delle tendenze segue la distanza dei punti di griglia. Inoltre è dimostrato che la struttura verticale delle sorgenti di calore e di umidità dipende fortemente dai profili di referenza scelti per la convezione profonda.

1 Introduction

Numerical weather prediction (NWP) is of paramount importance for modern operational weather forecasting. This technique of mathematically modelling and numerically predicting atmospheric processes provides valuable guidance for the elaboration of short-range weather forecasts describing the weather of "today and tomorrow" and appears indispensable for medium-range (3-7 days) weather prediction for the extra-tropical latitudes (Bengtsson, 1991). The present study is designed to contribute to the development of a *high-resolution* NWP model. The development of such models is motivated by the need to obtain more accurate weather forecasts for the increasing requirements of public and commercial interest. The specific objects of the present study will first be placed in the broader context of NWP.

1.1 Key issues of numerical weather prediction

Weather prediction was first recognized to be an initial (and boundary) value problem described by an appropriate set of (partial differential) equations by Bjerknes (1904). He claimed the essential ingredients to be the momentum and mass conservation equations, the equation of state for air, and the first and second principles of thermodynamics. This system of seven equations involves seven unknowns, namely the three components of the velocity field and the density, pressure, temperature and moisture fields. Thus given an initial condition, it can in principle be solved. This deterministic view of the weather prediction problem forms the basis of present day's NWP.

There are two distinct tasks: The determination of initial conditions, i.e. the description of the actual state of the atmosphere at a given time, and the solution of the time-dependent system of equations. These problems were rendered technically feasible by the advent of electronic computers. At first, drastic simplifications of the equations, e.g. reducing the whole system to one single barotropic equation, were necessary. Subsequently more and more features of the original governing equations were retained in pace with the increasing power of computers (institutions concerned with NWP were always among the first customers of the most recent supercomputers!). But even today, despite the availability of the newest computers, numerical modellers rely on simplifications and approximations of the basic equations and of the atmospheric processes to be represented. However, it must be emphasized that technical limitations are not the only problems encountered in NWP. The improvement of our understanding of the complex nature of atmospheric processes and their manifold interactions on various space and time scales presents a continuous scientific challenge.

The representation of the atmospheric state valid at a given time which serves the prediction model as initial condition is determined by the so-called data assimilation process. The first step in this process is the numerical (objective) analysis of observations which involves an interpolation procedure in space and time of the irregularly scattered observational data of different type to a regular 3/4-dimensional grid. First guess fields from climatology, former analyses or short-term predictions, constraints from meteorological principles and from characteristics of the observing systems and of the numerical model are incorporated in this procedure. Initialization makes the analysed fields compatible with structures supported by the prediction model. In this process meteorologically irrelevant

features which would evolve as detrimental perturbations are eliminated. The prediction model itself is also involved in the data assimilation process. It is integral to the initialization and provides forecast fields as first guesses for the analysis. Data assimilation can either be designed as an intermittent (e.g. Bengtsson, 1991) or quasi-continuous process.

The governing equations of the prediction problem are cast in a discrete form in space and time. For the horizontal representation the finite difference, finite element and spectral transform methods have been used. A variety of time integration schemes has been developed to carry the evolution of the model atmosphere forward in time. All NWP models utilize the equivalent of a 3-dimensional grid in physical space and the spacing between grid points defines the *resolution* of a NWP model. Thus the explicit description of atmospheric processes by a NWP model is always confined to phenomena larger than a certain model-related scale. This minimum scale is always larger than that of some weather-significant processes. The subgrid-scale processes must be described in terms of parameters resolved and predicted by the model, a problem known as *parameterization*.

Processes of major importance subject to parameterization are radiation, turbulence, convection, cloud and precipitation formation. The main effects attributable to atmospheric turbulence are accounted for by horizontal and vertical diffusion schemes and planetary boundary layer parameterization schemes, which essentially represent the vertical eddy fluxes of momentum, sensible and latent heat near the earth surface. In addition dissipation of momentum in the free atmosphere due to subgrid-scale orographic effects is sometimes included. The effects of the subgrid-scale condensation and vertical transport of heat and moisture by shallow and deep convection are accounted for by *cumulus parameterization schemes*. The somewhat artificial and arbitrary separation into subgrid-scale and grid-resolvable-scale phenomena leads to the formal distinction of convective and grid-scale clouds and precipitation. Cloud and precipitation formation in convective and stable situations and corresponding latent heat release is described by microphysics parameterization schemes. There exists a variety of parameterization schemes for each category with differing degrees of sophistication.

1.2 Past and current trends in operational NWP

During the past 10-15 years the evolution of operational NWP systems has been marked by a steady improvement in analysis and initialization techniques, numerical methods and parameterization schemes (e.g. Bengtsson, 1991 for the ECMWF system). This progress was accompanied by a steady increase of horizontal and, to a lesser extent, vertical resolution, and the evolution was constrained by the finite computer power. For example, the European Centre for Medium Range Weather Forecasts (ECMWF), one of the world leaders in the field, started to operate a global grid point model with a grid spacing of 1.875° (~210km) and 15 vertical levels in September 1979. The spectral model T63 introduced in May 1983 had about the same horizontal resolution. In May 1985 the Gaussian grid associated with the T106 model had a spacing of about 125km. One year later the number of vertical levels was increased to 19. In September 1991 the spectral model T213 (the associated Gaussian grid has a mesh size of ~62km) with 31 vertical levels became operational. By this last step the global ECMWF model reached a horizontal resolution which compares well with that one of the most advanced limited area models (LAM) of national weather

services. High-resolution operational LAMs are designed to resolve flow features at the lower end of the meso-α scale. (A generally accepted subdivision of horizontal scales for atmospheric processes (Orlanski, 1975) denotes flow features belonging to length scales of respectively 200-2000km as meso-α-scale, 20-200km as meso-β-scale and 2-20km as meso-γ-scale. These scales are associated with model grid spacings of 50-500km (meso–α), 5-50km (meso-β) and 0.5-5km (meso-γ).)

At present many national weather services utilize meso-α-scale LAMs: Models with mesh widths of about 50km are running in e.g. Denmark, Finland, Germany, Japan, Norway and the United Kingdom. All these models are hydrostatic primitive equation models with not more than 20 vertical levels. Hydrostatic models with even higher resolution are operational in France (35km) and Norway (25km). The only operational non-hydrostatic model (15km) is run in the United Kingdom with an integration area covering the British Isles and it has 32 levels.

1.3 Object of the present work

High-resolution NWP models are designed to predict in more detail and with increased accuracy weather parameters such as precipitation, cloudiness, low-level winds and surface temperatures, in particular local minima and maxima. Nevertheless, grid lengths of 30km or more are insufficient to meet such demands in a mountainous country like Switzerland. Therefore an effort is under way at the Swiss Meteorological Institute to develop a meso-β-scale NWP model for operational weather prediction purposes. The strategy adopted is to reduce the mesh width of an existing meso-α-scale LAM to achieve a grid spacing of about 15km (Quiby et al., 1988). Similar initiatives are under way in several countries (cf. Bougeault, 1992).

A series of challenging questions are raised by enhancing the horizontal resolution of a well developed NWP model:

1.) How does the overall behaviour of the model change with increasing resolution?

2.) Which components of the model are (particularly) scale-sensitive and have eventually to be revised or even replaced?

3.) How can the potential improvement of a higher resolution version of the model under consideration be assessed?

4.) What kind of observational data are required to verify meso-β-scale model results?

Several specific problems in this context will be addressed with the objective of contributing to the development of an operational meso-β-scale NWP model.

1.3.1 Specific problems

Precipitating weather systems, in conjunction with their sometimes devastating accompanying phenomena such as gale winds, hail and flooding, have an immediate human impact and influence a broad range of activities, e.g. agriculture, construction, traffic. Therefore precipitation, its timing (onset and duration), location and intensity, is certainly a key parameter in weather prediction and has significance for operational hydrology. Furthermore simulated precipitation signatures resulting from numerical prediction give an in-

dication of the model's ability to properly represent the circulation features that actually occurred in nature.

In the following investigations the ability of a NWP model to simulate precipitation events with increasing horizontal resolution is examined. To gain insight into the processes involved three major aspects are investigated in detail.

a.) Mesh width reduction

The dependency of precipitation simulation on horizontal resolution is an aspect of primary interest. In particular the influence of the convective parameterization scheme and the relative importance of specific details of cumulus parameterization have to be examined. To assess simulated high-resolution precipitation characteristics qualitatively and quantitatively appropriate observational data and evaluation methods are required. In complement to temporally and spatially dense raingauge measurements weather radar data offer an opportunity for such an approach.

A sound understanding of the parameterization of convection and the availability of a powerful diagnostic tool are considered to be essential for the interpretation of the results emerging from these investigations.

b.) Cumulus parameterization

The representation of cumulus convection with associated condensation, vertical turbulent transports, cloud and precipitation formation is a significant problem in mesoscale modelling. Here special attention will be directed to the convective adjustment concept. The fundamental properties of the adjustment type family of parameterization will be explored and related to other classes of parameterization schemes. Given the need for a so-called deep-convection reference profile the derivation of a realistic quasi-equilibrium thermodynamic and moisture structure of the post-convective atmosphere from observational data poses a challenging problem.

c.) Model diagnostics

A good diagnostic package is needed for incisive analysis of model internal processes and interactions. In the context of precipitation simulation the influence of the precipitation-forming processes, grid-scale and convective, on the evolution of the model atmosphere is of particular interest. Depending on the design of the NWP model under consideration and the envisaged capabilities of the diagnostic procedure, the development of an appropriate tool can imply considerable formal, numerical and technical problems. It is desirable to test model intrinsic structures, e.g. vertical heating and moistening profiles of precipitating weather systems, against observed features.

1.4 Outline

Three main chapters form the body of the following text. Each chapter is focused on one of the aforementioned principal aspects.

In chapter 2 the problem of cumulus parameterization in NWP is addressed. After a brief general introduction the convective adjustment concept is explained in more detail. An observational study to find a parametric representation of the thermodynamic structure of the convectively adjusted atmosphere, an essential ingredient for convective adjustment schemes, forms a key part of this chapter. The deep-convection reference profiles used in subsequent numerical experiments are introduced and qualitatively discussed with respect to observed features. Some formal considerations of the adjustment concept concerning convective condensation rates and convective vertical transports in relation to the mass flux concept conclude the chapter.

Mesh width experiments with the Europa Modell of the Deutscher Wetterdienst are discussed in chapter 3. In recent years this meso-α-scale model has been developed from an experimental version (Müller et al., 1987) to one in routine operation since January 1991 (Majewski, 1991). The development of a meso-β-scale high-resolution model version is a joint project of the Deutscher Wetterdienst and the Swiss Meteorological Institute. First the two basic versions of the model are presented together with an outline of the experimental design and the weather situations under consideration. Experiments are carried out with the original mesh width of the Europa Modell (~60km) reduced by a factor two and four. Special emphasis is put on consideration of the influence and the behaviour of the cumulus parameterization scheme which is of the adjustment type. The dependency of the simulation results on details of the convective adjustment scheme, namely the specification of the deep-convection reference profile and the adjustment time scale, is of particular interest. Various aspects of simulated precipitation such as accumulated area average precipitation amounts, time series of hourly precipitation sums, horizontal structures of instantaneous precipitation rates and the evolution of these fields in time are investigated and qualitatively and quantitatively compared to observational data. Major findings and problems are discussed in a broader context and conclusions drawn at the end of the chapter.

In chapter 4, first the formalism to diagnose the physics of convection is introduced. Results obtained from observational studies are briefly mentioned as well as the different strategies which have been applied to numerical models so far. The formalism is then carefully related to the governing equations of NWP models. The formulation of the governing equations of the Europa Modell in terms of total enthalpy and total specific water content poses specific difficulties for the determination of water vapour condensation rates. This peculiarity gives rise to careful theoretical and numerical considerations. A strategy is derived to retrieve heat and moisture budgets from the Europa Modell and the corresponding diagnostic tool is developed. Results obtained for convective weather events are presented and their significance with respect to mesh width and cumulus parameterization discussed.

The main conclusions are drawn in chapter 5 and some final remarks are made in the last chapter.

2 Cumulus parameterization by convective adjustment

2.1 Introduction

Cumulus convection is a major atmospheric process. It influences atmospheric flow through the release of latent heat, through vertical turbulent transport of heat, moisture and momentum and through the interaction of cumulus clouds with radiation. Cumulus convection has long been recognized to drive tropical cyclones, mesoscale convective complexes and squall lines. Also it significantly influences the development of mid-latitude cyclones, polar lows and explosive marine cyclones. With respect to the conventional horizontal grid spacings of current hydrostatic NWP models, convective systems contain components that are subgrid in scale.

The problem of cumulus parameterization is to describe the net effect of the subgrid-scale cloud elements on the resolvable scale, i.e. to relate convective condensation and circulation features, which cannot be explicitly resolved by the NWP model, to the variables predicted by the model. Thus an attempt is undertaken to formulate the collective effect of cumulus clouds without predicting individual clouds. To this end, a limited number of equations is sought that represent a statistical ensemble. The core of the parameterization problem is the choice of appropriate closure assumptions (Arakawa and Chen, 1987).

In the last three decades there has been extensive research into the nature of atmospheric convection and scale interaction in cumulus regimes. These studies have been undertaken from an observational, theoretical and modelling point of view. Reviews of the cumulus parameterization problem in NWP have been undertaken that focus on the aspect of dynamical regimes (Frank, 1983), on the closure assumptions and observational verification (Arakawa and Chen, 1987), on major aspects of commonly used schemes (Tiedtke, 1988) and on the problem with respect to mesoscale models (Molinari and Dudek, 1992).

Here the discussion will be confined to aspects that relate specifically to the basic concepts of the so-called convective adjustment schemes and to the parametric representation of the thermodynamic structure of the convectively adjusted atmosphere. The validity of a parameter set designed to describe the structure of the post-convective atmosphere (Betts, 1986) is assessed for a mid-latitude continental environment in western Europe by examination of a set of routine radiosonde ascents at the sounding station Payerne in Switzerland. The characteristics of the deep-convection reference profiles used in numerical experimentation are examined with respect to observed features. The problem of finding convective condensation rates and convective mass fluxes which are consistent with the heat and moisture increments produced by convective adjustment schemes is addressed in a formal way.

2.2 General remarks on cumulus parameterization philosophies

The existence of a clear separation in space and time between the scale being parameterized and that being explicitly resolved by the model grid and a strong direct coupling between the two scales simplifies the parameterization of a given process. If these conditions were met for the representation of cumulus activity in numerical models, the clouds within a grid box could be regarded as a statistically homogeneous entity controlled by the grid-scale variables. Arakawa and Chen (1987) suggested, on the basis of an analysis of the

macroscopic behaviour of moist convection, that cumulus clouds appear to be parameterizable, at least in large-scale models. A serious obstacle to cumulus parameterization comes from the mesoscale organization of convective clouds. In effect the overlap between the cloud scale and the mesoscale poses conceptual problems for the parameterization of cumulus convection as the grid spacing decreases (Arakawa and Chen, 1987; Molinari and Dudek, 1992). There appears to be a need, at least for NWP models of the meso-β scale and larger, to parameterize the convective-scale components and at least parts of the mesoscale structures.

The closure problem of cumulus parameterization can be illustrated by consideration of the budget equations for dry static energy and specific water vapour content:

$$\frac{d\bar{s}}{dt} = \frac{\partial \bar{s}}{\partial t} + \bar{\vec{v}} \bullet \nabla \bar{s} + \bar{\omega} \frac{\partial \bar{s}}{\partial p} = Q_1 \tag{2-1}$$

$$\frac{d\overline{q_v}}{dt} = \frac{\partial \overline{q_v}}{\partial t} + \bar{\vec{v}} \bullet \nabla \overline{q_v} + \bar{\omega} \frac{\partial \overline{q_v}}{\partial p} = -\frac{Q_2}{L_v} \tag{2-2}$$

Here $s=c_pT+gz$ is the dry static energy, c_p the specific heat of air at constant pressure, T the temperature, g the acceleration of gravity, z the height, ω the vertical p-velocity, p the pressure, L_v the latent heat of vaporization, q_v the specific water vapour content and $\vec{v}$ the wind vector. The overbar denotes the area average over a large-scale domain. The quantities Q_1 and Q_2 are the apparent heat source and apparent moisture sink (Yanai et al., 1973), respectively. A more detailed discussion of the above equations and of their importance in the context of convection is given in chapter 4. The important point to be stressed here is that the four quantities $\frac{\partial \bar{s}}{\partial t}$, $\frac{\partial \overline{q_v}}{\partial t}$, Q_1 and Q_2 are unknown in the two equations. If no additional degrees of freedom are introduced, two equations have to be established to close the system and to determine the unknowns (Arakawa and Chen, 1987).

Four types of closure assumptions are identified in most existing cumulus parameterization schemes (Arakawa and Chen, 1987). Type I assumptions postulate the existence of equilibrium states. Type II assumptions constrain the processes that produce the apparent heat source (Q_1) and the apparent moisture sink (Q_2). Type III assumptions directly constrain the intensity of a cumulus ensemble. Type IV assumptions directly couple Q_1 and Q_2 with large-scale processes. A complete closure can be established by type IV assumptions or by some combination of type II with either type I or type III assumptions.

Three requirements of closure assumptions are (Arakawa and Chen, 1987): They must not lose / destroy the predictability of large-scale fields, they should be universally valid and they should be observationally verifiable.

Most existing convective parameterization schemes can be grouped into four families, some representatives of which are listed below:

1.) *Convective adjustment schemes*: Manabe et al. (1965), Krishnamurti et al. (1980), Betts (1986), Betts and Miller (1992).

2.) *Kuo-type schemes*: Kuo (1965, 1974), Anthes (1977), Molinari (1982), Geleyn (1985).

3.) *Mass flux schemes*: Arakawa and Schubert (1974), Geleyn et al. (1982), Bougeault (1985), Tiedtke (1989).

4.) *Schemes designed for mesoscale models*: Kreitzberg and Perkey (1976), Fritsch and Chappell (1980), Frank and Cohen (1987).

Classification in one of the first two families implicitly gives an information about the closure assumptions used: Adjustment schemes have in common that they use type I closure assumptions, thus constraining the thermodynamic state of the equilibrium atmosphere. Kuo-type schemes use type IV assumptions to close the system.

In contrast, mass flux schemes do not necessarily have common closure assumptions: Tiedtke (1989) closes his bulk cumulus ensemble model by a type IV assumption, whilst Arakawa and Schubert (1974), using a spectral cloud ensemble model, rely on a quasi-equilibrium closure. In mass flux schemes the effects of the clouds on the resolvable-scale variables are parameterized in terms of the convective mass fluxes and, typically, convection is assumed to influence the environment through environmental subsidence and detrainment at the top of the updraft or the bottom of the downdraft (Arakawa and Schubert, 1974). Mass fluxes occurring in cloud models used by Kuo-type schemes are only internally needed to determine thermodynamic cloud properties, but they do not influence the environment explicitly.

From a modelling point of view, Grell et al. (1991) present a most instructive separation of cumulus parameterization schemes into three components: *dynamic control*, *static control* and *feedback*. The *dynamic control* determines how the environment modulates convective activity, its location and intensity. Following Grell et al. (1991) three types of dynamic control can be distinguished in the aforementioned parameterization schemes: Convective adjustment schemes, Kreitzberg-Perkey and Fritsch-Chappell depend on instantaneous stability criteria defining available buoyant energy. Adjustment tends to establish an equilibrium state. In contrast, the dynamic control of Kuo-type schemes and of Tiedtke (1989), e.g., are based on some large-scale advective properties like integrated moisture convergence, integrated vertical advection of moisture or low-level convergence. Although convective instability is still required for the onset of convection, the amount of latent heat released is independent of the available buoyant energy. As a third variant, the Arakawa-Schubert scheme relates convective activity to the rate of destabilization by the environment, which is balanced by stabilization through convection in a quasi-equilibrium way.

In the context of mesoscale modelling the validity of the quasi-equilibrium assumption is open to question. The concept (Arakawa and Schubert, 1974) can be summarized as follows (Chen and Bougeault, 1992; personal communication): Through environmental forcing convective available potential energy (CAPE) is generated in the atmosphere on the large scale. Once convection is triggered, CAPE is consumed by release of latent heat forming precipitation and therefore the environment is heated and dried. Convective activity tends to stabilize the atmosphere whilst destabilization by the large-scale processes may continue. If the large-scale forcing is stationary, an equilibrium state is reached after a characteristic time of convective development. But since large-scale forcing will change in time, convection has to adjust continuously. Therefore the intensity of convection does not only depend on instantaneous environmental forcing, but also on its past history. However,

in a large-scale domain (several hundreds of kilometers in horizontal dimensions) environmental forcing has a time scale of, say, 10^5s. Convective adaptation on the other hand occurs within 10^3-10^4s. Thus the reaction of convection to changes in large-scale forcing can be considered to be instantaneous. This is the basis of the quasi-equilibrium hypothesis. In a mesoscale model (mesh width 10-100km) the time scale of the phenomena explicitly simulated on the grid might be comparable to the convective adjustment time scale, and therefore quasi-equilibrium may no longer be an acceptable assumption. In addition, Frank (1983) argues that situations exist, in particular in mesoscale convective systems in mid-latitudes, where the release of latent heat by convection substantially influences the divergent component of the larger-scale flow field and thus convection partially drives the larger-scale flow and does not simply adjust to it. In contrast, semi-prognostic tests with a mesoscale NWP model in comparison with observations seem to provide some indication that the quasi-equilibrium assumption holds for mid-latitude convective situations with strong larger-scale forcing (Grell et al., 1991).

The modification of the environment by the convection is defined by the *feedback*. In particular, the feedback specifies the vertical distribution of total convective heating and drying. Again four approaches have been elaborated with respect to the aforementioned schemes: In adjustment schemes the temperature and moisture differences between the reference and the actual profiles are taken to modify the grid-scale variables without explicitly considering the physical processes causing heating and moistening. In Kuo-type schemes differences between the in-cloud and the environmental profiles are used instead. In a second variant, heating and moistening profiles are arbitrarily specified. Mass flux schemes assume the clouds to have a steady-state character. Latent heat release in the clouds is not used to warm the environment but to maintain the cumulus mass flux. Subsidence and detrainment calculations determine the modification of the environment. Kreitzberg-Perkey and Fritsch-Chappell perform subsidence calculations as the mass flux schemes, but in addition laterally mix the decaying cloud with the environment.

The *static control* determines the thermodynamic properties of the convective process in a general sense. For adjustment schemes the construction of the deep-convection reference profile can be regarded as the static control. The most simple cloud model used in Kuo-type schemes assumes that the in-cloud thermodynamic properties are those of a pseudo-adiabat. A variety of one-dimensional cloud models has been developed including entraining and detraining up- and downdrafts and microphysical parameterizations.

The parameterization of cumulus convection remains one of the major unsolved problems in NWP. This is particularly true in the context of mesoscale weather forecasting. Even fundamental aspects of cumulus parameterization like the closure assumptions are still subject to debate (Emanuel and Raymond, 1992). Other critical aspects are the description of the conditions initiating convection (the trigger problem) and the validation of parameterization schemes. The latter aspect requires both, a sound methodology and an adequate observational basis. Arakawa and Chen (1987) claim for the verification of closures by observations, but at present there are no observations available on the mesoscale for that purpose (Molinari and Dudek, 1992). Most recent developments of cumulus parameterization schemes aim at the formulation of prognostic equations for certain characteristic quantities of convection (Chen and Bougeault, 1992; personal communication) and at

a more sophisticated interaction between parameterized and grid-resolved scales in mesoscale models (Molinari and Dudek, 1992).

2.3 The convective adjustment concept

The basic idea of the so-called adjustment schemes is the direct representation of the quasi-equilibrium structure of the convective atmosphere. Observations suggest that the presence of deep moist convection strongly constrains the vertical temperature and moisture structure of the atmosphere. The essence of the adjustment schemes for the parameterization of subgrid-scale convective activity in NWP models is the reference profile, which characterizes the thermodynamic quasi-equilibrium structure of the convective atmosphere. Through the adjustment process the temperature and moisture structures of the model atmosphere are simultaneously relaxed towards this quasi-equilibrium state. The particular reference profile used can either be based on some a priori concept of what the quasi-equilibrium state of the atmosphere could be, or can be approximately inferred from observations. It appears appealing to guide the model to approach and maintain a realistic vertical temperature and humidity structure on the grid scale in the presence of convection.

An attractive feature of adjustment schemes is their relative conceptual and computational simplicity. For instance, an efficient direct solving algorithm for the reference temperature profile of convective adjustment schemes has recently been proposed by Akmaev (1991). The relaxation towards a predefined quasi-equilibrium structure sidesteps all the details of how the subgrid-scale cloud and mesoscale processes achieve and maintain this structure. Uncertainties involved in attempting to determine this state indirectly using increasingly complex cloud models are avoided. Diagnostic studies have revealed the great complexity of convective systems: in addition to convective-scale up- and downdrafts, mesoscale circulation features and microphysical processes such as detrainment of hydrometeors, freezing, melting, water loading and evaporation are important (see for instance the conceptual model of a mid-latitude squall line presented by Houze et al., 1989). It appears difficult and computationally very expensive to model all these phenomena in a sufficiently realistic way at every grid point of a numerical model.

Several variants of adjustment schemes have been developed. The so-called *hard* convective adjustment (Manabe et al., 1965) replaces the convectively unstable model grid point sounding by the reference profile within one time step. Commonly a pseudo-adiabat has been chosen as the vertical temperature and humidity reference structure. Applied to the tropical atmosphere this procedure can cause temperature and humidity increments of about 3°K and 6g/kg respectively in the initial time step. Although changes in the subsequent time steps are generally much smoother, the initial adjustment can irrecoverably destroy the temperature and humidity fields, since horizontal gradients of these fields in the tropical atmosphere are known to be small (Krishnamurti and Moxim, 1971). As an attempt to mitigate the drastic consequences of hard adjustment, so-called *soft* convective adjustment has been developed (Krishnamurti et al., 1980). In this case, relaxation towards the pseudo-adiabat is assumed to occur only on a fraction σ of the grid element area. Over the remaining area $(1-\sigma)$, the vertical profiles of temperature and humidity remain invariant due to various, unstated processes. In this way, it is possible for the large-scale conditional instability to be gradually and smoothly removed and for the weak thermal and humidity

gradients to be maintained. The fractional area σ has to be determined by a relative humidity criterion (– a closure assumption). For their semi-prognostic tests of the GATE phase III period, Krishnamurti et al. (1980) found optimally tuned rainfall results for an area average relative humidity value of 82.4% and a fractional area σ=0.037. One of the major drawbacks of these schemes is the fact that the quasi-equilibrium structure of convective atmospheres, and in particular of the tropical atmosphere (on which these earlier studies concentrated) is not pseudo-adiabatic (Betts, 1986; Xu and Emanuel, 1989). The third and more recent variant is called *lagged* convective adjustment (Betts, 1986; Betts and Miller, 1992). Here a relaxation time τ is defined within which the actual grid point sounding approaches the specified reference state and which is representative of the convective and mesoscale processes. The pseudo-adiabatic structure is no longer used for the reference state.

In summary, the local temperature tendencies applied to an unstable grid point can be written as follows:

$$\Delta\overline{\psi}_{cum} = (\psi^{Ref} - \overline{\psi}), \qquad \textit{hard} \text{ convective adjustment} \qquad (2\text{-}3)$$

$$\Delta\overline{\psi}_{cum} = \sigma\,(\psi^{Ref} - \overline{\psi}), \qquad \textit{soft} \text{ convective adjustment} \qquad (2\text{-}4)$$

$$\Delta\overline{\psi}_{cum} = \frac{(\psi^{Ref} - \overline{\psi})}{\tau} \times \Delta t, \qquad \textit{lagged} \text{ convective adjustment} \qquad (2\text{-}5)$$

Here ψ stands for temperature (T) and specific water vapour content (q_v), subscript "cum" indicates the change due to cumulus convection, the superscript "Ref" and the overbar denote the reference profile and the grid point profile respectively, Δt is the model time step, σ the fractional area on which adjustment takes place and τ the convective adjustment time scale. Note that for hard and soft adjustment the irreversible moist adiabat (pseudo-adiabat) has been used as reference profile, for lagged adjustment more sophisticated reference states have been defined (see below).

In searching for realistic reference profiles representing the quasi-equilibrium structure of the atmosphere undergoing deep convection the question must be addressed as to whether common characteristics exist for such situations and how can they be described. For example Zipser (1977) collected a set of soundings which are likely to represent the atmospheric structure after the passage of tropical squall lines. The typical "onion" shape of these soundings reflects the effects of the two circulation components different in scale of such convective systems: Near the surface cool, near-saturated air from the convective downdrafts is separated by a marked stable layer from much warmer and drier air aloft produced by the mesoscale unsaturated downdraft. Despite falling precipitation significant subsaturation occurs in this layer. Above the melting level distinctly smaller subsaturation and a slightly stable temperature structure result from the saturated convective-scale and mesoscale updrafts. "Onion-shape" post-convective soundings are also found in mid-latitude continental environments (Fig. 2-4h, page 40). Given the fact that both, cumulus-scale and mesoscale organization are characteristic features of major convective systems around the world (Houze, 1989), it can be inferred that deep-convection reference profiles should represent the effects of both scales of motion. This may be true for mesh sizes of NWP

models down to a few tens of kilometers, at least for more complex arrangements of convective systems (cf. Fig. 10 in Houze et al., 1990).

Based on observational evidence from different tropical and sub-tropical data-sets, Betts (1986) designed a simple parametric representation of the quasi-equilibrium state of convective atmospheres. A few parameters define the deep-convection reference profiles of temperature and humidity. The numerical values of these parameters may be inferred from diagnostic studies. Betts and Miller (1986) present an optimum parameter set derived from a GATE data-set and tuned by means of a single column version of the ECMWF grid point model.

2.4 On the parametric representation of the tropospheric thermodynamic structure for mid-latitude convective situations[1]

In contrast to most earlier studies of the adjustment scheme, the present investigation attempts to assess the validity of the characteristic features of the Betts (1986) deep-convection reference profile for mid-latitude summer convection over western Europe. It is of particular interest to explore the similarities (and differences) between the profiles more representative of the tropical oceans and those of extra-tropical continental environments. To this end numerical values for the important parameters are also determined and compared with those proposed by Betts and Miller (1986).

In the next subsection the data selection and preparation procedures are explained. Subsection 2.4.2 recalls briefly the main features of the Betts (1986) deep reference profile. Recent modifications of the Betts-Miller scheme (Betts and Miller, 1992) are also mentioned. The important parameters computed from the present data-set are given in subsection 2.4.3.

2.4.1 Data selection and preparation

The present investigation concentrates on a set of upper air soundings of the radiosonde station Payerne (46°49′ N latitude, 6°57′ E longitude) in Switzerland for the summer months, i.e. May to September, of the years 1981 through 1988.

Days with convective activity over the region were selected using a synoptic "weather situation" classification scheme (Schüepp, 1979). The primary selection criteria to be satisfied were weak gradients in the geopotential height field at 500hPa (i.e. weak advection) and thunderstorms reported at the sounding site Payerne. These selection criteria are likely to ensure that convection was a, if not the, dominating process during the respective episodes.

After several additional checks, both objective (e.g. restriction to events where the maximum surface temperature was measured in the afternoon) and subjective (e.g. elimination of events influenced strongly by additional non-convective effects), 75 days remained for the given period of 8 years.

---

[1] This section is an adapted and updated version of the article with the same title published in Quart. J. Roy. Meteor. Soc., **116**, 1349-1357 (Binder, 1990).

For these days the two sets of observations at noon and midnight would be likely to reveal a convective adjustment process between 12UTC and 00UTC. (At Payerne local noon precedes 12UTC by about half an hour.)

In addition the 12UTC soundings were subject to further modification. The maximum surface temperature measured during the afternoon was inserted as the ground level temperature of the sounding. Then the low-level temperature profile of the sounding was replaced by the dry adiabat up to the level of intersection with the original sounding. This was an attempt to reconstruct the pre-convective sounding as closely as possible. The water vapour mixing ratio was left unchanged.

All soundings were interpolated to 50hPa intervals with 950hPa as the lowest level. The mean actual ground pressure at Payerne was 960.5hPa (standard deviation 2.6hPa). The 950hPa level was therefore about 90m above ground.

2.4.2 The deep-convection reference profile

Three pressure levels in the atmosphere are required to construct the deep-convection reference profile according to Betts (1986): cloud base (p_B), the melting level (p_M) and cloud top (p_T).

For the present data-set cloud base is provided by the condensation level of a 950hPa rising air parcel. Table 2-1 gives the mean values and standard deviation of these characteristic levels for the set of 75 Payerne soundings. It is important to note that the variability of the air mass in convective situations over the extra-tropical continental station is much higher than over tropical oceans. For example the melting level for days with convective activity can be found below 750hPa in May and above 600hPa in August. Similarly the soundings start from boundary layer temperatures which can differ by 10 degrees. Tropopause height is another variable quantity. This variability renders the construction of average (or composite) soundings much more problematic than for tropical and sub-tropical environments (Jordan, 1958; Frank, 1977; Barnes and Sieckman, 1984). Therefore, this variability was explicitly taken account of in the following evaluations. From Table 2-1 it is also recognized that on average the melting level pressure increases by about 11.5hPa through the convective adjustment process.

A prime feature of the Betts deep reference profile is the existence of a vertical temperature gradient which is conditionally unstable with respect to the pseudo-adiabat below the melting level and stable above (unlike the uniform stability structure of most soft ad-

Table 2-1. Characteristic pressure levels for 75 Payerne soundings: Mean values and (standard deviation) in hPa

	pre-convective (12UTC)	post-convective (00UTC)
cloud base	806.5 (38.6)	
melting level	669.9 (36.6)	681.4 (37.3)
cloud top	234.2 (38.4)	

justment schemes). In the present context neutral stratification of the atmosphere is defined by a vertical temperature structure following an irreversible saturated adiabatic ascent.

Instability of the temperature profile is expressed by a gradient parameter α (Eq. (15) in Betts (1986)) the meaning of which is the following:

$$(\frac{\partial\theta}{\partial p})_{\text{Ref}} = (1-0.1\alpha)\,(\frac{\partial\theta}{\partial p})_{\theta_{ES}} \qquad (2\text{-}6)$$

$(\frac{\partial\theta}{\partial p})_{\text{Ref}}$ is the vertical gradient of potential temperature of the reference profile and

$(\frac{\partial\theta}{\partial p})_{\theta_{ES}}$ is the vertical gradient of potential temperature of the pseudo-adiabat.

The vertical potential temperature profile of the reference sounding can be characterized by α as follows:

$\alpha<0$: absolutely stable.

$\alpha=0$: pseudo-adiabat θ_{ES}, by definition.

$\alpha<1$: conditionally unstable.

$\alpha=1$: moist virtual adiabat θ_{ESV}, by definition (reversible moist ascent).

Eq. (A30) in Betts (1982) indicates that $(\frac{\partial\theta}{\partial p})_{\theta_{ESV}} \approx 0.9\,(\frac{\partial\theta}{\partial p})_{\theta_{ES}}$

$\alpha>1$: unstable with respect to the moist virtual adiabat.

Starting from cloud-base temperature, the parameter α is used to construct the lower part of the reference temperature profile up to the melting level, using Eq. (2-6). Extrapolation downwards from cloud base to the surface may be carried out in the same way. Above the melting level the reference temperature profile is relaxed towards the temperature at cloud top of the pseudo-adiabat through cloud base. This is done by interpolating linearly the θ-difference at the melting level between the estimated temperature and the temperature of the pseudo-adiabat through cloud base.

The reference dew-point sounding is defined by prescribing the saturation-level departures $\mathcal{P}_B$, $\mathcal{P}_M$ and $\mathcal{P}_T$ at the three characteristic pressure levels. After Betts (1982) $\mathcal{P}$ represents the pressure difference that an air parcel has to be lifted to reach saturation and is therefore a measure of subsaturation. At intermediate pressure levels, and below cloud base, the dew-point temperatures are inferred from linearly interpolated and extrapolated values of $\mathcal{P}$ respectively.

It is interesting to note that despite the specification of a global constant reference profile $\mathcal{P}^{\text{Ref}}$, the grid-scale subsaturation $\overline{\mathcal{P}}$ does have a spatial and temporal variability in the presence of deep convection related to the grid-scale vertical velocity $\overline{\omega}$ according to

$$\overline{\mathcal{P}} \approx \mathcal{P}^{\text{Ref}} - \overline{\omega}\tau \qquad \text{(Relation (10) in Betts (1986)).} \qquad (2\text{-}7)$$

The deep convective adjustment is only applied if the precipitation rate (PR), defined by

$$PR = \int_{p_B}^{p_T} \frac{q_v^{Ref} - \overline{q_v}}{\tau} \frac{dp}{g}, \qquad (2\text{-}8)$$

is positive (no liquid water storage!). Thus, given moisture convergence and upward vertical motion, the atmosphere first moistens until a threshold is reached, where convective precipitation starts to fall. Under steady-state forcing $\overline{\omega}\tau$ moistening of the atmosphere continues until relation (2-7) is met, where all grid-scale moisture supply is rained out. Precipitation continues for a while after cessation of the large-scale forcing ($\overline{\omega} = 0$) until the humidity structure of the reference profile is reached (after Betts, 1986).

A sample deep-convection reference profile of the Betts (1986) type is displayed in Fig. 2-4d (page 40). This was constructed with a parameter set derived from the Payerne data-set (see below). The salient features are the conditionally unstable temperature profile below, the kink of the temperature profile at, and the stable character above the 0°C-level. Cloud base is around 800hPa and the temperature and dew-point soundings are extrapolated down to 950hPa as outlined above. The sounding has the largest saturation-level departures at low levels.

Betts and Miller (1992) introduced some modifications to the construction of the deep-convection reference profile. The most important changes are related to the specification of a distinct quasi-equilibrium reference structure for the boundary layer. The properties of an unsaturated downdraft are represented by a temperature and unsaturated moisture profile parallel to a pseudo-adiabat. In addition, an independent adjustment time scale for the boundary layer related to the downdraft mass flux has been introduced. These modifications have implications for the formulation of the energy correction and the determination of precipitation. Furthermore a cloud-top mixing algorithm was incorporated in the definition of cloud top. Above the melting level a quadratic fit in temperature T is applied, rather than the linear fit in potential temperature θ, to bring the temperature profile back to the environmental temperature at cloud top. The energy correction now also includes the cloud-top level.

2.4.3 Results

The 00UTC Payerne soundings for the selected 75 events are assumed to give a representation of the reference state the atmosphere tends to achieve through the convective process.

For comparison numerical values of the (α,$\mathcal{P}$)-parameter set are also computed from GATE observations. Barnes and Sieckman (1984) present tabulated composite "environmental" and "wake" (pre- and post-convective) soundings for fast and slow moving convective systems during GATE.

a.) Temperature profile

The α-values representative for 50hPa layers are computed after Eq. (2-6) with the sounding data used as the reference profile. For the reasons mentioned earlier, 50hPa layers between 750hPa and 600hPa can occur either below or above the melting level. Accordingly, two separate means of α have to be computed for the layers of the respective pressure range.

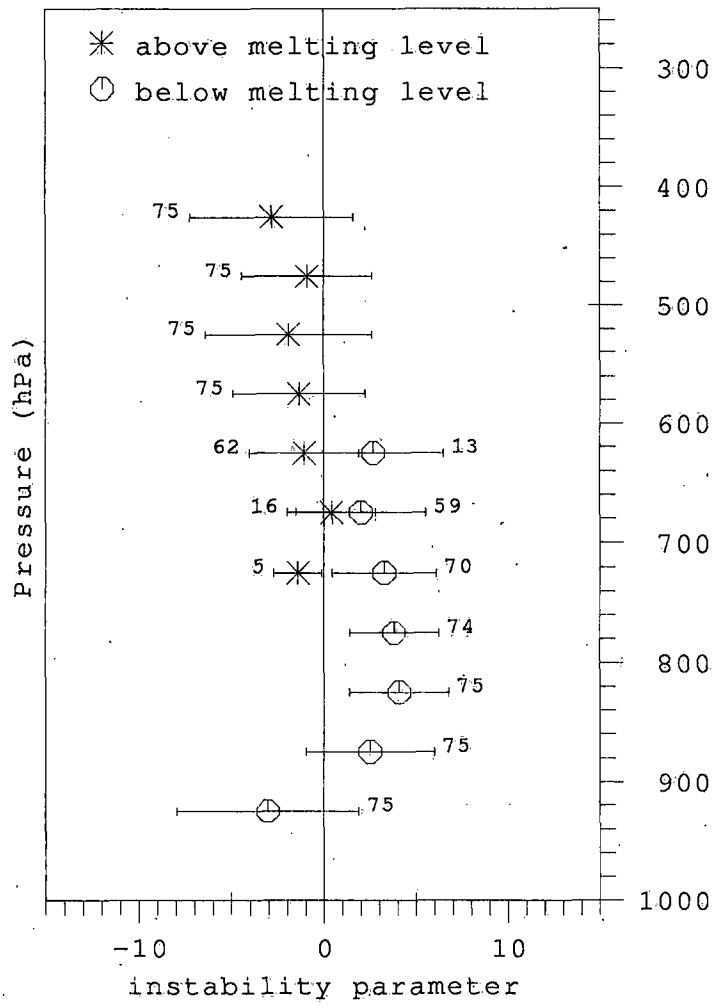

Fig. 2-1: Mean values for the instability parameter α for 50 hPa layers as a function of pressure. The two different symbols represent mean α-values for layers below and above melting level respectively. Also indicated are the standard deviations (horizontal bars) and the number of soundings contributing to each mean value.

Fig. 2-1 shows the mean values of α for 50 hPa layers derived from the Payerne dataset. Arithmetic means of α are separately computed for layers below and above the melting level and represented by two different symbols. It is apparent from Fig. 2-1 that, apart from the lowest layer, the melting level divides the vertical temperature structure of the post-convective atmosphere into two different regimes. On average, α-values below melting level are larger than 1.0 (see Table 2-2) and therefore the temperature profile of the atmosphere is conditionally unstable even with respect to the moist virtual adiabat. Above the melting level the shift of α towards negative values is indicative of the stability of the atmosphere. Recently, similar temperature structures have been found for the North American High Planes by Zhang and McFarlane (1991).

From the numerical values of α in Table 2-2 we conclude that the parameter α adopts a vertically-averaged value of about 3.0 below the melting level for the class of soundings considered here. Betts and Miller (1986) found an optimally tuned value of 1.5 from a

Table 2-2. Instability parameter α for 50 hPa layers

Layer mean pressure (hPa)	Layers below melting level			Layers above melting level		
	α mean	α std. dev.	no. of soundings	α mean	α std. dev.	no. of soundings
925	-3.0	4.9	75			
875	2.5	3.5	75			
825	4.1	2.7	75			
775	3.8	2.4	74	2.9	0.0	1
725	3.3	2.8	70	-1.4	1.3	5
675	2.0	3.5	59	0.4	2.4	16
625	2.7	3.8	13	-1.0	3.0	62
575				-1.3	3.6	75
525				-1.9	4.5	75
475				-0.9	3.5	75
425				-2.8	4.4	75

GATE data-set, whereas 1.7 and 1.5 are derived from "wake" soundings of fast and slow moving systems during GATE (Table 2-3). Over the continent the low-level atmosphere seems to maintain a more unstable lapse-rate than over the tropical ocean.

This result is of some physical interest. For example it indicates that the convection starts from a much more unstable pre-convective sounding in the continental case. The composite environmental GATE soundings, evaluated from 18 and 14 soundings in the so-called fast and slow environment respectively, tabulated in Barnes and Sieckman (1984), exhibit a layer with a dry adiabatic lapse-rate about 560m deep just above the ocean surface. The construction of a constant potential-temperature profile starting from the surface maximum temperature applied to the 75 pre-convective 12UTC Payerne soundings provides a depth for this layer of 1350 ± 500 m over land. It is also not uncommon to find a superadiabatic stratification just before convection is initiated.

One important process for the transition from the stable to the conditionally unstable lapse-rate around the melting level is the melting of frozen precipitation particles. Local temperature decreases at the melting level through the removal of environmental heat for melting, and therefore stability is increased above and decreased below. It is not surprising that tropical and extra-tropical oceanic and continental soundings exhibit this same feature. Numerical lapse-rate adjustment experiments for the tropical atmosphere by Cohen and Frank (1989) revealed that ice processes are important for the presence of the inflection point in the temperature profile at the melting level. Although present in their initial conditions, this feature was not maintained if the model did not provide for ice processes.

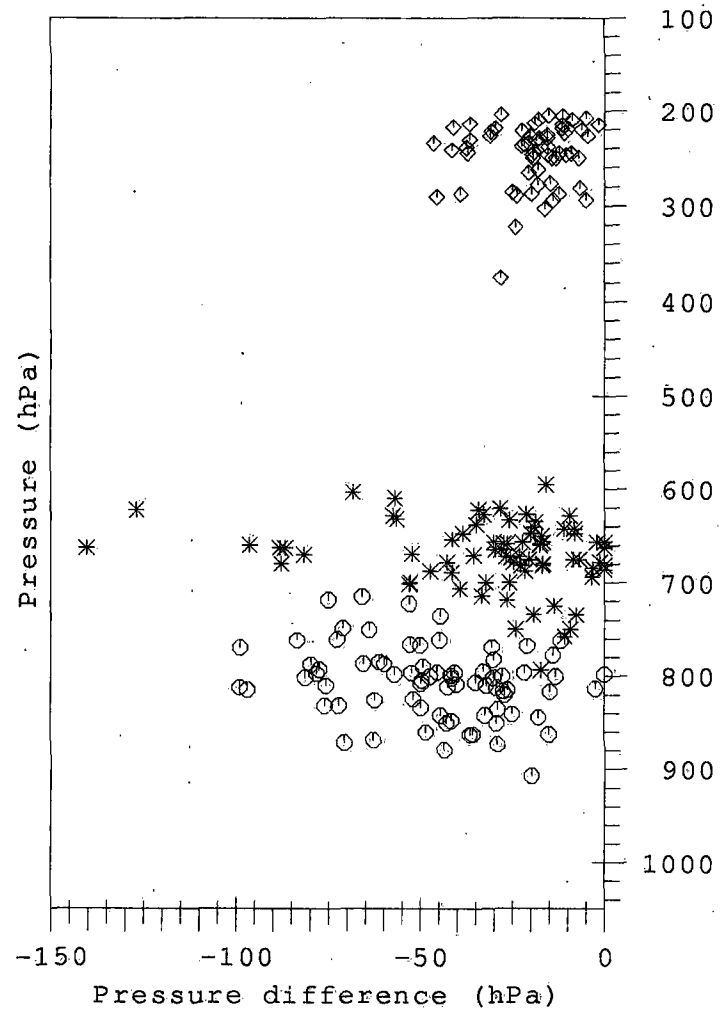

Fig. 2-2: Scatter-plot of saturation-level departures at cloud base, melting level and cloud top for 75 sounding pairs. The individual $\mathcal{P}$-values are plotted at their true pressure level.

b.) Humidity profile

The saturation pressure departures $\mathcal{P}_B$, $\mathcal{P}_M$ and $\mathcal{P}_T$ are calculated in the followin way. For each 12UTC sounding the three characteristic levels p_B, p_M and p_T are deter mined. The subsaturation at these pressure levels for the corresponding 00UTC soundin is then computed. A scatter-plot of $\mathcal{P}$-values for each of the characteristic levels is dis played in Fig. 2-2. Again it is apparent that the pressure values for cloud base, the meltin level and cloud top vary considerably. Also the subsaturation exhibits a strong variabilit The median is used as a representative value of $\mathcal{P}_B$, $\mathcal{P}_M$ and $\mathcal{P}_T$ respectively instead of th arithmetic mean, because of the asymmetry of the frequency distribution of $\mathcal{P}$, partly du to the fact that radiosondes do not report condensed water. In Fig. 2-3 the medians of $\mathcal{P}$ ar plotted at the mean pressure levels of p_B, p_M and p_T, and the arrows indicate the $\mathcal{P}$-median of all 75 adjusted Payerne soundings at 50hPa intervals. This Figure demonstrates that th linear interpolation (and extrapolation below cloud base) of $\mathcal{P}$-values between the charac teristic levels is a good approximation of the real median profile. Again, as for α, the lowes level is an exception.

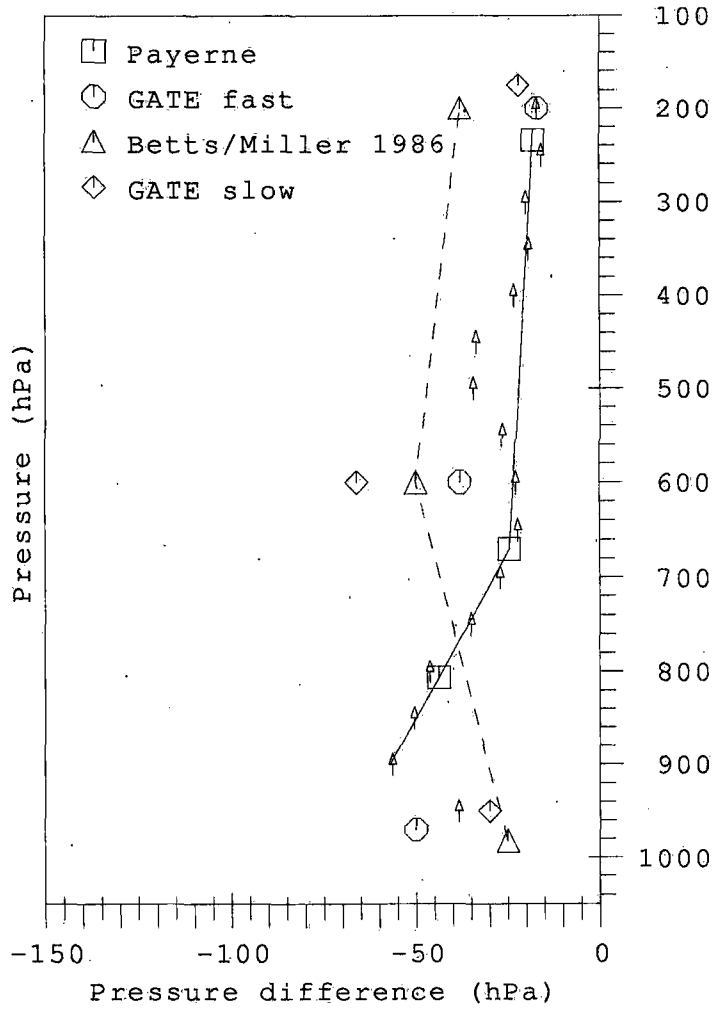

Fig. 2-3: Parameterized vertical moisture profile in terms of saturation-level departures versus pressure from the present investigation (Payerne), Betts and Miller (1986) and GATE composite soundings for fast and slow moving cloud lines (Barnes and Sieckman, 1984). Median values are used for the present study, Arrows indicate median values of $\mathcal{P}$ evaluated at constant pressure every 50hPa from the Payerne data-set.

The $\mathcal{P}$-values from this investigation, GATE observations and Betts and Miller (1986) are given in Table 2-3 and plotted in Fig. 2-3.

In contrast to the Betts-Miller profile we find a profile with largest saturation-level departures at low levels and smaller values between melting level and cloud top. Similar vertical humidity characteristics are also found in some tropical soundings. There is evidence in Betts (1986) and Table 2-3 of the more unstable and drier (in terms of $\mathcal{P}$) lower troposphere in the wake of fast moving squall lines, during GATE, attributable to strong downdrafts. Other examples are the post-squall soundings from different locations in the tropics reported by Zipser (1977). Strong downdrafts produce low-level drying and if convection is cut off, more instability is left in the lower layers. On the other hand, slow moving tropical squall lines with weak downdrafts tend to exhibit the structure evaluated by

Table 2-3. Deep-convection reference profile parameters from different sources

	α	$\mathcal{P}_B$ (hPa)	$\mathcal{P}_M$ (hPa)	$\mathcal{P}_T$ (hPa)	No. of soundings
Payerne	3.0	-44	-25	-18	75
GATE fast	1.7	-50	-38	-17	27
GATE slow	1.5	-30	-66	-22	7
Betts-Miller	1.5	-25	-50	-38	model

GATE observations after Barnes and Sieckman (1984)

Betts and Miller (1986) (Table 2-3). Also, in contrast to the continental case, the warm tropical ocean provides a source for recovering the moisture content of the lowest layers.

For the set of routine soundings considered here it is not possible to work out "a posteriori" the detailed nature of the convective event nor the particular region of the convective system the radiosonde ascended through. This is in contrast to data-sets sampled during field experiments, which are designed to investigate particular phenomena. Although minimized by the selection criteria outlined in subsection 2.4.1, the somewhat arbitrary timing of the routine soundings with respect to the convective events contributes to the scatter of the characteristic quantities explored in this study.

Given the high variability of the moisture profile, the question of the horizontal representativity of the parameterized reference profile arises. The Payerne soundings are, due to the vicinity of the Alps and the Jura mountains, certainly more "local", at least in the lower half of the troposphere, than GATE soundings over the open ocean.

Note also that the 950hPa level is in most cases situated within the moist cool stable layer (Zipser, 1977), which is itself attributable to the outflow from the saturated convective-scale downdrafts. Thus it might be anticipated that the deviation of α- and $\mathcal{P}$-values from the simple reference profile for the lowest layer and level considered are in reasonable accordance with former findings. It is clear that the lowest layer needs a more elaborate treatment than the simple reference profile provides (cf. Betts and Miller, 1992).

2.5 Convection reference profiles used in subsequent numerical experimentation

In this section an introduction is provided to the deep-convection reference profiles of the adjustment scheme used in the numerical experiments with the experimental and operational versions of the Europa Modell (EUM, Müller et al., 1987; EM, Majewski, 1991) of the Deutscher Wetterdienst. Emphasis is placed on the construction of these reference profiles and their characteristics are discussed with respect to the findings of the previous section. Details about the trigger condition and the definition of the convection domain are given in subsection 3.2.2.

Briefly, the model convective precipitation is represented as follows: A fraction of the cloud water built up in supersaturated layers is removed and accumulated successively from upper to lower layers. In unsaturated layers, in particular below cloud base, precipitation can evaporate.

The initial grid point sounding for which deep-convection reference profiles are derived is displayed in Fig. 2-4i (page 40). The relative humidity is 100% over the whole depth of the atmosphere. The convection domain extends approximately from 880hPa to 210hPa. In order to test the sensitivity to initial moisture, reference profiles have also been constructed corresponding to an initial sounding with the same temperature structure but a constant relative humidity of 90% (profile not shown).

a.) A comment on equivalent potential temperature and moist static energy

Since moist static energy will be used as the conserved thermodynamic quantity for the construction of the following deep-convection reference profiles, it is pertinent at this stage to comment on the relationship between equivalent potential temperature and moist static energy.

Above the lifting condensation level, irreversible water-saturated adiabatic (also called moist or pseudo-adiabatic) ascent is usually considered to be the process determining the thermodynamic properties of a rising parcel of moist air which does not mix with the environment. Under this process equivalent (or pseudo-) potential temperature is conserved (by definition). It is assumed that all condensate immediately falls out and none is carried along in the updraft. The ice phase is not considered, thus latent heat of fusion is neglected and water vapour saturation pressure is calculated with respect to water and not with respect to ice. Formulae with various degrees of approximation for the pseudo-potential temperature are available (e.g., Holton, 1979; Bolton, 1980). The most commonly used formulae for pseudo-potential temperature are

$$\theta_e = \theta exp(\frac{L_v Q_v(T,p)}{c_p T}) \quad \text{and} \quad \theta_e = \theta exp(\frac{L_v q_v(T,p)}{c_p T_{LCL}}) \tag{2-9}$$

for the saturated and unsaturated case respectively. θ is potential temperature, q_v (Q_v) is specific (saturation) water vapour content and T_{LCL} is the temperature at the lifting condensation level (cf. Bolton, 1980). In fact, these formulae are not really needed to calculate an irreversible moist adiabat, since the water-saturation pseudo-adiabatic ascent can be computed by stepwise dry adiabatic lifting of an air parcel and an iterative procedure to account for the production of condensate and the release of latent heat (cf. Haltiner and Williams, 1980).

Another approximation to the undiluted water-saturation adiabatic ascent is given by conservation of moist static energy, defined by $h_p=c_pT+L_vq_v+gz$. In the context of convection the pseudo-adiabat is often used to find the top of the convective clouds. It has been recognized (Madden and Robitaille, 1970) that slightly lower parcel equilibrium heights result from calculations using pseudo-potential temperature rather than moist static energy (for instance 9 hPa at a pressure level of 180 hPa). From a careful theoretical consideration Betts (1974) concluded, that "if static energy is considered as a conserved quantity, the implicit assumption is made that kinetic energy is all locally dissipated; while if potential temperature is used, one is assuming the maximum available kinetic energy is generated and none is locally dissipated in the chosen atmospheric volume."

For illustration we derive the energy equation for a saturated parcel under undiluted irreversible adiabatic ascent. Assuming that no other heat sources exist apart from the latent heat released by saturated adiabatic expansion the first law of thermodynamics can be written (e.g. Haltiner and Williams, 1980)

$$c_p\frac{dT}{dt}-\frac{1}{\rho}\frac{dp}{dt}=-L_v\frac{dq_v}{dt}, \tag{2-10}$$

where ρ is density. In the unsaturated case the term on the right hand side vanishes. For a derivation of pseudo-potential temperature defined by Eq. (2-9) starting from Eq. (2-10) see Holton (1979). Expanding the total derivative of the time change of pressure yields

$$c_p\frac{dT}{dt}-\frac{1}{\rho}\vec{v}\bullet\nabla p=\frac{1}{\rho}\frac{\partial p}{\partial t}-L_v\frac{dq_v}{dt}, \tag{2-11}$$

where $\vec{v}$ denotes the 3-dimensional wind velocity vector. Multiplying the equation of motion from the left by $\vec{v}\bullet$, substituting the vertical velocity w by dz/dt and insertion into Eq. (2-11) gives

$$c_p\frac{dT}{dt}-\frac{1}{2}\frac{d}{dt}|\vec{v}|^2+g\frac{dz}{dt}=\frac{1}{\rho}\frac{\partial p}{\partial t}-L_v\frac{dq_v}{dt}. \tag{2-12}$$

Rearrangement then results in

$$\frac{d}{dt}(c_pT+L_vq_v+gz+\frac{1}{2}|\vec{v}|^2)=\frac{1}{\rho}\frac{\partial p}{\partial t}. \tag{2-13}$$

Omitting the kinetic energy term and the local rate of pressure change we get the conservation of moist static energy under water-saturated pseudo-adiabatic ascent. Neglect of kinetic energy suggests the name "static" energy.

The use of static energy as a conserved variable is most convenient for budget considerations (e.g. Yanai et al., 1973). The different energy forms sensible heat (enthalpy, c_pT), latent heat (L_vq_v) and potential energy (gz) then appear as natural variables. In diagnostic studies these quantities can be directly inferred from radiosonde measurements. Furthermore, the mathematical treatment of static energy (dry and moist) is simpler than that of potential and equivalent potential temperature.

It is felt that the main limitations of the method to determine the parcel equilibrium height in order to estimate the vertical extent of the convection domain does not come from

the choice of pseudo-potential temperature or moist static energy as the conserved variable. Consideration of undiluted irreversible water-saturated parcel ascent (i.e. along a pseudo-adiabat) as the reference process for a rising moist air parcel appears to be a much more critical approximation to the real process: Entrainment and detrainment effects strongly affect parcel buoyancy. Provisions should be taken for ice processes (latent heat of fusion) which have a non-negligible effect in the upper troposphere. The immediate fallout of condensate, liquid or frozen, is also a simplification and avoids the problem of accounting for the heat capacities of these particles.

Finally it shall be mentioned that present NWP models do not dispose of a vertical discretization which would "feel" a discrepancy of, say, 10hPa in convective cloud top pressure that might arise from estimates using potential temperature as opposed to static energy.

b.) The VA profile (Vertical Averaging)

The deep-convection reference profile originally used by EUM (cf. Müller et al., 1987) is constructed by vertical mass-weighted averaging of moist static energy $h_p=c_pT+L_vq_v+\Phi$ and total specific water content $q_{vc}=q_v+q_c$, which is the sum of specific water vapour content (q_v) and specific cloud water content (q_c). $\Phi=gz$ is the geopotential. The average is taken over the vertical extent of the convection domain. Thus,

$$h_p^{Ref}(p) = \overline{h_p(p)}^p = const \quad \text{and} \quad q_{vc}^{Ref}(p) = \overline{q_{vc}(p)}^p = const. \qquad (2\text{-}14)$$

The overbar denotes the grid-point value, the value of the reference profile is marked by the superscript "Ref" and the vertical average is indicated by the overbar with the suffix "p". The reference sounding in terms of temperature (T), specific water vapour (q_v) and cloud water content (q_c) is diagnosed from moist static energy and total water content by means of the water vapour saturation criterion.

The reference profile obtained by this procedure from the initially saturated grid-point sounding is displayed in Fig. 2-4a. The vertically averaged total specific water content is about 4g/kg, which means distinct supersaturation above 550hPa. In this supersaturated subdomain the temperature and dew-point structure correspond to a pseudo-adiabat and substantial cloud water is available. Below, without inclusion of a precipitation process, the reference atmosphere is unsaturated and the temperature profile follows a dry adiabat. The dew-point structure corresponds to a line of constant specific humidity. This structure follows immediately from the diagnostic step splitting averaged moist static energy and total water content into temperature, water vapour and cloud water content. If upper-level cloud water is released as precipitation, the temperature and dew-point profile in the unsaturated lower-level part of the atmosphere are modified by evaporative cooling and moistening. In the upper part cloud water content is reduced, but the thermodynamic profile remains unchanged. In terms of relative humidity the reference atmosphere is driest at the bottom of the convection domain. A significant discontinuity in the temperature and dew-point profile can occur at this level. In general, the overall shape of the reference sounding is not completely dissimilar to the "onion" of Fig. 2-4h, although warming and drying at low levels appear to be exaggerated.

Due to the approximately exponential decrease of water vapour saturation with height, vertical mass-weighted averaging of total specific water content leads to abundant supersaturation at upper levels. Since only part of the removed cloud water can be re-evaporated at lower levels, significant precipitation is produced by this scheme. For this particular example, transition from the initial to the reference thermodynamic atmospheric structure produces $7.0\,\mathrm{kg\,m^{-2}}$ of precipitation.

The reference profile belonging to the initial condition with reduced humidity exhibits the same characteristics (Fig. 2-4e). Due to the lower moisture content of the atmosphere and therefore reduced vertically averaged moist static energy and total water content, the whole profile is slightly shifted towards lower temperatures and the precipitation potential is reduced to $5.4\,\mathrm{kg\,m^{-2}}$.

*c.) The MA profile (**M**oist **A**diabat)*

The first step to construct this deep-convection reference profile is again vertical mass-weighted averaging of moist static energy and total water content (Eq. (2-14)). Secondly, for every model level a hypothetical saturation temperature $T_s(p)$ and the associated saturation water vapour content $Q_v(T_s(p))$ is calculated from $h_p^{Ref}(p)$. A new reference profile for total water content is then computed by

$$q_{vc}^{Ref}(p) = \frac{\overline{\overline{q_{vc}(p)}^{p}}}{\overline{Q_v(T_s(p))}^{p}} \times Q_v(T_s(p)). \qquad (2\text{-}15)$$

The conventional thermodynamic variables T, q_v and q_c are then diagnosed from $h_p^{Ref}(p)$ and $q_{vc}^{Ref}(p)$. The first factor on the right hand side of Eq. (2-15) determines, whether the reference profile is saturated or subsaturated over the whole convection domain. Saturation is achieved, if the available moisture is sufficient to saturate the atmosphere at the hypothetical saturation temperature. In case of saturation, the thermodynamic reference sounding follows a pseudo-adiabat, since h_p independent of pressure approximates a pseudo-adiabat (Fig. 2-4b). If subsaturation results for the reference atmosphere, the lapse-rate is slightly conditionally unstable in the entire convection domain (Fig. 2-4f). The dew-point depression increases from top to bottom. At the interface between boundary layer and convection domain a clear jump towards cooler temperatures in the convection domain is apparent.

Obviously, much moisture is needed to produce a saturated reference profile. The initial profile with decreased humidity does not provide enough moisture for saturation, and therefore no precipitation is released during the transition from the initial to the final state, in contrast to the VA profile. Even with the saturated initial profile, only one tenth ($0.7\,\mathrm{kg\,m^{-2}}$) of the precipitation obtained with the VA construction is produced by the MA scheme.

*d.) The MX profile (**MiX**ed)*

The VA and MA reference profiles can be mixed by linear combination as first pointed out by Doms (1990b). Such a linear combination maintains the "onion-shape" characteristic of the reference profile and eliminates the excessive heating of the pure VA profile

at the bottom of the convective domain. More precipitation is produced than in the MA case, since supersaturation in the upper part of the convection domain is likely in most cases. Drying of the lower troposphere by convective vertical upward moisture transport provides the necessary humidity.

The efficiency of the scheme can easily be varied by the weight of linear combination. Formally the mixed moisture reference profile reads

$$q_{vc}^{Ref,MX}(p) = \beta \times q_{vc}^{Ref,MA}(p) + (1-\beta) \times q_{vc}^{Ref,VA}(p) . \qquad (2\text{-}16)$$

In the bottom row of Fig. 2-4 three examples of this type of reference profile are displayed with linear combination weights from left to right $\beta = 0.25, 0.50, 0.75$. $\beta = 0$ reproduces the original VA profile and $\beta = 1.0$ the MA profile. The precipitation potential of the three examples in Fig. 2-4j/k/l is 5.3kgm^{-2}, 3.7kgm^{-2} and 2.0kgm^{-2} respectively.

e.) The EH[1] profile

First the vertical mass-weighted average of moist static energy is computed. Then two subdomains are distinguished: The lower subdomain includes all levels at the bottom of the convection domain for which the grid-point value of moist static energy is larger than the vertically averaged value. In this layer a first guess value of the reference total specific water content $q_{vc}^{fg}(p)$ is calculated by use of the initial grid-point temperature, i.e.

$$q_{vc}^{fg}(p) = \frac{\overline{\overline{h_p}(p)}^{p} - c_p \overline{T}(p) - \overline{\Phi}(p)}{L_v}, \text{ where } \overline{h_p}(p) > h_p^{Ref}(p) \text{ at low levels.} \qquad (2\text{-}17)$$

For the levels above, up to the top of the convection domain, a hypothetical saturation temperature $T_s(p)$ and the associated saturation water vapour content $Q_v(T_s(p))$ is calculated

---

Fig. 2-4: Initial grid-point sounding and associated deep-convection reference profiles constructed by different methods drawn on a skew *T-log(p)* diagram. Displayed are a selection of pressure levels and isotherms, the temperature and dew-point sounding and a pseudo-adiabat as an indication of local static stability.

a) VA profile, initial relative humidity= 100%
b) MA profile, 100%
c) EH profile, 100%
d) BMP: Betts-Miller profile constructed with the Payerne parameter set
e) VA profile, initial relative humidity= 90%
f) MA profile, 90%
g) EH profile, 90%
h) "onion-shape" post-convective original Payerne sounding of 21 August 1983 00UTC
i) initial unstable grid-point sounding extracted from an EUM simulation
j) MX profile, β=0.25, initial relative humidity = 100%
k) MX profile, β=0.50, 100%
l) MX profile, β=0.75, 100%

---

[1] EH are the initials of the name of the person who has proposed this reference profile.

initial relative humidity = 100%

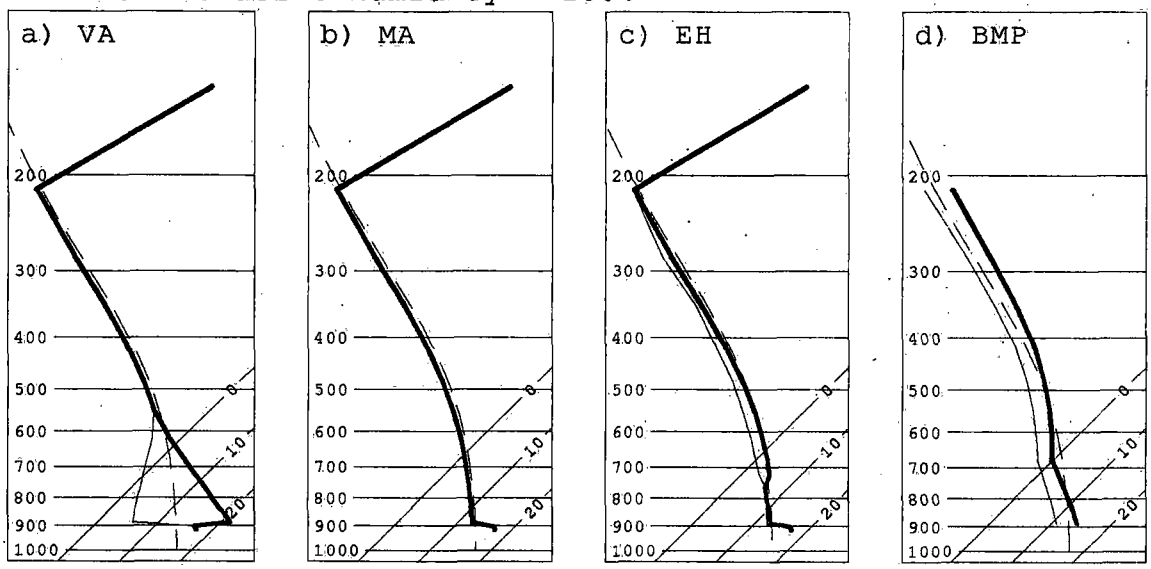

initial relative humidity = 90%

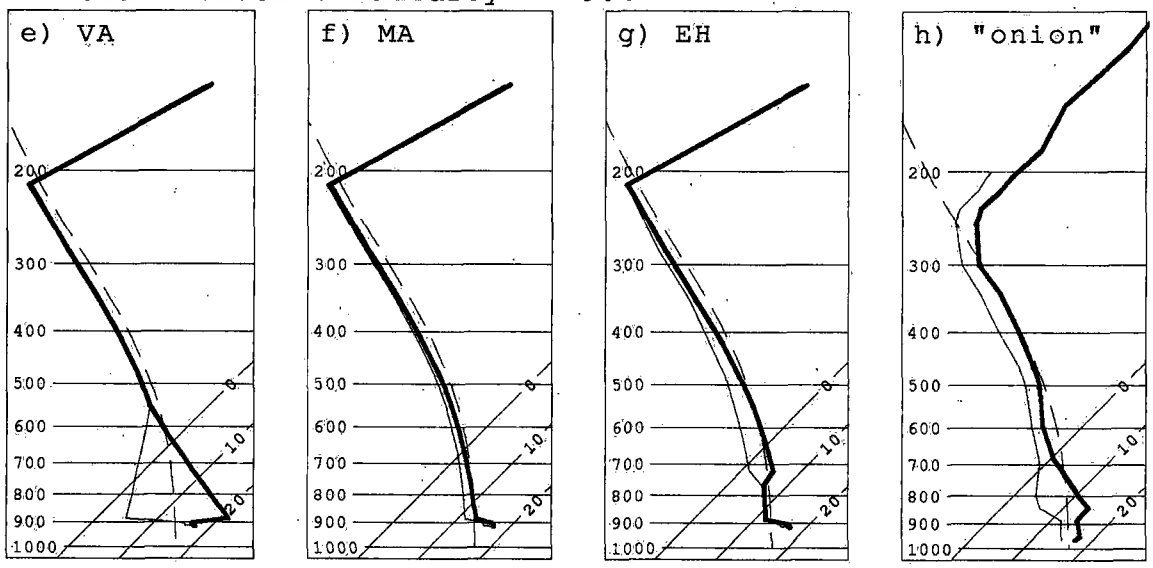

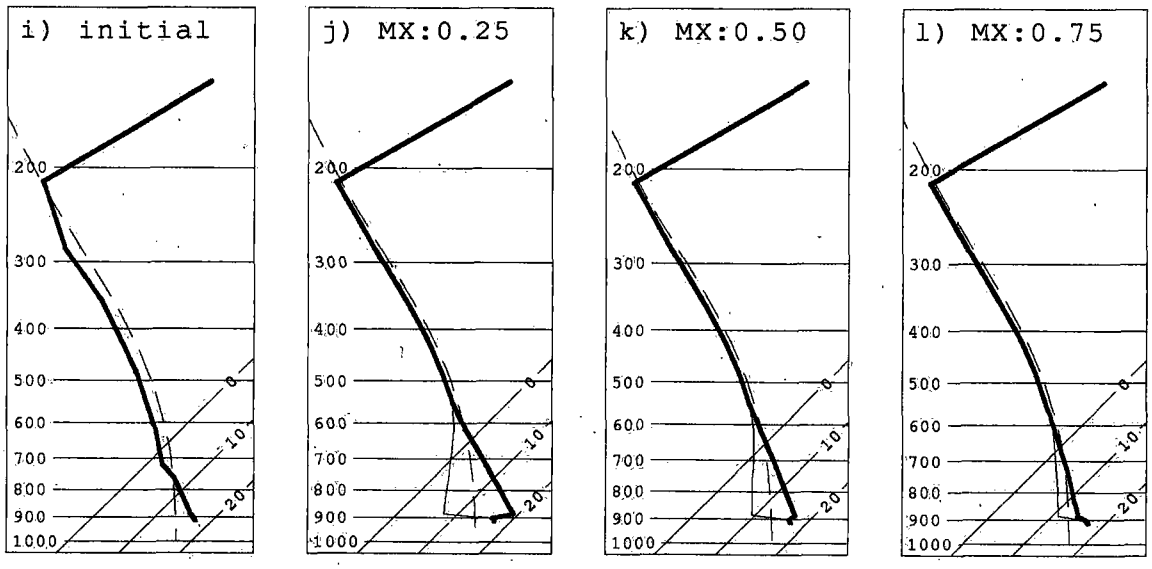

from $h_p^{Ref}(p)$. The maximum of a predefined fraction γ of this saturation water vapour content and the initial grid-point water vapour value is then taken as the first guess value for the total water content,

$$q_{vc}^{fg}(p) = max\{\gamma \times Q_v(T_s(p)), \overline{q_v}(p)\}. \tag{2-18}$$

For operational use γ has been set to 0.6. The final total water vapour reference profile is defined as follows:

$$q_{vc}^{Ref}(p) = \frac{\overline{\overline{q_{vc}(p)}^{p}}}{\overline{\overline{q_{vc}^{fg}(p)}^{p}}} \times q_{vc}^{fg}(p) \tag{2-19}$$

Temperature and dew-point soundings resulting from the EH scheme are plotted in Fig. 2-4c and g. Saturation occurs in the lower subdomain, where the thermodynamic structure follows a pseudo-adiabat. An absolutely stable layer separates the lower part of the profile from the upper part, where subsaturation is found. In fact, the EH reference profile is a combination of the saturated MA case in the lower part of the convection domain with the unsaturated MA case in the upper part. Precipitation can only be built in the lower part, where cloud water is present. The precipitation potential is $1.8 kgm^{-2}$ and $0.7 kgm^{-2}$ for the transition from the saturated and unsaturated initial profile to the corresponding EH profile respectively.

f.) Discussion

The properties of the deep-convection reference profiles introduced in this section are discussed in relation to characteristics of post-convective atmospheres deduced from observations. It has been recognized that the 0°C-isotherm is a characteristic level in the parametric representation of convective reference profiles. Across the melting level the lapse-rate changes from conditionally unstable below to absolutely stable above. Largest subsaturation in terms of saturation-level departure is found at low levels, at least in mid-latitude continental environments. The Betts-type deep-convection reference profile incorporates these features by construction (Fig. 2-4d).

It has already been noticed that the VA reference profiles carry some resemblance with the observed "onion-shape" structure. The pseudo-adiabatic (moist neutral) temperature structure in the upper part of the convection domain and the conditionally unstable lapse-rate in the lower part appear to be realistic. However, the transition between these two regimes is by no means related to the melting level. In addition, the features of the humidity structure with saturation aloft and strong subsaturation at low levels are probably too pronounced. Significant temperature and dew-point temperature discontinuities at the bottom of the convection domain occur. Since the lowest part of the convection domain experiences strongest drying, the scheme produces a maximum of convective precipitation.

The MA reference profile either follows a pseudo-adiabat over the entire convection domain and is therefore moist neutral or it is unsaturated and has a conditionally unstable lapse-rate over the whole depth. Moist neutrality in the lower layers in the first case and the unstable temperature structure in the upper layers in the second case do not conform to observations. Temperature and dew-point discontinuities also occur at the bottom of the con-

vection domain. This scheme produces a minimum of convective precipitation, since saturation over the whole depth of the convection domain is needed prior to release of precipitation.

The MX profile appears to be a reasonable compromise between the first two variants. Although not linked to the melting level, the lapse-rate changes from conditionally unstable to pseudo-adiabatic with height and drying occurs in the lower layers. Temperature discontinuities at the lower boundary of the convection domain are significantly reduced (e.g. Fig. 2-4k). Convective precipitation is decreased since subsaturation is significantly reduced in the lower troposphere.

The thermodynamic characteristics of the EH profile are hardly supported by observations.

The VA scheme has been used in the EUM experiments and, for comparison purposes, in a few experiments with EM. The operational version of EM is based on the EH profile. As an alternative, the MX scheme with $\beta = 0.5$ has been used in the following numerical experiments. The Betts-Miller convective adjustment scheme was not available for use in EUM and EM.

2.6 Condensation rates and mass fluxes for the adjustment process

Adjustment schemes for the parameterization of moist convection circumvent all the details of how convective overturning takes place. It is of general interest to know whether some of the quantities crucial in other types of cumulus parameterization can also be determined for adjustment schemes. In this section two questions are addressed:

1.) Is it possible to attribute convective condensation rates to a moist convective adjustment scheme?

2.) Is it possible to determine mass fluxes responsible for the vertical exchange of thermodynamic and moisture quantities in a convective adjustment scheme?

2.6.1 Adjustment schemes and convective condensation rates

Using the budget formalism of Yanai et al. (1973) for a NWP model (Anthes, 1977) the rates of change of the model variables due to parameterized convection (subscript "cum") can be written as follows (see also chapter 4 for further details):

$$\left.\frac{\partial \bar{s}}{\partial t}\right|_{cum} = -\frac{\partial}{\partial p}\overline{\omega' s'} + L_v c^* \qquad (2\text{-}20)$$

$$\left.\frac{\partial \bar{q}_v}{\partial t}\right|_{cum} = -\frac{\partial}{\partial p}\overline{\omega' q'_v} - c^* \qquad (2\text{-}21)$$

$$\left.\frac{\partial \bar{q}_c}{\partial t}\right|_{cum} = -\frac{\partial}{\partial p}\overline{\omega' q'_c} + c^* \qquad (2\text{-}22)$$

Notation for the variables is conventional. c^* is the local condensation or evaporation rate and the other terms denote the vertical convergence of convective vertical eddy fluxes. Adopting the Reynolds averaging technique the variables are split into a grid element av-

erage part (overbar) and a deviation therefrom (prime). In the context of lagged convective adjustment schemes the left hand side of Eqs. (2-20) to (2-22) is defined by

$$\left.\frac{\partial\overline{\psi}}{\partial t}\right|_{\text{cum}} = \frac{\psi^{\text{Ref}} - \overline{\psi}}{\tau}, \tag{2-23}$$

where ψ stands for the thermodynamic and moisture variables. The superscript "Ref" denotes the value of the reference profile and τ is the adjustment time scale. Thus, the problem is to determine the right hand sides of Eqs. (2-20) to (2-22).

Assuming that the convection domain extends over N model layers, the system of equations (2-20) to (2-22) is underdetermined if we try to solve for the flux divergences, since there are $3N$ equations and $3N+N$ unknowns. It is more reasonable to ask for the eddy fluxes over the interfaces between the layers.

With no loss of generality we look at the construction of reference profiles for quantities which are conserved under convective adjustment in an atmospheric column, namely moist static energy (h_p) and total specific water content (q_{vc}). Examples of such reference profiles used by EUM and EM have been given in the previous section. Linear combination of Eqs. (2-20) and (2-21) yields Eq. (2-24), where flux divergences are written in difference form. Eq. (2-25) is the sum of Eqs. (2-21) and (2-22). Note that the eddy fluxes can be linearly combined like the prognostic quantities themselves. These new equations do no longer contain the condensation rate. For the sake of simplicity precipitation is not considered.

$$\left(\frac{\partial\overline{h_p}}{\partial t}\right)_k\Bigg|_{\text{cum}} = \frac{(h_p^{\text{Ref}} - \overline{h_p})_k}{\tau} = -\frac{(\overline{\omega' h'_p})_{k+1/2} - (\overline{\omega' h'_p})_{k-1/2}}{\Delta p_k} \tag{2-24}$$

$$\left(\frac{\partial\overline{q_{vc}}}{\partial t}\right)_k\Bigg|_{\text{cum}} = \frac{(q_{vc}^{\text{Ref}} - \overline{q_{vc}})_k}{\tau} = -\frac{(\overline{\omega' q'_{vc}})_{k+1/2} - (\overline{\omega' q'_{vc}})_{k-1/2}}{\Delta p_k}, \quad k=1\,..\,N \tag{2-25}$$

The model level numbering starts at the top of the model atmosphere. Here, we consider only those N layers k belonging to the convection domain. Half levels denoted by $k \pm 1/2$ are the interfaces between the model layers. There are no convective vertical eddy fluxes over the bottom and the top of the convection domain, thus for ψ being h_p and q_{vc},

$$(\overline{\omega'\psi'})_{N+1/2} = 0 \quad \text{and} \quad (\overline{\omega'\psi'})_{1-1/2} = 0. \tag{2-26}$$

Enforcing conservation of moist static energy and total specific water content, i.e.

$$\sum_{k=1}^{N} \left((\psi^{\text{Ref}} - \overline{\psi})_k \times \Delta p_k \right) = 0, \tag{2-27}$$

the eddy fluxes for each variable can be uniquely determined, since there remain N-1 equations and N-1 unknowns for each quantity. The inference is that the set of equations (2-20) to (2-22) has no unique solution for the layer by layer convective condensation rates

c_k^* (k=1 . . N) and the vertical eddy fluxes $(\overline{\omega' s'})_{k+1/2}$, $(\overline{\omega' q'_v})_{k+1/2}$ and $(\overline{\omega' q'_c})_{k+1/2}$ (k=1 . . N-1). The c_k^* appear as arbitrary unknowns in Eqs. (2-20) and (2-21) for s and q_v, which are a linear decomposition of Eq. (2-24). Exactly the same argument holds for the water equations.

2.6.2 Adjustment schemes and convective mass fluxes

The problem posed is to find convective mass fluxes which accomplish the adjustment tendencies defined by Eq. (2-23). Following Yanai et al. (1973) and Chen and Bougeault (1992, personal communication) use of the definitions

$$\psi = \overline{\psi} + \psi' \text{ and} \tag{2-28}$$

$$\overline{\psi} = a\psi_c + (1-a)\,\psi_e \tag{2-29}$$

yields an expression for the vertical eddy flux

$$\overline{\omega'\psi'} = a\,(\omega_c - \omega_e)\,(\psi_c - \overline{\psi}) = \omega^*\,(\psi_c - \overline{\psi})\,. \tag{2-30}$$

Here a is the fractional area covered by cumulus clouds. This area could even be subdivided into up- and downdraft subdomains (e.g. Fritsch and Chappell, 1980). Subscripts "c" and "e" denote the value of quantity ψ in the cloud and the environment respectively. ω^* represents the mass flux by the vertical velocity difference between the cumulus clouds and the environment. Note that we do not make use of the approximations $a<<1$ and $\omega_c>>\omega$ which are often applied in considerations of larger-scale systems (e.g., Yanai et al., 1973). In particular the first inequality does not necessarily hold in mesoscale models with mesh widths of 10 to 20km. Insertion of Eq. (2-30) into Eqs. (2-24) and (2-25) gives for $\psi=h_p$, q_{vc}

$$\frac{(\psi^{Ref} - \overline{\psi})_k}{\tau} = -\frac{\omega^*_{k+1/2}\,(\psi_c - \overline{\psi})_{k+1/2} - \omega^*_{k-1/2}\,(\psi_c - \overline{\psi})_{k-1/2}}{\Delta p_k}\,. \tag{2-31}$$

The reference profile ψ^{Ref} represents the atmospheric structure on the grid scale, thus giving the result of all convection induced processes within the grid element. It can differ from the cloud profile ψ_c, which can be defined by an elaborate cloud model or most simply by a pseudo-adiabat. The important fact is that ψ_c is regarded as independently defined in the present context.

The convection domain is assumed to extend over N model layers denoted by k increasing from top to bottom. Values ψ at the layer boundaries $k \pm 1/2$ are calculated as mass-weighted averages. The layer thicknesses are given in pressure increments Δp_k. There is no mass flux due to convection across the lower and upper boundaries of the convection domain, i.e.

$$\omega^*_{N+1/2} = 0 \text{ and } \omega^*_{1-1/2} = 0. \tag{2-32}$$

Starting the integration from the lower boundary an expression for the vertical velocity is easily derived:

$$\omega^*_{k-1/2} = \frac{1}{\tau\,(\psi_c - \overline{\psi})_{k-1/2}} \times \sum_{l=N,k,-1} (\psi^{Ref} - \overline{\psi})_l \Delta p_l, \qquad 1 \le k \le N. \quad (2\text{-}33)$$

For k=1 the vertical velocity vanishes as a consequence of Eq. (2-27) and therefore the upper boundary condition is correctly reproduced.

More generally expressed, for each conserved quantity a set of N-1 equations with N-1 unknowns is solved independently. Therefore the result will be in general two individual, non-identical vertical velocity profiles. This fact fundamentally contradicts the basic mass flux idea. To put it differently, given any reference profile ψ^{Ref} and a cloud profile ψ_c, in general it is not possible to find a mass flux profile which simultaneously satisfies the heat and total water fluxes required by the construction of the respective reference profiles.

To complete the argument, assume that a particular case is found where a common $\omega^*(p)$ profile for both h_p and q_{vc} applies. We then modify the initial grid point profile $(\overline{q_{vc}})_k$ at two levels j and j-1 in such a way that the reference profile as well as the cloud profile remain unchanged. It then follows from Eq. (2-33) that the new vertical velocity profile $\hat{\omega}^*(p)$ associated with this modified initial profile differs from the original $\omega^*(p)$ at the three levels j+1/2, j-1/2 and j-3/2.

In order to give a specific example, simple vertical mass-weighted averaging is assumed for the construction of the reference and the cloud profile. Increments δq are added to the initial total water content profile in two supersaturated adjacent layers j and j-1 which satisfy

$$\delta q_j \Delta p_j + \delta q_{j-1} \Delta p_{j-1} = 0. \quad (2\text{-}34)$$

By this procedure neither vertically integrated total moist static energy nor total specific water are altered and therefore the vertical averages remain unchanged. From Eq. (2-33) it then follows, that

$$\hat{\omega}^*_{j-1/2} = \omega^*_{j-1/2} - \frac{1}{\tau\,(\psi_c - \overline{\psi})_{j-1/2}} \delta q_j \Delta p_j. \quad (2\text{-}35)$$

Evidently, adjustment increments can not be satisfied by a mass flux approach. These two concepts are fundamentally different.

2.7 Conclusions

Some fundamental issues of cumulus parameterization in NWP have been discussed in the present chapter. Special emphasis has been put on the convective adjustment concept, aspects of which have been investigated from an observational and theoretical point of view. A discussion of the characteristic features of the reference profiles to be used in subsequent numerical experimentation has also been included. The main conclusions are as follows:

1.) The convective adjustment concept has several attractive features: conceptual simplicity, a possible immediate link to observations and computational efficiency.

2.) Deep-convection reference profiles representing the quasi-equilibrium state of convective atmospheres can, in principle, be inferred from observations.

3.) A carefully selected set of 75 pre-convective and post-convective sounding pairs from convective episodes during the summer months of the years 1981 to 1988 over a continental station in Western Europe, i.e. Payerne in Switzerland, has been examined to assess the validity of the deep-convection reference profile of Betts (1986) and to derive a corresponding parameter set.

The existence of a conditionally unstable temperature profile below melting level of the convectively adjusted atmosphere is consistent with the Betts deep-convection reference profile. This instability of the lapse-rate is even more pronounced than that evaluated by Betts and Miller (1986) for tropical environments. One reason for the change of the stability characteristics at the 0°C-level are ice processes (melting). The humidity structure differs considerably from the one deduced by Betts and Miller (1986) mainly based on a GATE data-set. However, tropical convective systems with strong downdrafts do exhibit similar vertical moisture structures.

The results of this study indicate that the Betts (1986) parametric model for deep-convection can be adapted to extra-tropical continental convection provided an appropriate parameter set is chosen. It is also worth noting that for convective parameterization in NWP models it would not be inappropriate to use "local" parameter sets, diagnostically derived and representative of the respective environment.

4.) From a phenomenological point of view, in particular criteria relating to static stability and saturation, the deep-convection reference profiles available for experiments with EUM and EM turn out not to be entirely satisfactory.

5.) It has been demonstrated that, for fundamental reasons, it is impossible to determine convective condensation rates from a convective adjustment scheme.

6.) In general, it can be shown that there does not exist a convective mass flux profile which can be associated with heat and moisture transports required by the adjustment increments. Adjustment and mass flux concepts are fundamentally different.

3 Scale and parameterization dependencies of precipitation simulation

3.1 Introduction

Most advanced LAMs operated by national weather services have mesh widths of the order of 50km and hence are able to resolve meso-α-scale flow structures. The current trend is to develop for operational purposes hydrostatic meso-β-scale models with grid spacings of 10-20km. Problems usually reported from preliminary experiments are the resolution dependency of the hydrological cycle and the need to respect some relation between horizontal and vertical resolution (Bougeault, 1992).

The beneficial impact of enhanced horizontal resolution in NWP has long been recognized. In the 1960s the dynamics of a front and associated rainfall was simulated with considerable success by a 10-level primitive equation model with a grid spacing of 40km (Bushby and Timpson, 1967). Higher horizontal resolution allows for the explicit representation of smaller scale eddies and hence better definition of the fine structure of meteorological systems. Simulation of a frontal passage over the Alps with a high-resolution limited area version of the ECMWF grid point model (Dell'Osso, 1984) with an approximate horizontal grid length of 37km provided better structures of the wind field and, concomitantly, the forecast of precipitation was improved both with respect to location and quantity. Certainly part of the success of such simulations is attributable to the finer-scale orography and the associated more realistic external forcing. The French Péridot model, introduced at the beginning of 1985, was the first operational meso-β-scale model. It has a mesh width of about 35km and 15 levels. After two and a half years of operational experience Imbard et al. (1988) summarized the main problem areas to be the sensitivity of forecast quality to lateral boundary conditions and the impact of the cumulus parameterization scheme, and they acknowledged the better adaptation of the model flow fields to local orography.

Boundary value updating is a specific problem of LAMs. The forecast quality depends crucially on the quality of the boundary values provided by the host model (Anthes et al., 1985). There is some evidence that forecast errors can depend as strongly on perturbations of the lateral boundary conditions as on imperfect initial conditions within the limited area domain (Vukicevic and Errico, 1990). A high update frequency is apt to counteract distortions of weather systems simulated by the nested model due to inadequate treatment of information penetrating through the boundary zone (Majewski, 1990). The permanent spin-up problem noted by Yessad (1992) which particularly affects the hydrological cycle might be mitigated by an optimal harmonization of the coupled models with respect to basic structures and parameterization schemes.

Model orientated investigations (Persson and Warner, 1991) indicate that most of today's mesoscale models are inconsistent with respect to the relation between horizontal and vertical resolution. In general the number of vertical levels ought to be significantly increased to attain a reasonable ratio between vertical and horizontal grid spacing. Despite this inconsistency operational LAMs are known to produce reasonable forecasts. A recent sensitivity study by Houghton et al. (1991) reveals that the impact of increased horizontal resolution is more pronounced than that of enhanced vertical resolution. Nonetheless a definite and seemingly positive impact of vertical resolution enhancement is also recognized.

The representation of cumulus convection is a difficult problem for high-resolution LAMs. As the mesh size decreases more of the circulation features connected to convective systems will be resolved on the grid scale. Thus the nature of components to be parameterized can depend on the mesh size. At which grid length parameterization of moist deep convection ceases to be a necessary ingredient of mesoscale models is still unclear, although it is an essential question for meso-β-scale models with grid spacings between 10 and 20km. Such models belong just to the scale regime where this question is most difficult to answer. For models with grid lengths larger than 100km (Bougeault and Geleyn, 1989) or 50km (Molinari and Dudek, 1992) the best choice is the so-called "traditional" approach (Molinari and Dudek, 1992): Cumulus parameterization is applied at conditionally unstable grid points, explicit condensation at the stable grid points. Fully explicit condensation is appropriate for mesh sizes smaller than one or a few kilometers, at best. For models with horizontal grid distances of about 20km to 50km the so-called "hybrid" approach has recently been proposed by Molinari and Dudek (1992). In such a scheme only the convective scale is parameterized and a coupling between implicit (parameterized) and explicit clouds is established by the direct transfer of microphysical quantities from the parameterization scheme to the grid-scale forecast equations. For the "critical" regime (5km to 20km), to which some of the scheduled meso-β-scale models will belong to, the possibility increases that conditional instability occurs at saturated grid points and therefore convective clouds will develop directly on the grid-scale. An optimum solution for this scale of NWP models has still to be found.

In the present study, starting from an up-to-date meso-α-scale model, namely the Europa Modell of the Deutscher Wetterdienst, the following questions are addressed: What is the potential of a meso-β-scale model to simulate precipitation? What specific problems arise? What is the role and importance of the cumulus parameterization scheme? What is the sensitivity of the model to horizontal resolution and parameterization of convection?

A series of experiments is carried out in order to answer these questions. Model simulations are conducted with successively decreasing mesh widths, beginning with the original mesh size of about 60km reduced to 30km and finally 15km. The basic model uses the convective adjustment concept for cumulus parameterization. Three different deep-convection reference profiles are tested within this framework. Various aspects of the simulation of essentially four weather situations, two convectively dominated events and two summertime frontal events, are examined. These aspects include the bulk properties of the precipitation fields such as domain average accumulated and hourly precipitation amounts, horizontal patterns of instantaneous convective and grid-scale precipitation rates, and time series of precipitation type partitioning.

Meaningful verification of meso-β-scale precipitation fields requires dense observational information. Advantage is taken of the availability of high-resolution (in space and time) observational precipitation data from a weather radar and an automatic raingauge network to scrutinize the simulated precipitation fields. In particular, quantitative precipitation estimates of the three sources are discussed.

The present chapter is organized as follows: Section 3.2 introduces some pertinent features of the models under consideration, in particular their parameterization schemes for convection and cloud physics. The detailed experimental set-up and the weather situations

examined are also presented for various aspects of resolution and parameterization dependency. Sections 3.3 and 3.4 discuss properties of domain average precipitation and horizontal precipitation patterns respectively. Attempts to make quantitative precipitation estimates and comparison with model data are presented in section 3.5. Results are discussed in section 3.6 and conclusions drawn in the last section.

3.2 Preliminaries

3.2.1 Model characteristics

The main features of the two models forming the basis of the subsequent experiments are briefly mentioned. The experimental version of the Europa Modell (EUM) of the Deutscher Wetterdienst (DWD) is described in detail by Müller et al. (1987). In its basic configuration it is that of a hydrostatic meso-α-scale NWP model based on the primitive equations. It is cast in flux form on a Arakawa-A grid staggered in time with terrain following co-ordinates. The full physics parameterization package includes horizontal diffusion and vertical turbulent transports, convective and grid-scale precipitation with cloud microphysics and radiation. At the end of the year 1990 the exploitation of EUM was replaced by an alternative version, called EM, which became operational at the DWD on 15 January 1991. A description of EM is given in Majewski (1991). Although EM is a descendant of EUM, the step from EUM to EM was accompanied by several changes with respect to the basic structure of the model and the model physics.

The prognostic variables of both models are surface pressure (p_s), the horizontal wind components (u, v), total enthalpy (h) and total specific water content (q_{vc}). h is the sum of sensible heat ($c_p T$) and latent heat ($L_v q_v$), whereas q_{vc} is the sum of specific water vapour content (q_v) and specific cloud water content (q_c). The (h, q_{vc})-system has the property of treating phase changes between water vapour and liquid water implicitly, thus no condensation or evaporation rates become apparent. The common variables temperature (T), water vapour (q_v) and cloud water (q_c) can be diagnostically determined from (h, q_{vc}) by assuming water saturation in clouds.

A summary of the characteristics of the two models is given in Table 3-1. The physics of EM have been improved as described by Doms (1990a): Vertical diffusion uses a modified Crank-Nicholson scheme with a vertically varying weight factor. Horizontal diffusion is applied on the hybrid levels, but correction terms derived from a complete co-ordinate transformation of the divergence of the diffusion flux are added in the heat and moisture equations to account for the slope of the model surfaces. The space dependent diffusion coefficients are calculated from the *total* deformation of the velocity field. Usually only contributions from shearing and stretching are incorporated but not from dilatation of the flow. In order to guarantee a positive dissipation function of momentum the flow variables u and v are no longer diffused independently. The revised diffusion coefficients should provide a measure to counteract the development of grid point storms.

Cumulus convection is parameterized by a convective adjustment scheme. The deep-convection reference profiles used in EUM and EM are different (cf. section 2.5). EUM had an option to use a 1-dimensional cloud model representing an entraining parcel with microphysics with a Kuo-type moisture convergence closure (Anthes, 1977) for cumulus con-

Table 3-1. Main features of EUM and EM

property	EUM (Müller et al., 1987)	EM (Majewski, 1991)
prognostic variables	p_s, u, v, h, q_{vc}	p_s, u, v, h, q_{vc}
primitive equations	flux form	advective form
horizontal grid	Arakawa-A staggered in time (Eliassen grid)	Arakawa-C
horizontal co-ordinates	polar stereographic, true at 60°N	rotated geographical, north pole at φ=32.5°N, λ=170°W
mesh width	63.5km	0.5° (~55km)
vertical structure	$\sigma = \frac{p-p_t}{p_s-p_t}$, 3 p-levels on top, p_t=250hPa	$p(\eta) = A(\eta) + B(\eta)p_s$, classical hybrid
number of vertical levels	18	20
time integration	leap-frog explicit	leap-frog semi-implicit
time step	75s	300s

vection. This scheme is no longer available with EM. EM also uses a completely new radiation scheme (a precursor of Ritter and Geleyn, 1992).

3.2.2 Precipitation schemes

Formally the model distinguishes between grid-scale and convective precipitation parameterized with respectively a Kessler-type scheme including an ice phase and a convective adjustment scheme.

a.) Convective precipitation

First a brief account is given of some essential features of the construction of the convective adjustment scheme for moist deep convection. The procedure is applied at each grid point column independently and consists of the following steps:

1.) Definition of convection domains:
Locate, if present, conditionally unstable layers in a given column. The top of the unstable layer is defined by the level at which the difference between the moist static energy of the root level (i.e. bottom of unstable layer) and the saturated moist static energy of the actual level is a maximum. This formulation of conditional instability is equivalent to Holton's (1979) which is given in terms of equivalent potential temperature. The use of static energies is most common in budget calculations (e.g. Yanai et al., 1973) and cumulus parameterization. In practice the difference between

potential temperature and static energy considerations is small. An account of the two thermodynamic quantities has been given in section 2.5.

In EUM an entrainment rate is defined which is inversely proportional to the thickness of the unstable layer. In EM the entrainment rate is constant and set to $1/4000\,m^{-1}$. Observations suggest an inverse relation between entrainment rate and the linear dimensions, i.e. the radius (Simpson and Wiggert, 1969) or the vertical depth (e.g. Austin and Houze, 1973) of a cumulus cloud. Such an inverse proportionality has been used by several authors in convective parameterization schemes (e.g. Houze et al., 1980; Fritsch and Chappell, 1980; Frank and Cohen, 1987). The inherent uncertainty in the specification of the entrainment rate can amount to a factor of two (Cheng and Houze, 1980). Shallow cumuli 1-2km deep seem to entrain environmental mass at a rate of about $1/1000\,m^{-1}$ and deep cumulus clouds at a rate of about $1/5000\,m^{-1}$ to $1/10000\,m^{-1}$ (Austin and Houze, 1973). Tiedtke (1989) chose two different constant values for deep ($1/10000\,m^{-1}$, typical for very deep tropical towers) and shallow ($3/10000\,m^{-1}$, typical for large trade cumuli) cumulus clouds. In comparison to the curves of Cheng and Houze (1980) the entrainment rate used in EM corresponds to cloud depths between 4 and 7km, which appears not to be unreasonable. The EM-entrainment is too weak for small cumuli.

2.) Cloud top is found at the intersection point of the entraining parcel ascent from the root level with the grid point sounding. A convection domain extends from the root level to cloud top. Several convection domains can exist in the same atmospheric column.

3.) Construction of the reference profile for the convection domain:
For construction and characteristics of the references profiles used in EUM and EM the reader is referred to section 2.5.

4.) Precipitation process:
In general a given reference profile might divide the convection domain into saturated and unsaturated subdomains. In the saturated subdomain a fraction α_R of supersaturation (cloud water) is removed as rain. Rain is accumulated layer by layer from top to bottom. Within the subsaturated convection subdomain a portion of the convective precipitation is used to saturate a fraction σ_U of the grid point area, σ_U assumed to be the area occupied by saturated updrafts. Below the convection domain evaporation of remaining convective precipitation saturates subgrid-scale rain shafts which occupy a fraction σ_R of the grid point area.

5.) Convective tendencies:
The level by level differences between the initial vertical profile of h and q_{vc} and the (h, q_{vc})-profile resulting from the above procedure are then divided by the adjustment time scale τ to define the convective tendencies to be used in the prognostic equations.

6.) Parameter setting:
The values assigned to the free parameters of the adjustment scheme used in EUM and EM experiments are given in Table 3-2.

A second type of cumulus parameterization, henceforth referred to as KUO, was available with EUM. This scheme used a simple 1-dimensional stationary cloud model to

Table 3-2. Parameters of the convective adjustment scheme

Parameter		EUM	EM
entrainment	ε	inversely prop. to depth of unstable layer	1/4000 m^{-1}
rain out fraction	α_R	1.0	1.0
updraft area	σ_U	0.4	0.4
rainfall area	σ_R	0.1	0.1
adjustment time scale τ		3.0h (EUM/EU1)	1.0h (EM3)
used for (model configuration),		3.0h (EU2)	0.75h (HM4)
cf. Table 3-3		0.5h (EU4)	0.5h (HM8)

determine the properties of the convective clouds and a moisture convergence closure to compute the number of clouds per grid element. The cloud model is formulated for vertical velocity, horizontal wind, moist static energy and total specific water content. Entrainment is considered for these four quantities. The equation for the vertical velocity in the cloud contained the buoyancy force, the equations of energy and humidity accounted for the cloud microphysical processes. A three step procedure was applied to solve the cloud model equations:

First, unstable layers are detected with the same criterion as for the adjustment scheme. The first guess cloud top is approximated by the height of the intersection point of the root level moist static energy curve with the saturation moist static energy of the environment at the respective level. The depth of the cloud is then used to estimate an updraft radius which in turn enters the common formula for the entrainment rate after Simpson and Wiggert (1969).

In the second step the cloud model is vertically integrated starting from the root level with the inclusion of entrainment effects as well as autoconversion and nucleation rates. The cloud top is now defined where vertical motion within the cloud becomes negative. Reduction of buoyancy by liquid water is taken into account.

In the third step integration from top to bottom yields missing conversion rates of cloud physics and precipitation fluxes. These processes modify cloud temperature, specific water vapour and cloud water content, but not vertical velocity via the buoyancy term. All necessary properties of the in-cloud sounding are now determined.

The scheme is closed after Anthes (1977). The fraction $(1-b)$ of total moisture convergence used for cloud formation increases linearly from zero to 1 if vertically averaged relative humidity is larger than 50%. The fractional area (a) covered by convective clouds is then defined by

$$a = \frac{(1-b)\,I}{P_{tot}}, \qquad (3\text{-}1)$$

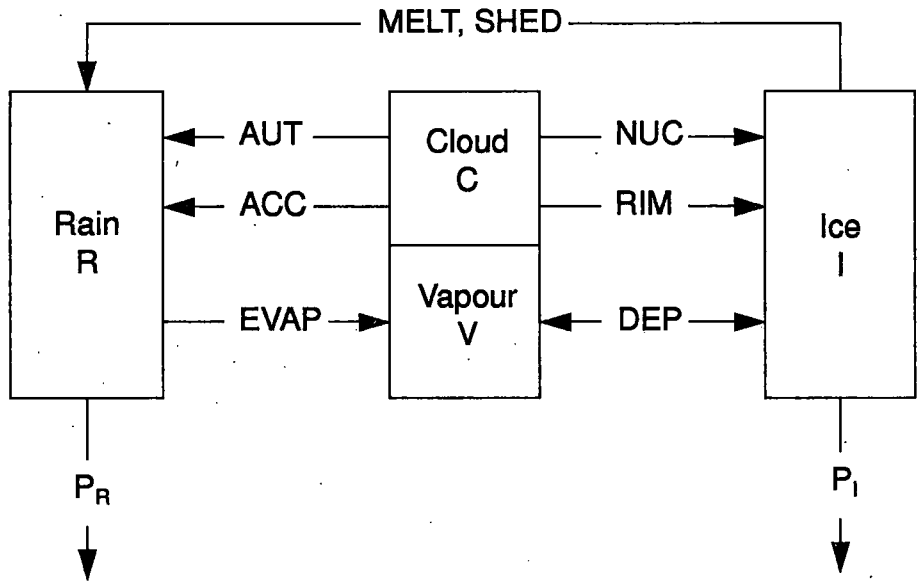

Fig. 3-1: Schematic diagram of parameterized cloud microphysics: Processes involved in rain (P_R) and snow (P_I) formation (after Müller et al., 1987).

where I is the total 3-dimensional moisture convergence over the cloud depth and P_{tot} is total convective precipitation at cloud base. a is then used to calculate the cumulus convection tendencies transmitted to the prognostic model equations.

$$\left.\frac{\partial h}{\partial t}\right|_{cum} = -\frac{\partial}{\partial p}\left(\frac{a\overline{\omega_c}^{p}}{1-a}(h_{pc}-h_p)\right) + aL_f(S_{cloud}), \tag{3-2}$$

where $\overline{\omega_c}^{p}$, h_p and S_{cloud} denote vertically averaged in-cloud vertical velocity, moist static energy and cloud microphysical conversion rates respectively. Index "c" stands for in-cloud values and L_f is the latent heat of fusion. An analogous equation holds for total specific water content. Thus the grid-scale effects of convection are computed as the sum of the divergence of convective transports (using the vertically averaged cloud mass flux) and the microphysical conversion rates both multiplied by the fractional cloud cover derived from the closure scheme.

b.) Grid-scale precipitation

A detailed account of the stable precipitation scheme is given in Müller et al. (1987) and a part of the following description is taken from that source. The parameterization of the cloud microphysics accentuates the role of the ice phase for precipitation formation by emphasizing the Bergeron-Findeisen process. The parameterization scheme is of the Kessler type and allows for interactions between water vapour, cloud water, rain and ice including autoconversion of cloud water to rain (AUT) and to ice, here called nucleation (NUC), accretion (ACC), riming (RIM), shedding (SHED), melting (MELT), deposition (DEP), and evaporation of raindrops (EVAP) (see Fig. 3-1). Assuming stationarity and

neglecting advection the rainfall rate (P_R) and the snowfall rate (P_I) can be integrated vertically by

$$\frac{\partial P_R}{\partial p} = S_{AUT} + S_{ACC} + S_{SHED} + S_{MELT} - S_{EVAP} \tag{3-3}$$

$$\frac{\partial P_I}{\partial p} = S_{NUC} + S_{RIM} - S_{SHED} - S_{MELT} + S_{DEP} \tag{3-4}$$

Definitions of the conversion rates (S) can be found in Müller et al. (1987). Autoconversion and nucleation are the processes initiating precipitation formation. The remaining conversion rates can only become non-zero if precipitation falls into the layer under consideration.

Since h and q_{vc} are the prognostic variables of the model (EUM and EM), the condensation rate of water vapour to cloud water (COND) does not appear explicitly in the scheme. Condensation and evaporation of cloud water is implicitly treated by diagnosing temperature, water vapour and cloud water from h and q_{vc} by use of the water vapour saturation criterion. The tendencies of h and q_{vc} from the stable precipitation process are given by

$$\frac{\partial h}{\partial t} = L_f (S_{DEP} + S_{RIM} + S_{NUC} - S_{MELT}) \tag{3-5}$$

$$\frac{\partial q_{vc}}{\partial t} = -S_{DEP} - S_{RIM} - S_{NUC} - S_{AUT} - S_{ACC} + S_{EVAP} \tag{3-6}$$

A case study of a frontal system showing the relative importance of the individual conversion processes is discussed in Müller and Wacker (1988). It is demonstrated that in deep clouds most precipitation is generated via the ice phase by an effective seeder-feeder mechanism.

It is important to note that both the grid-scale and the convective precipitation parameterization schemes use grid point values of time level n-1 to evaluate tendencies to be applied at time level n to the prognostic equations in order to predict time level n+1. Therefore both routines called at time step n work in parallel. Thus if one scheme removes moisture from the atmosphere, the other scheme does not take it into account at the same time step. This is in contrast to, e.g., Sundqvist et al. (1989) who in their model make a strict separation between grid points subject to convection (which is of the Kuo type) and saturated stably stratified grid columns.

3.2.3 Model configurations

The original mesh widths of EUM and EM have been reduced by a factor of two and four in order to test the implications on high-resolution precipitation simulations. For the reduced grid spacings smaller integration areas had to be chosen. A summary of the model configurations used in experimentation is given in Table 3-3. Corresponding integration domains are presented in Fig. 3-2. Closer examination of model simulation results will be focused on an area covering the Alps and the surrounding region (Fig. 3-3). The representation of the orography reflects the HM8 grid structure. The domain is approximately

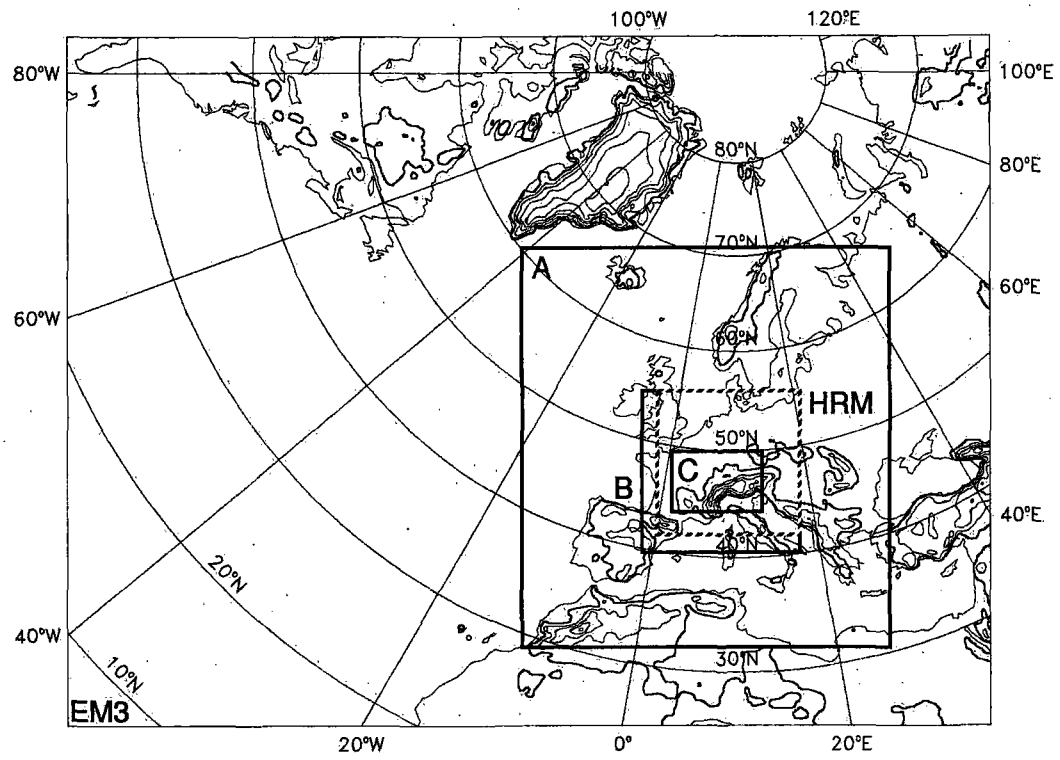

Fig. 3-2: Model domains used in EUM and EM/HM configurations displayed on a stereographic map with an indication of main orographic features (isoline spacing 500m).

558km x 428km in horizontal dimensions and corresponds to the Swiss radar composite image.

Table 3-3. Model configurations

acronym	mesh width	grid points	domain index	time step
EUM	63.5km	73x69	A	75s
EU1	63.5km	31x31	B	75s
EU2	31.75km	61x61	B	37.5s
EU4	15.875km	55x47	C	18.75s
EM3	0.5°	181x129	EM3	300s
HM4	0.25°	55x51	HRM	150s
HM8	0.125°	109x101	HRM	75s

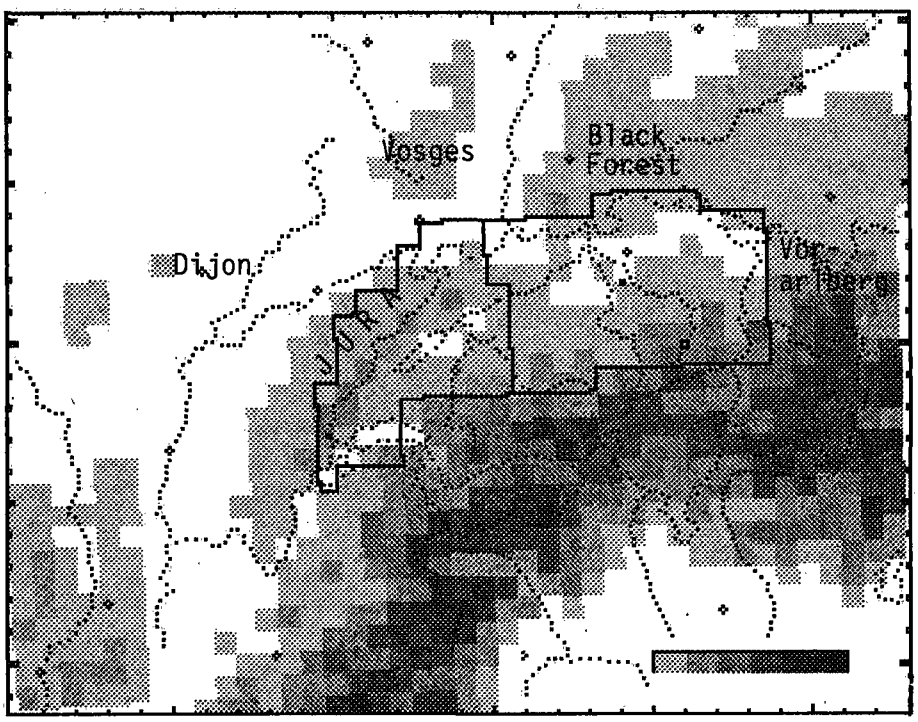

Fig. 3-3: Hypsometric representation of the HM8 model orography with the Swiss borders, major waters (both dotted) and some geographical features indicated. Grey scaling represents steps of 500m. Also outlined are the domains used for verification of precipitation.

a.) Initial and boundary conditions for EUM

EUM did not have its own analysis system. Initial and boundary values are interpolated from ECMWF T106-analysis fields. The interpolation method has been developed by Majewski (1985). It is designed to preserve as much as possible the balanced state of the large scale analyses initialized by normal modes despite the completely different grid structures and model orographies. This is achieved by using tension splines for horizontal and vertical interpolation, careful computation of the mass field by a two step adjustment of the surface pressure in the fine grid, vertical interpolation of temperature with conservation of the layer mean temperature and adjustment of the wind field in the boundary layer by solving the stationary Ekman equation using the same parameterizations of the turbulent fluxes as the limited area model. Boundary values are updated every 6 hours according to the ECMWF data assimilation cycle and assimilated by the limited area model by the boundary relaxation technique after Davies (1976). The interpolation technique was applied for all EUM configurations, in particular to the EU4-grid, which means a considerable jump in horizontal scale. EUM and its high-resolution versions are directly nested into the global T106 model. Due to this technique the initial fields of the LAM do not have real mesoscale features except those induced by the more detailed orography of the high-resolution model.

b.) Initial and boundary conditions for EM/HM

Initial and boundary values for EM are prepared exactly the same way as for EUM, since EM was run at ECMWF's computing centre. (The operational suite at DWD in Of-

fenbach FRG has its proper data assimilation cycle, cf. Majewski (1991). In the operational mode boundaries are updated every 3 hours by forecast fields of the global model.) In our experiments EM was guided by 6-hourly ECMWF analyses transformed to the EM3 grid. In contrast, initial and boundary values of HM are transformed EM3 forecast fields. HM boundaries are updated every hour. The only information about atmospheric moisture provided by ECMWF analyses are relative humidity fields. Therefore EUM and EM can not have clouds in the initial conditions. The hydrological cycle has first to be spun up. Cloud water fields of EM3 can then be interpolated to the HM configurations and thereby used in the initial and boundary conditions of HM simulations. The transformation programme of Majewski (1985) has been extended by Schubiger and de Morsier (1992) to accomplish this task. The high-resolution configurations of EM are therefore nested into EM3, which is nested within the global T106 model.

3.2.4 Weather situations

EUM and EM experiment series have been conducted for four main weather situations which will be briefly described in the following.

a.) 15 May 1988 (MAY88): purely convective

Synoptic surface pressure and 500hPa geopotential height gradients as well as temperature gradients were weak over Central Europe on this day. A weak mesoscale low pressure system over the Adriatic was linked to weak easterly winds in the lower troposphere north of the Alps. At higher altitudes winds were from south to south-westerly directions. The airflow was in general weak. A rather humid and unstably stratified airmass straddled the Alps. Convection was triggered by radiative forcing in the diurnal cycle. In the sequel the weak easterly winds were strongly disturbed by the developing convection. Flow in the lower levels was gradually directed towards the Alps. Radar observations show that convection was initiated over orography (Jura, Vosges, Alps). During the afternoon convection spread out over the whole northern part of Switzerland and thereby slowly drifted eastwards.

b.) 26/27 August 1989 (AUG89): summertime cold front

On 27 August 1989 a low-level low pressure system was located over northern Germany. During the next 24 hours it moved slightly to the east and deepened significantly. The associated stormy winds caused heavy damage at the coast of the Baltic Sea in Germany ("Kieler Sturm"). Low-level winds were weak in the afternoon of 26 August 1989 in the Alpine region. Showers began to develop in the unstably stratified air. The frontal system approaching from the north attached to the low pressure system created favourable conditions for enhanced shower activity during the night. The cold front then crossed northern Switzerland around 9UTC on 27 August 1989. To the rear of the front the north-westerly to northerly winds were partly blocked by the Alps. In the unstable low-level air intense shower activity developed. Comparably few thunderstorms occurred since there was a stably stratified layer at a height of about 4km during the whole period.

c.) 26/27 June 1991 (JUN91): summertime cold front

A well defined cold front with pre-frontal cloudiness in the warm sector reached from the North Sea over south-east England and Brittany to the north-western edge of the Iberian Peninsula on 26 June 1991 00UTC. At that time the Alpine region was cloudless. The front moved rather quickly into the continent towards Central Europe. Pre-frontal thunderstorms were triggered during the morning at the western edge of the Alps prior to the arrival of the front around noon. The principal rain band crossed Switzerland from west to east between 10UTC and 17UTC. There was no shower activity behind the front. Atmospheric vertical stratification was unstable up to about 3km and very stable between 3km and 7km. New thunderstorms formed in the Alpine region in the second half of the night in the moist warm air advected from southern France ahead of a second low pressure system over the English Channel. The air mass was then squeezed between the Alpine chain and the approaching front from the west triggering new convective activity along the north-western edge of the Alps around 27 June 1991 06UTC.

d.) 6/7 July 1991 (JUL91): purely convective

The synoptic situation on these two days was characterized by an Ω-type pattern over Central Europe with the western low pressure centre over the western exit of the English Channel and the high pressure centre located over southern Scandinavia. Southerly winds were observed over France and weak easterly winds over the region north of the Alps. Thus strong horizontal shear occurred at the western edge of the Alps. Payerne soundings also showed strong vertical shear between 2km and 3km from easterly to southerly directions. In this shear zone heavy convection developed over the Alps in western Switzerland and France in the afternoon of 6 and 7 July 1991. Huge convective complexes were built which moved slowly northwards and dissipated in the Alsace region. In the evening of 7 July convection also reached the eastern part of Switzerland thus extending much further to the east than on the previous day. Weather forecasting was difficult this weekend but very important to the public since great festivals took place in Switzerland. On Saturday 6 July 1991 heavy damages were caused in the western part of Switzerland by hail storms and wind velocities of $30\,m\,s^{-1}$ were observed during hours.

3.2.5 Set-up of experiments

Table 3-4 gives a summary of the experiments carried out for the 4 weather situations, the 7 model configurations and the 3 different deep-convection reference profiles (plus the KUO and the NO version). Individual experiments will henceforth be referred to by indication of these three entries. An experiment *series* includes all model configurations for a given weather event and a given convective adjustment scheme. Only the MAY88 case has been simulated with EUM and EM. The HM runs of MAY88 and JUL91 all used the EM3/EH runs for initial and boundary conditions. Thus the reference profiles for EM3- and HM runs can be different. For the JUN91 case HM runs were started from 12h-forecasts of the respective EM3 runs. For all other experiments initial times for EUM/EM and the high-resolution models were identical. Adjustment time scales used for the different high-resolution experiments can be seen from Table 3-5.

Table 3-4. Set-up of experiments

weather situation (cf. 3.2.4)	model configuration (cf. 3.2.3)	cumulus parameterization (cf. 2.5 and 3.2.2)	initial conditions (cf. 3.2.3)	forecast range
MAY88	EU1, EU2, EU4	VA	T106	15.5.88 00UTC +24h
MAY88	EUM, EU2	KUO	T106	15.5.88 00UTC +24h
MAY88	EUM, EU4	NO	T106	15.5.88 00UTC +24h
MAY88	EM3	EH	T106	15.5.88 00UTC +24h
MAY88	HM4, HM8	EH	MAY88/EM3/EH	15.5.88 00UTC +24h
MAY88	EM3	VA	T106	15.5.88 00UTC +24h
MAY88	HM4, HM8	VA	MAY88/EM3/*EH*	15.5.88 00UTC +24h
AUG89	EUM, EU4	VA	T106	26.8.89 12UTC +36h
JUN91	EM3	EH	T106	25.6.91 12UTC +48h
JUN91	HM4, HM8	EH	JUN91/EM3/EH	26.6.91 00UTC +36h
JUN91	EM3	MX	T106	25.6.91 12UTC +48h
JUN91	HM4, HM8	MX	JUN91/EM3/MX	26.6.91 00UTC +36h
JUL91	EM3	EH	T106	6.7.91 12UTC +36h
JUL91	HM4, HM8	EH	JUL91/EM3/EH	6.7.91 12UTC +36h
JUL91	EM3	MX	T106	6.7.91 12UTC +36h
JUL91	HM4, HM8	MX	JUL91/EM3/*EH*	6.7.91 12UTC +36h

VA/MX/EH: *convective adjustment scheme with different deep-convection reference profiles, cf. section* 2.5.

KUO: *Entraining parcel with moisture convergence closure*; NO: *no cumulus parameterization.*

3.3 Domain average precipitation

A first interesting general result from inspection of the simulations is the increase of accumulated domain average total precipitation with increasing horizontal resolution. This tendency is independent of the specific choice of the reference profiles for the adjustment scheme and the value chosen for the adjustment time scale (Fig. 3-4). The complete set of experiments yields domain average total precipitation amounts between $0.6 kg m^{-2}$ and $10.0 kg m^{-2}$ for the low resolution runs and between $1.8 kg m^{-2}$ and $14.5 kg m^{-2}$ for the high-resolution runs (EU4, HM8). Increasing precipitation with decreasing mesh width is a common feature, although these simulations represent different weather events with different forecast ranges, use different reference profiles, adjustment times and are even carried out by two models with rather different basic structures. Most of the EM experiments exhibit

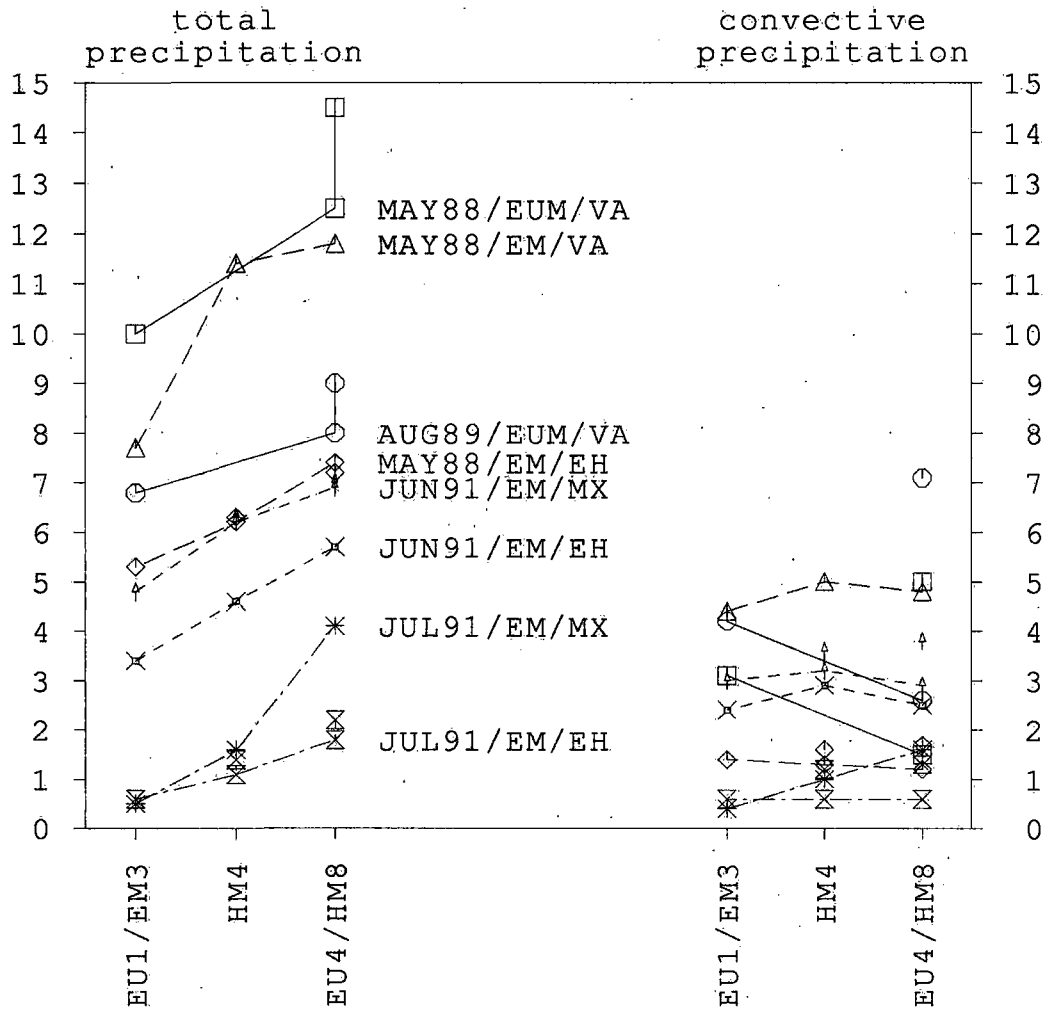

Fig. 3-4: Total (left) and convective (right) domain average accumulated precipitation amounts in $kg\,m^{-2}$. Each experiment series has its own symbol. Disconnected symbols give values of runs with adapted convective adjustment time scale τ. For the notation of experiments see Table 3-5. The horizontal axis separates the three different horizontal resolutions of each model.

a nearly linear increase of total area average precipitation with increasing resolution. In contrast the experiments MAY88/EM/VA show a marked increase when reducing the grid spacing from 0.5° to 0.25° and only a slight additional increase for the 0.125° run. For the JUL91/EM/MX series of experiments a major jump in simulated precipitation amount is found for the HM4 to HM8 step. Also indicated in Fig. 3-4 are the precipitation amounts resulting from the runs with changed adjustment time scale τ. Reducing τ from three hours to half an hour strongly increases the resulting precipitation amounts in the EUM experiments. Only slight changes are observed for the EM experiments, where the basic value for τ is one hour.

In contrast to domain average total precipitation the convective part of it does not increase with decreasing mesh width. From Fig. 3-4 it is recognized that convective precipitation amounts are more or less independent of the grid length. Consequently the percentage of convective precipitation decreases with increasing horizontal resolution. Re-

Table 3-5. Domain average accumulated total precipitation amounts in kgm^{-2}. (percentages of convective precipitation are given in parentheses)

EUM experiment	EUM/EU1	EU2		EU4	
adjustment time scale	τ=3.0h	τ=3.0h		τ=3.0h	τ=0.5h
MAY88/.../VA	10.0 (31)	-	-	12.5 (12)	14.5 (34)
AUG89/.../VA	6.8 (62)	-	-	8.0 (33)	9.0 (79)
MAY88/.../VA	2.0 (40)	3.3 (21)	-	7.4 (12)	-
MAY88/.../KUO	2.1 (57)	3.5 (54)	-	-	-
MAY88/.../NO	1.7 (-)	3.1 (-)	-	7.0 (-)	-

EM experiment	EM3	HM4		HM8	
adjustment time scale	τ=1.0h	τ=1.0h	τ=0.75h	τ=1.0h	τ=0.5h
MAY88/.../VA	7.7 (57)	-	11.4 (42)	-	11.8 (41)
MAY88/.../EH	5.3 (26)	6.2 (21)	6.3 (25)	7.4 (16)	7.2 (24)
JUN91/.../MX	4.8 (63)	6.2 (52)	6.3 (57)	6.9 (42)	7.0 (54)
JUN91/.../EH	3.4 (71)	4.6 (63)	-	5.7 (44)	-
JUL91/.../MX	0.5 (70)	-	1.6 (62)	-	4.1 (39)
JUL91/.../EH	0.6 (100)	1.1 (55)	1.4 (86)	1.8 (33)	2.2 (59)

duction of the adjustment time scale in the convective parameterization scheme enhances convective precipitation, particularly pronounced for EUM. The partitioning between grid-scale and convective precipitation depends strongly on the weather situation considered and on the reference profile used (cf. Table 3-5). The two weather situations of more frontal character (AUG89 and JUN91) tend to produce a larger part of convective precipitation than those with weak synoptic forcing (MAY88). Surprisingly little convective precipitation is simulated by the MAY88/EM/EH experiments.

A rationale for the systematic increase of grid-scale precipitation with decreasing mesh width (see also item c.) in this section) is given in subsection 3.6.1.

a.) Adjustment time scale τ

The adjustment time scale τ determines the lag of the convective response to the larger-scale forcing. The model atmosphere approaches the specified thermodynamic reference state with small τ, whereas with larger τ it moves towards the larger-scale forcing. Following the arguments of Betts (1986) a relationship for τ can be established, which reads as follows:

$$\bar{\mathcal{P}} \approx \mathcal{P}^{\mathrm{Ref}} - \bar{\omega}\tau \qquad (3\text{-}7)$$

where $\overline{\mathcal{P}}$ and $\overline{\omega}$ denote the saturation-level pressure departure and vertical motion of the environment respectively. $\mathcal{P}^{Ref}$ is the corresponding value of the quasi-equilibrium reference state. Since the role of convective parameterization in a numerical model is to produce precipitation before grid-scale saturation is reached in order to simulate real atmospheric behaviour on one hand and to prevent grid-scale instability due to conditional instability of the saturated model atmosphere on the other hand, constraints for τ or $\overline{\omega}$ can be derived from equation (3-7). If the convective parameterization scheme is to prevent grid-scale saturation, i.e. $\overline{\mathcal{P}} = 0$, we find the relation (Betts, 1986)

$$\tau < \mathcal{P}^{Ref} / \overline{\omega}_{max} \tag{3-8}$$

where $\overline{\omega}_{max}$ is the maximum vertical velocity of the large-scale forcing. Betts (1986) postulated τ to be 2h and 1h for the ECMWF models T63 and T106 respectively, therefore implying values of $\overline{\omega}_{max}$ for a major tropical disturbance of -20hPa/h and -40hPa/h depending on model resolution.

Given 3h, 1h and 0.5h for τ in the EUM and EM experiments and assuming a vertically averaged value of $\mathcal{P}^{Ref}$ for mid-latitude continental conditions after Binder (1990) of about -30hPa expression (3-8) yields maximum vertical velocities $\overline{\omega}_{max}$ of -10, -30 and -60hPa/h respectively. The above considerations suggest that the adjustment time scale τ should be reduced when going to a finer grid, since local forcing is better resolved and $\overline{\omega}_{max}$ will therefore increase with decreasing grid length.

These estimates indicate that the choice of 3h for the relaxation time in the EUM experiments is too large and therefore the convection scheme works very inefficiently, especially in the high-resolution experiments. The values of 1h for EM3 and of 0.5h for HM8 appear to be much more appropriate. Shortening the adjustment time by a factor 6 in the EU4 experiments causes a massive increase of convective precipitation (Fig. 3-4). It is interesting to note, that EU4 experiments with smaller τ values do not only produce more convective precipitation, but also total precipitation is enhanced. This is not the case for HM4 and HM8 experiments, where total precipitation amounts are more or less independent of the adjustment time scale (Fig. 3-4). In the latter case the choice of τ primarily influences the partitioning between grid-scale and convective precipitation.

It has also been recognized that a proper choice of the adjustment time scale reduces the occurrence of grid point storms. Again this fact is most pronounced for the two values used in EU4 experiments but has also been confirmed by HM8 experiments. In case of a shorter adjustment time, conditional instability and moisture, both being significant factors for the development of grid-scale vertical circulations, are more efficiently removed from the model atmosphere by the cumulus parameterization scheme.

b.) Deep-convection reference profiles

Three different thermodynamic reference profiles have been used for the representation of the convectively adjusted atmosphere, called VA, MX and EH. For a discussion of the construction and some basic properties of these profiles refer to section 2.5. Model runs using different reference profiles have only been carried out with EM. The EH scheme is presently used in the operational version of EM3 (until summer 1992).

Fig. 3-4 shows that the experiments conducted with the EH profile always produced the smallest amounts of total as well as convective precipitation. The only exception is the JUL91/EM3/EH simulation, which produced slightly more precipitation than the analogous MX experiment. This fact is independent of the choice of the adjustment time scale.

The increase of convective and total precipitation is particularly pronounced for the VA profile. Convective precipitation amounted to only about 20% in the MAY88/EM/EH experiments. Its portion increased to over 40% in the corresponding VA runs, whilst total precipitation increased by about 50%. In absolute terms convective precipitation was approximately tripled by the change of the reference profile.

Simple vertical averaging of total enthalpy and total specific water content, essentially the construction of the VA profile, causes abundant supersaturation in the upper part of the convection domain and strong drying in the lower part. Supersaturation is removed as convective precipitation, which is partly re-evaporated in the lower atmosphere and therefore reduces drying to a certain limited extent. This concept of VA tends to produce intense convective precipitation, especially if the initial atmosphere is humid. Drying the lower part of the convection domain, where the moisture storage capacity is largest, by vertical mixing and precipitating cloud water from the upper part is an efficient way of removing moisture from the atmosphere.

In contrast, the EH scheme tends to saturate the lower part of the atmosphere by approaching a moist adiabatic structure, thus storing a lot of moisture. Relaxation towards a unsaturated structure in the upper part of the convection domain provides less humidity for precipitation.

For HM4 and HM8 experiments the increase of total precipitation amounts of VA runs versus EH runs is larger than the difference which can be attributed to the intensified convective precipitation. This is an indication of a probable interaction between convection and grid-scale precipitation-forming processes. Heating of the lower levels by the VA scheme possibly contributes to the development of vertical grid-scale circulations, which then remove moisture from the atmosphere by enhanced vertical moisture transports, condensation and precipitation. In fact, this is a feature convective parameterization schemes should not support.

The MX profile preserves the "onion" shape of the reference sounding, but heating and drying at lower levels is significantly reduced compared to VA. Essential is the fact, that the lower part of the atmosphere is unsaturated, whereas the upper part is relaxed towards a moist adiabatic structure. Therefore it also produces precipitation more efficiently than the EH scheme, as is reflected by the experimental results.

Apart from the reference profile, other details of the cumulus parameterization scheme can also have a significant impact on precipitation amounts. For the MAY88/EU4/VA set-up experiments addressing the sensitivity of the VA scheme to the constraint implied on the lower boundary of the convection domain and to the entrainment rate have been carried out. Originally the lowest model level allowed to form the bottom of the convection domain is level 15 (of 18). Allowing vertical mixing to include lower levels clearly increases the absolute amount of moisture involved in convective overturning. In case of a humid boundary layer supersaturation of the upper part of the atmosphere increases and therefore convective precipitation is enhanced in the context of the VA scheme.

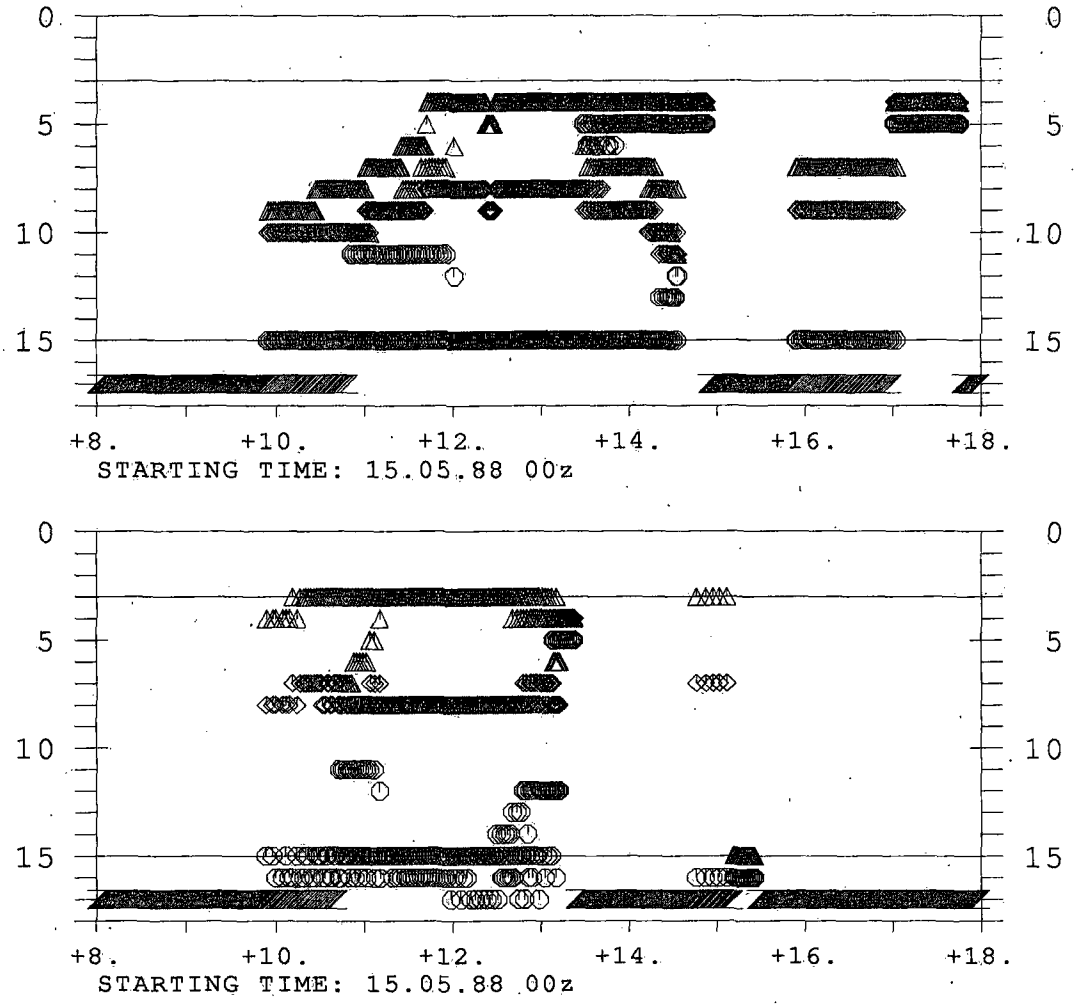

Fig. 3-5: Time variation of the convection domain at a single grid point for the original (upper panel) VA convective adjustment scheme and VA without entrainment and the constraints on the vertical extent of the convection domain released (lower panel). Horizontal and vertical axes give forecast time in hours and model level respectively (level 3 and 15 are the original upper and lower boundaries of the convection domain). Indicated are the lower (circles) and upper (triangles) boundaries of the convection domain and the base of the saturated subdomain (squares). Static stability of the vertical column is indicted at level 17.

Entrainment effects are introduced into the lapse-rate considerations used to determine the top of the convection domain. Exclusion of entrainment therefore leads to deeper layers subject to convective overturning. Due to the reduced moisture storage capacity of the upper atmosphere again supersaturation and in turn convective precipitation is enhanced. The temporal development of the convection domain at a given grid point of the control experiment and an experiment without entrainment and released constraint on the bottom of the convection domain is displayed in Fig. 3-5. In both experiments convection starts just before +10h of integration time. The control experiment needs approximately two hours to reach the maximum vertical extent of the convection domain, whereas the sensitivity experiment only needs a dozen time steps. After +13h the grid column is stabilized and convective overturning ceases. A little "shower" follows around +15h. In contrast the control

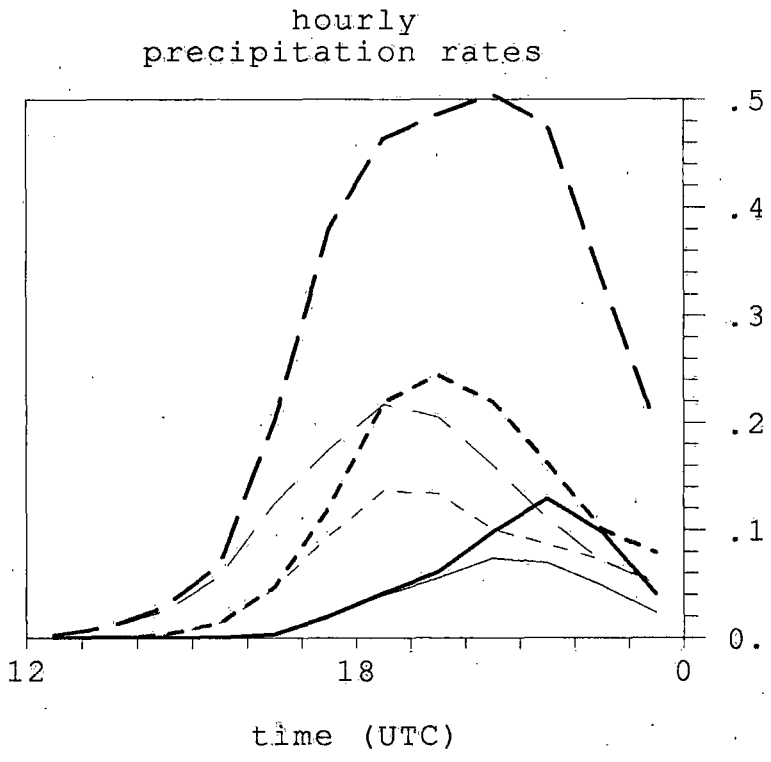

Fig. 3-6: Time series of precipitation type partitioning for EM3 (solid), HM4 (short dashed) and HM8 (long dashed), 6 July 1991 12UTC +24h...+36h. Total and convective (MX profile, adapted τ) precipitation is plotted by bold and thin lines and scaled in $kgm^{-2}h^{-1}$.

run removes convective instability only until +15h, with a second event of one hour duration between +16h and +17h. Thus the VA scheme works much more efficient without entrainment. It is worth noting that entrainment does not influence the onset of convection, but rather the duration of an event. During the major event convective cloud base is found at level 8 in both experiments. But since the no-entrainment experiment mixes atmospheric layers from lower levels to a higher cloud top than the control experiment, more convective precipitation is produced. Domain average accumulated convective precipitation is more than doubled without entrainment. It can also happen that entrainment suppresses convection at certain grid points.

c.) Time variation of precipitation type partitioning

Essential and typical features of the time variation of precipitation type partitioning are illustrated by the JUL91/EM/MX experiment series using adapted adjustment time scales (Fig. 3-6). This particular case can be considered representative of other mesh width experiments since it distinctly shows features which were found in general. The present example has been selected for demonstration because the simulations describe the development of a single huge convective complex in the western part of the domain. Therefore domain averages are not affected by systems at different stages of development scattered over the domain.

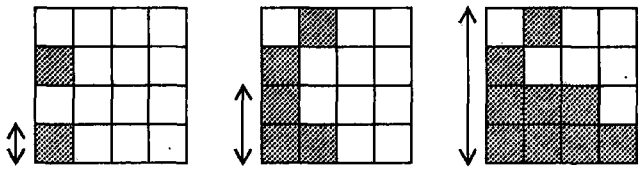

Fig. 3-7: A subgrid-scale property occupying grid elements of different sizes at different stages (see text for explanation).

Plotted are time series of domain average hourly total and convective precipitation rates at three different horizontal resolutions. Properties already discussed for accumulated precipitation become apparent: precipitation is enhanced with decreasing mesh width and in parallel convective precipitation gets less important. The onset of precipitation depends on horizontal resolution: the finer the mesh, the earlier convection is triggered. In the present case the time lag is about 2 hours for every step reduction. The first phase of precipitation development is of purely convective origin. After a few hours grid-scale precipitation is also produced. Coarser grids delay the onset of grid-scale precipitation. Grid-scale precipitation intensifies more rapidly but reaches its maximum later than convective precipitation. The peak rate of convective precipitation accounts for only 75%, 63% and 46% of the total precipitation rate at the same time for EM3, HM4 and HM8 respectively, thus reflecting the decreasing portion of convective precipitation mentioned earlier for precipitation sums. Peak rates of total precipitation are always reached later than the convective peak rate. The described evolution of precipitation type partitioning is consistent with the way convective and stratiform precipitation develops in real mesoscale convective systems (e.g. Houze and Hobbs, 1982).

The earlier onset of precipitation in fine mesh models can be explained by generalizing an argument introduced by Kristjánsson (1991) in the context of cloud cover estimation. Let us assume that a certain critical condition has to be matched on the grid-scale in order to trigger a given process. For example low-level instability is needed for convection to take off or grid-scale saturation is necessary for grid-scale precipitation formation. Fig. 3-7 illustrates the development of the critical property in an element of the coarsest grid, subdivided into grid elements with dimensions of one half and one quarter of the original mesh, at three different stages. Elements of the finest grid where the critical condition is met are shaded. At the first stage, if we discuss convection as an example, convective overturning will start at two grid points of the finest grid. Continued radiative forcing destabilizes further grid elements, so that in stage II five high-resolution elements are conditionally unstable. The arrangement of these elements indicates, that the critical condition is now also met for one element of the next coarser grid (if more than 50% of the elements forming the next larger element match the condition, it is assumed, that the coarser element matches the condition as well). Finally at stage III even the largest element is subject to convection.

To put it concisely, it is easier to meet a critical, meteorologically relevant condition on a finer grid. This argument is particularly meaningful in geographical regions, where external forcing, such as orographic lifting, can be more adequately resolved on a finer grid. Hence the observed shift in onset of precipitation appears to be a logical consequence of resolution. It can also be interpreted as an indication of inadequate parameterization of the coarser grid model.

The transition from initially convectively to finally grid-scale dominated precipitation bears also some resemblance with the nature of real convective systems. Such a life cycle is outlined in Houze (1982,1989). With respect to the numerical models investigated here this issue will be discussed in item c.) of section 3.4.

Time traces of domain average precipitation in more advectively dominated weather situations (cold fronts in summer), i.e. AUG89 for EUM and JUN91 for EM, exhibit a comparably high and constant portion of convective precipitation (cf. Table 3-5). In such situations convection is continuously triggered at new grid points ahead and behind the progressing front. As a consequence convective systems at any stage are present in the domain at a given time. Therefore the life cycle of a single convective system is not reflected in the precipitation averages over a domain fixed in space.

It is interesting to note, that the evolution of precipitation type partitioning differs considerably, if a moisture convergence closure is used in the convective parameterization scheme instead of the quasi-equilibrium closure of the above adjustment scheme. In EUM simulations using the Kuo-type cumulus parameterization convective and grid-scale rainfall developed much in parallel. The portion of convective precipitation accounted to slightly more than 50% in general. Examination of horizontal patterns revealed that maxima of convective and grid-scale precipitation were significantly collocated (cf. also Fig. 3-12, page 79).

d.) A remark on atmospheric water content

Given the increase of precipitation with enhanced horizontal resolution the question may be raised whether the atmosphere of the fine-mesh model is substantially drier. Examination of EUM experiments (i.e. MAY88/EUM/VA and AUG89/EUM/VA) revealed that volume average specific cloud water content is usually below 1% of the total atmospheric moisture content. In the convectively dominated May case specific cloud water content reached a maximum of 0.4%. The maximum value for the more frontal August case was about 1%. The total precipitated water mass accounted for up to 27% (16%) of the cloud water mass in the May (August) case.

The efficiency of the cumulus parameterization scheme also has an important impact on the cloud water content of the model atmosphere. Model runs with the convective adjustment scheme switched off produced up to more than double the cloud water content found in runs with an adequately tuned convective adjustment scheme (i.e. 0.5h for the 16km model). This is a clear indication that parameterized convection removes water from the atmosphere which is otherwise stored as cloud water produced by the grid-scale vertical circulation. With respect to removal of water supersaturation the grid-scale precipitation-forming processes do not fully compensate for the missing or inefficient subgrid-scale convective parameterization.

Given the small percentages of cloud and rain water masses compared to total atmospheric water content, it is concluded that the cloud and precipitation-forming processes only marginally affect the overall atmospheric water budget and that therefore the atmosphere of fine-mesh models is not dramatically dried out. However, this does not reflect the important energetic and dynamical effects of cloud and precipitation processes!

3.4 Precipitation patterns in the horizontal

Consideration of bulk properties of precipitation simulation, as done in the previous section, certainly does not provide the basis for an evaluation of the skill of the various model configurations. Steps towards such an evaluation will be discussed in the present and the next section.

In this section emphasis will be put on the examination of horizontal structures of model simulated precipitation fields. The following aspects are considered: the dependency of horizontal precipitation patterns on horizontal resolution, the impact of different deep-convection reference profiles on these structures and finally the intercomparison and evolution of the formally separated convective and grid-scale precipitation patterns.

To assess the realism of the simulated precipitation fields they will be compared to observations of the Swiss weather radar network. Instantaneous model precipitation rate fields will be presented in the format of the Swiss radar composite image as so-called "pseudo-radar images". Although this might be the most convenient way of qualitatively comparing the observed and simulated precipitation fields a few remarks about the different nature of the two data types need to be borne in mind.

1.) Radar precipitation estimates are made for atmospheric boxes with horizontal dimensions of $2x2km^2$ and a height of 1km. Surface precipitation on a 2km grid is then associated with the maximum precipitation intensity found in each atmospheric column (maximum projection to ground view). Precipitation rates are represented by 7 logarithmically scaled intensity levels (cf. Table 3-6, page 80). Depending on orography and distance from the radar site radar detectability can be seriously affected. All processes like accretion or evaporation which modify the precipitation rate below the lowest visible radar height can not be accounted for. Thus radar precipitation rates can not be estimated from "homogeneous" conditions all over the area of the composite image. In particular precipitation detection by radar is difficult for the Alpine region and the region south of the Alps, since both Swiss radar stations are located in the northern part of the country. Precipitation south of the Alps can only be detected when convective storms reach echo tops above 6km.

2.) Instantaneous model precipitation rates give the rate of precipitation reaching the earth surface produced within one model time step. Precipitation falling to ground is the final product of all convective and/or grid-scale precipitation-forming processes in the whole vertical column. In particular low-level evaporation can reduce the quantity of condensate built up and collected at upper levels. In contrast to radar data, model simulated precipitation rates are "homogeneous" over the whole model grid. For the following investigations model precipitation rates have been discretized by the radar intensity classes.

3.) In order to alleviate intercomparison original radar data is averaged over model grid cells. This is done by arithmetically averaging precipitation rates of all radar pixels with their respective centres within a given model grid element. Whilst maxima of model precipitation are centred on grid points a priori, precipitation maxima observed by radar can be distributed over several model grid points, depending on their original position with respect to the model grid. Therefore adapted radar information can conceivably, and probably, exhibit smoother patterns.

a.) Mesh width

The impact of enhanced horizontal resolution on simulated precipitation fields is illustrated by two EUM simulations of the May 1988 case (MAY88/EUM/VA). Fig. 3-8a shows the precipitation field of the 64km run at 15 May 1988 12UTC after 12 hours of integration time. The squares reflect the structure of the model grid. Nearly uniform rainfall activity is found over the whole Swiss area. The precipitation patterns of the 16km run (Fig. 3-8b) are much more structured and independent convective systems can be distinguished. There is for instance a precipitation free area over the Swiss Plateau. The radar observations adapted to the 16km grid (Fig. 3-8d) show a remarkable coincidence with the simulated precipitation field. Looking at the 16km orography (Fig. 3-8f) we recognize that on this day convection was orographically initiated. The most striking example is probably convection over the chain of the Jura mountains, but orographic convection is also found over the Vosges mountains, the Black Forest area and Vorarlberg as well as in the pre-Alpine region (cf. Fig. 3-3 for an identification of the locations). All these clusters have their analogue in the 16km simulation. The convective complex near Dijon (north-western part of the radar image) does not show up in the model simulation. The model probably missed this event due to lack of mesoscale information in the analysed moisture field. Since the 64km orography (Fig. 3-8e) has much less structure than its 16km counterpart, orographic forcing for convection is very different. There is no orographic forcing for convection over the Jura mountains, since they do not exist in the 64km grid.

This promising example gives an impression of the potential of a meso-β-scale numerical prediction model to provide useful information of precipitation field structure not available from a model with conventional horizontal resolution (~60km).

b.) Deep-convection reference profiles

The next case study addresses the sensitivity of precipitation simulation on the specific deep-convection reference profile used in the convective adjustment scheme.

In the early afternoon of 7 July 1991 convective activity started over the Alps in the western part of Switzerland. A little later convective precipitation was observed by radar over the Jura and the French Alps (Fig. 3-9a). These convective complexes rapidly grew and merged forming a huge system which slowly drifted northwards (Fig. 3-9b). In the late afternoon further convective systems developed over the central part of Switzerland and in the region of Dijon. At 21UTC (Fig. 3-9c) the main complex was located north of Basle in the Vosges and Black Forest region, a second complex north of Dijon and a third one over north-eastern Switzerland. New convective cells also developed over the Alps in south-western Switzerland.

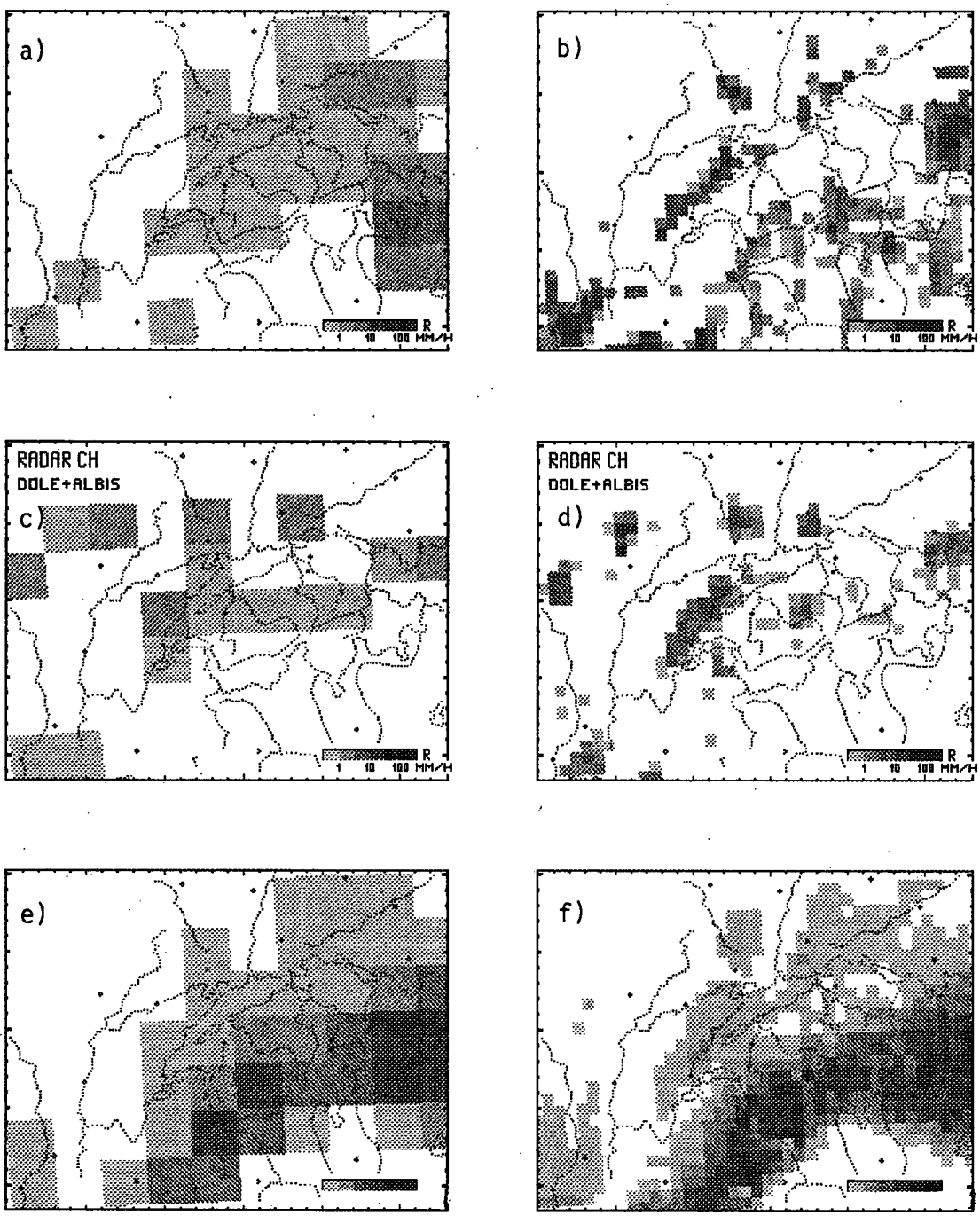

Fig. 3-8: EUM simulations and radar observations valid for 15 May 1988 12UTC. Presentation format corresponds to the Swiss radar composite image (horizontal dimensions 558km x 428km). Note that important shielding by the Alps sincerely constrains radar detectability in the south-east corner of the image.
EUM simulation time is 15 May 1988 00UTC +12h. The precipitation intensity scale is displayed in the lower right corner, see also Table 3-6.
a) instantaneous total precipitation rates of 64km EUM simulation
b) instantaneous total precipitation rates of 16km EUM simulation
c) radar observation adapted to the 64km model grid
d) radar observation adapted to the 16km model grid
e) 64km model orography (grey scaling indicates steps of 500m)
f) 16km model orography (grey scaling indicates steps of 500m)

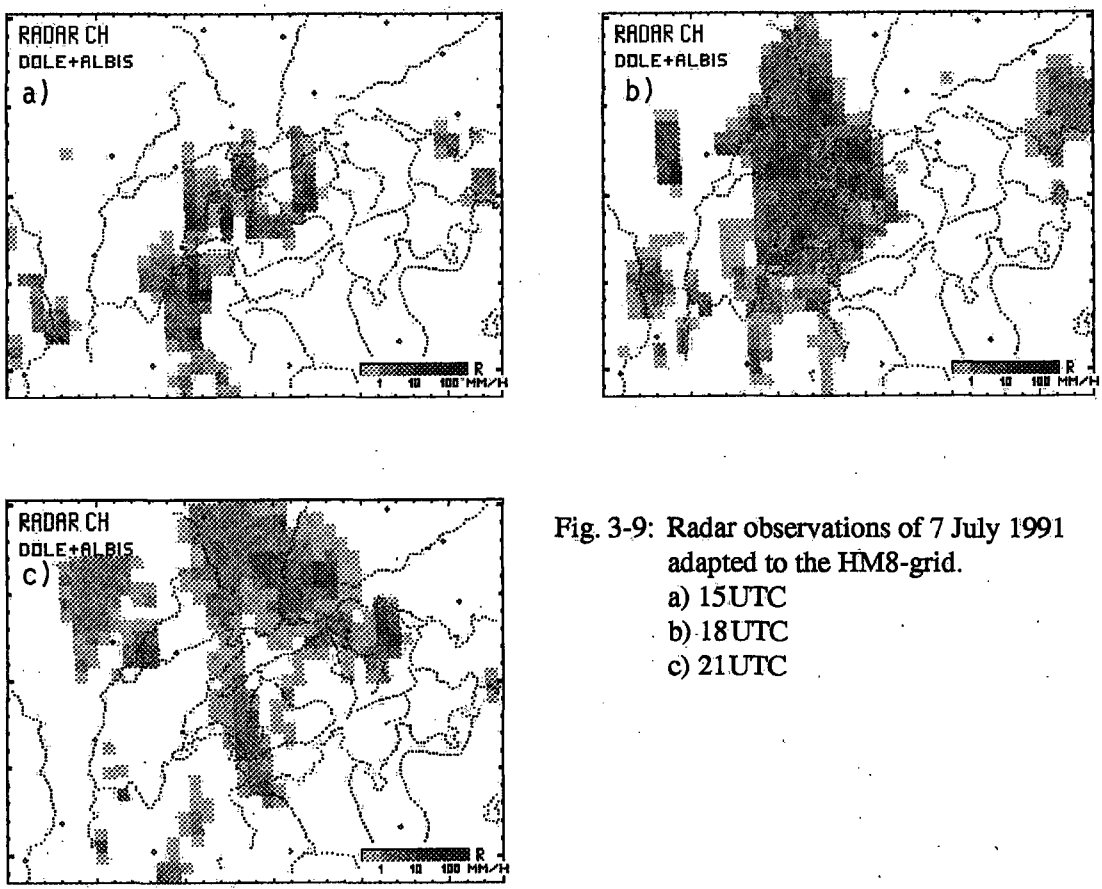

Fig. 3-9: Radar observations of 7 July 1991 adapted to the HM8-grid.
a) 15UTC
b) 18UTC
c) 21UTC

This weather situation was simulated by HM8 runs starting from 6 July 1991 12UTC with the EH and MX deep-convection reference profile respectively (Fig. 3-10).

The start of convective activity is obviously delayed in both experiments relative to observations (compare Fig. 3-10a/b with Fig. 3-9a). Neither of the simulations give an indication of the heavy convection going on in the western part of Switzerland. Within the next hours HM8/MX considerably developed convective activity (Fig. 3-10d). Despite the patchy pattern the overall shape of the precipitating area is suggestive of a structure similar to the observed huge complex, although position and lateral extent to the north are not correct. In contrast HM8/EH exhibits a very weak and scattered pattern at a position too far to the west of the real event. There is no indication of a contiguous precipitation system. On the other hand a new convective complex occurs in the Dijon area, which could conceivably correspond to an observed system, although slightly misplaced. In the HM8/MX simulation the Dijon region is unaffected by precipitation. Three hours later HM8/MX still shows the convective complex, but it has not moved northwards as in reality (Fig. 3-10f). There is still no precipitation in the Dijon region and in particular no rainfall is predicted in the north-eastern part of Switzerland. Maximum area average precipitation intensity in the HM8/MX run is attained at that time. With the exception of the Dijon complex precipitation activity in the HM8/EH run has almost ceased. This is in sharp contrast to observation.

In this primarily convectively dominated weather situation the HM8 runs proved to be extremely sensitive to the choice of the reference profile in the cumulus parameterization scheme. Two almost completely different developments evolved from the two forecast

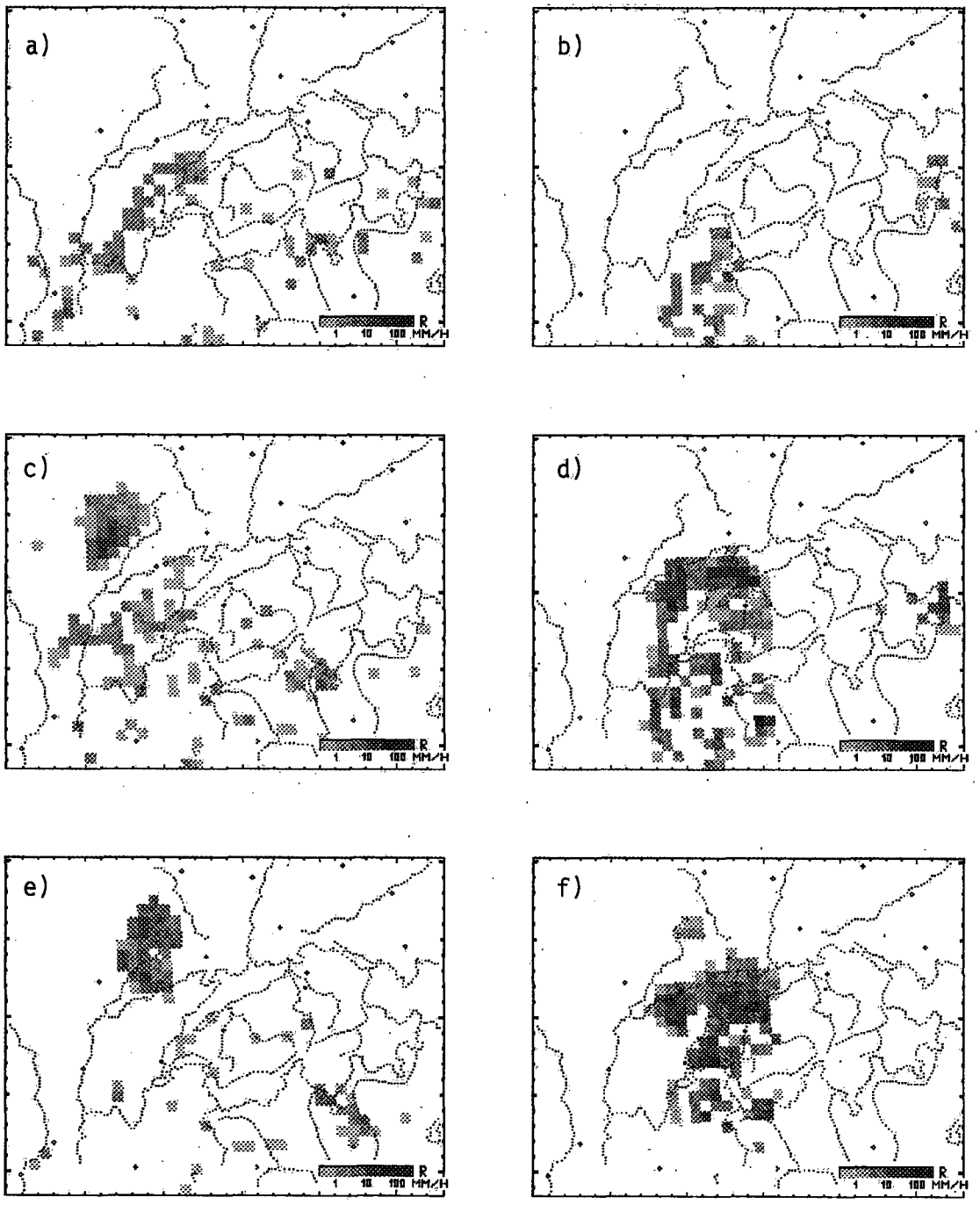

Fig. 3-10:HM8 experiments starting from 6 July 1991 12UTC. Instantaneous total precipitation rates are presented as pseudo-radar images (intensity scale in the lower right corner).

a) EH +27h (valid at 7 July 1991 15UTC) b) MX +27h (15UTC)
c) EH +30h (18UTC) d) MX +30h (18UTC)
e) EH +33h (21UTC) f) MX +33h (21UTC)

runs. HM8/MX produced intense convection whilst HM8/EH dramatically underestimated convective activity.

c.) Precipitation type partitioning

So far only *total* precipitation rates have been considered. Now the characteristics of convective and grid-scale precipitation patterns and their evolution in time will be investigated. Fig. 3-11 displays grid-scale and convective precipitation patterns at different forecast ranges of the JUL91/HM8/MX run discussed above. After +26 hours of integration time convective precipitation is initiated. At +27h precipitation is still of almost purely convective origin. The same is true one hour later. Convection is steadily expanding to further grid points. Only after +29h of simulation, i.e. three hours after the initiation of convection, there is a group of grid points producing rather intense grid-scale precipitation (Fig. 3-11c). Although precipitation intensity varies considerably from grid point to grid point, the convective precipitation pattern is more coherent than grid-scale precipitation, which appears to be tied to single grid points. This impression is also valid for +31h (Fig. 3-11d). It is remarkable that at this time area average grid-scale precipitation has become quantitatively more important than convective precipitation although occupying a smaller number of grid points (cf. Fig. 3-6). The lateral extent of the two precipitation types is similar after +33h. The grid-scale precipitation pattern has also become smoother. After +35h the precipitation system is in its decaying stage. Convection has almost ceased whilst grid-scale precipitation lasts a little longer with decreasing intensity.

This simulation exemplifies a few remarkable features which are characteristic of the other experiments carried out with EUM and EM as well.

1.) In accordance with real behaviour in nature a response to destabilization of the atmosphere is provided by initiation of convective processes, the model's convective parameterization scheme acting as a trigger mechanism. In contrast experiments without cumulus parameterization exhibited a distinct delay for the initiation of precipitation because there is some time needed to reach grid-scale saturation. In comparison with observations timing of the precipitation event was better in the experiment using cumulus parameterization.

2.) In general convective precipitation patterns are more coherent and more extended than their grid-scale counterparts. Grid-scale precipitation produces strong maxima on single grid points or on small groups of a few grid points with neighbouring grid points remaining unaffected. This feature disagrees with observations, where stratiform precipitation often appears wide-spread and convection is more localized.

3.) Given the above characteristics of horizontal patterns the life cycle of convective systems has also some differences from nature. Following the conceptual model of Houze (1982) deduced from and confirmed by observations (Houze, 1989) convective systems have an early stage dominated by the development of convective-scale vertical circulations such as updrafts resulting in a few isolated precipitating towers. In the mature stage a cloud shield has developed with the convective towers embedded. Stratiform precipitation falls from the cloud shield which usually covers a much wider area than the purely convective elements. This stage is characterized by two scales of circulation: the convective-scale up- and downdrafts and the mesoscale up- and downdrafts. In the weakening stage the convective-scale circulations have disappeared and only the stratiform cloud shield has survived which then is broken up and decays in the last stage.

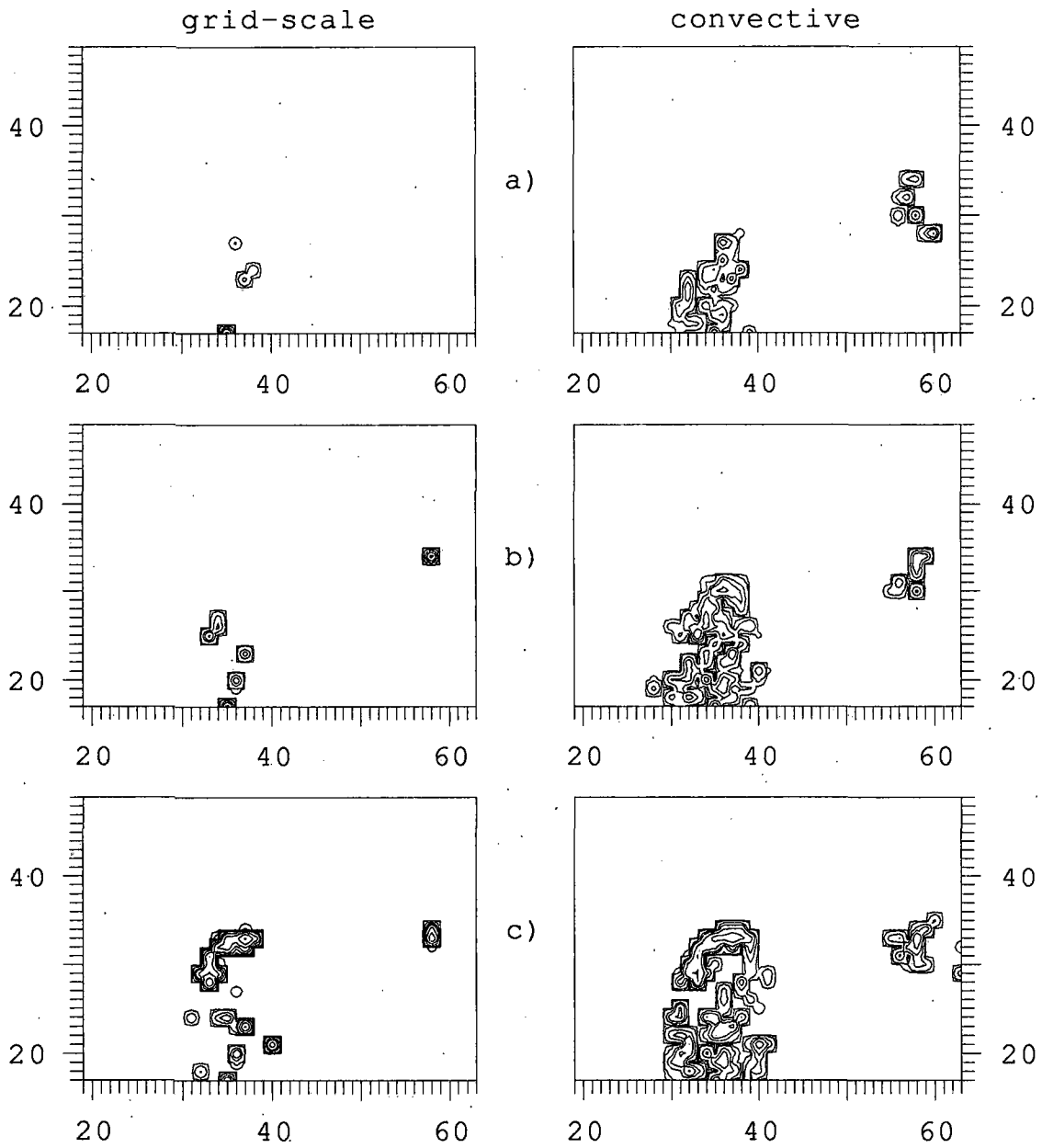

Fig. 3-11: Grid-scale (left) and convective (right) instantaneous precipitation rate patterns of JUL91/HM8/MX.
Domain corresponds to the Swiss radar composite frame approximately. Isolines for rain rates of 0.1, 0.3, 1.0, 1.8, 3.2, 5.6, 10.0, 17.8, 31.6, 56.2 and 100.0 $kgm^{-2}h^{-1}$.
a) 6 July 1991 12UTC +27h (verification time 7 July 1991 15UTC)
b) +28h (16UTC)
c) +29h (17UTC)

The simulation of 6/7 July 1991 does not show the proper development of the mesoscale component of the system which was in fact observed for the real system (cf. Fig. 3-9). On the contrary the grid-scale precipitation activity did not extend beyond the region of convective precipitation. At the end of the life of the simulated precipitation system convective and grid-scale precipitation areas are approximately con-

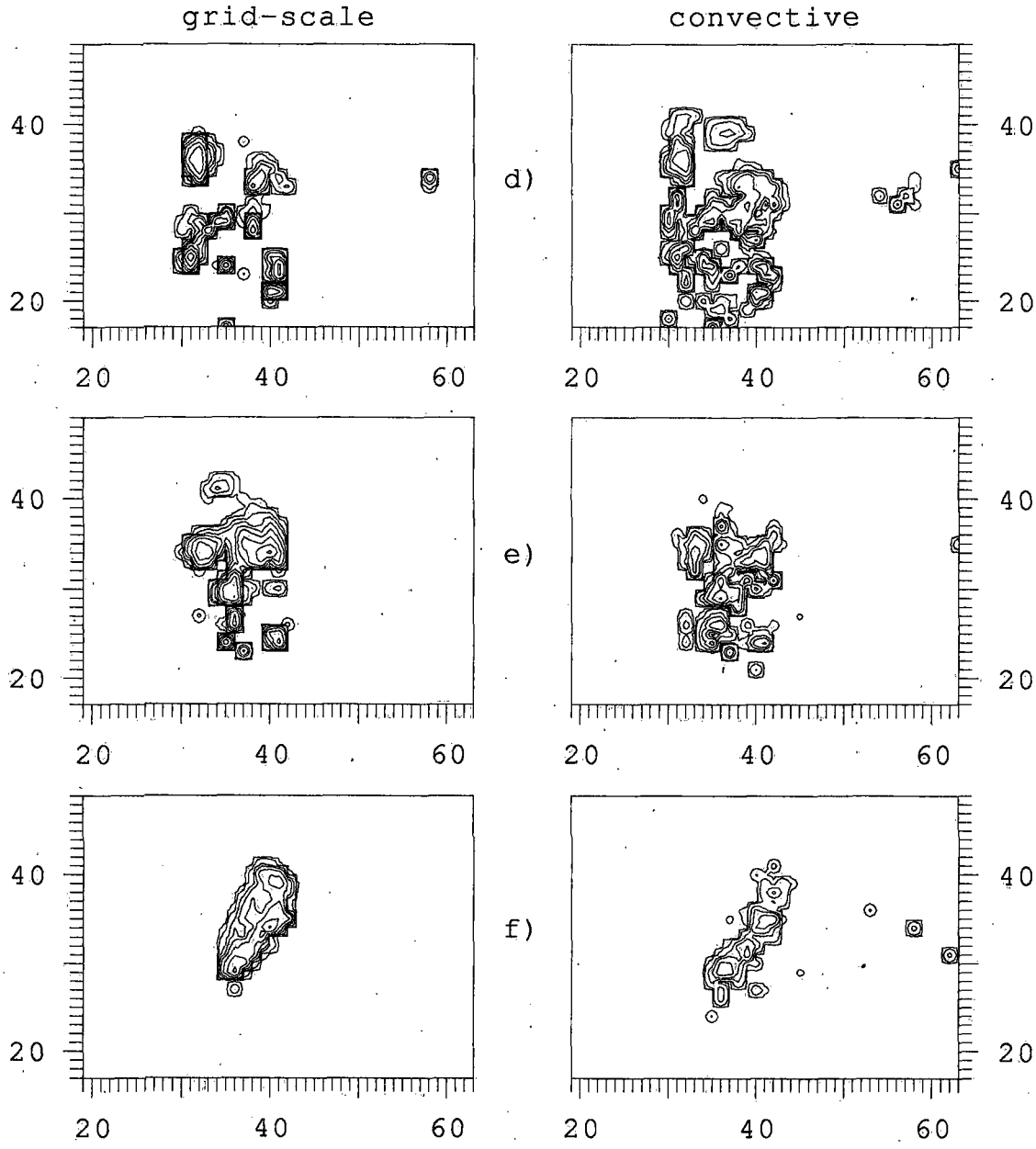

Fig. 3-11 continued.

d) +31 h (19UTC)
e) +33 h (21UTC)
f) +35 h (23UTC)

gruent. On the other hand the decreasing importance of convection with time is reasonable. One reason for this typical development of model simulations might be that grid-scale circulations at least partly participate in simulating convective overturning and we therefore observe the development of so-called grid point storms.

In summary, we found the following characteristic features of convective systems simulated by EUM and EM using a convective adjustment scheme for cumulus parameterization:

1.) Strong precipitation maxima are located next to precipitation-free grid points producing a rather patchy rainfall *rate* pattern.

2.) The ability to simulate realistic coherency, broadening and movement of the precipitation systems, i.e. to model a realistic *life cycle*, is underdeveloped.

3.) *Accumulated* precipitation amounts show convective precipitation covering a (much) larger area than grid-scale precipitation, the latter appearing intense and concentrated in space (grid point storms).

4.) In synoptically weakly forced situations grid point storms can stay over the same grid point or group of grid points for several hours accumulating unrealistic amounts of precipitation in these locations. This effect contributes to the distinguished patches in *accumulated* precipitation field patterns.

These facts are also evident from independent investigations. Only a few studies in the literature present the proper partitioning of grid-scale and convective precipitation for given model runs. Most of the investigations addressing the mesh width problem and/or the role and importance of the parameterization of convection for meso-β-scale models compare precipitation fields produced by experiments conducted with and without convective parameterization (Molinari and Dudek, 1986; Kalb, 1987; Bougeault and Geleyn, 1989). It is important to note that this point of view is not quite the same as separating convective and grid-scale contributions of total precipitation in a given experiment, since there are interactions between the two precipitation-forming schemes. Zhang et al. (1988) is the only study presenting the proper separation of resolvable-scale and convective precipitation (cf. their Figs. 2d/e for the control run, Figs. 13c/d for a so-called full physics simulation). Although they use a completely different model (PSU/NCAR version MM4) and in particular completely different schemes for the parameterization of convection (basically Fritsch and Chappell, 1980) and for resolvable-scale precipitation by solving prognostic equations for cloud and rain water variables, partitioned grid-scale and convective precipitation patterns for 12h accumulated rainfall look qualitatively the same as described above The same picture emerges from the convection/no convection comparisons of Molinari and Dudek (1986, Figs. 1a and 2), Zhang and Fritsch (1988a, Figs. 1g, 7c and 8c) and Bougeault and Geleyn (1989, Fig. 4).

In contrast, partitioned horizontal precipitation patterns in EUM simulations using the convective parameterization scheme with moisture convergence closure (KUO) developed much in parallel. As already mentioned this becomes obvious from time traces of domain average precipitation rates as well as from the horizontal structures themselves. Fig. 3-12 shows the 24h accumulated partitioned precipitation amounts for experiments using the moisture convergence closure and the convective adjustment scheme respectively (adjustment time scale was 3h, thus not adapted to the grid length of 32km). Note for instance the coinciding maxima at grid points (23,18), (29,18) and (33,22). The similarity of horizontal distribution is also found in the rainfall *rate* patterns at any time during the integration, although a little less pronounced than in the precipitation sums.

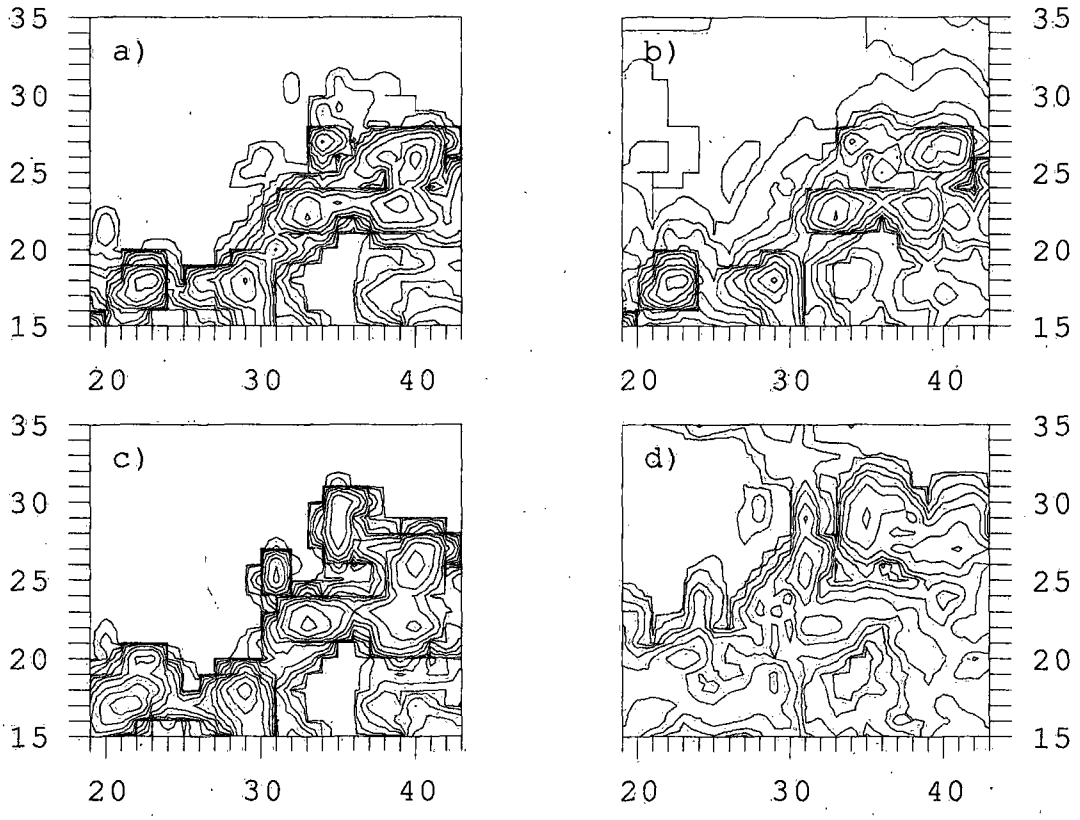

Fig. 3-12: Patterns of 24h accumulated grid-scale and convective precipitation for EUM simulations of 15 May 1988 00UTC +24h. Horizontal grid distance is about 32km. a) and c) show grid-scale precipitation patterns and b) and d) their convective counterparts. a) and b) represent the run using the moisture convergence closure (KUO), c) and d) using the usual adjustment scheme (VA, τ=3h). Isoline values as in Fig. 3-11.

3.5 Quantitative comparison of observed and simulated precipitation estimates

In Switzerland there are two completely independent and complementary real-time operational observing systems of precipitation. On one hand weather radar information from two radar instruments located near Zurich and Geneva is combined into an area covering composite image which is updated every ten minutes. On the other hand about 70 raingauge stations report surface rainfall (and a wealth of other parameters) at the same interval. These two sources of information are used to make quantitative estimates of area average precipitation for comparison with model forecasts.

3.5.1 Area averages from radar and raingauges

a.) Radar

Precipitation rate estimates of the Swiss weather radars are given in 7 levels of intensity which are logarithmically scaled with respect to rainfall rates (Table 3-6). The values available are related to the maximum reflectivity found along each vertical column and horizontal strip of the scanned volume which is divided into elementary boxes of 2x2x1 km^3. This maximum projection technique (Joss and Kappenberger, 1984) reduces the amount of

information to be stored and communicated by retaining ground, side and front views instead of the full volume information. It also carries an inherent tendency to overestimate quantitative precipitation amounts (neglect of bright band and low-level evaporation effects). Information of the two radars Albis (near Zurich) and La Dôle (near Geneva) is combined to the Swiss radar composite image, which makes use of the more reliable data of each radar and covers an area of 558x428km^2 (Galli, 1984).

Several distinct difficulties are related to estimation of precipitation rates from radar reflectivity measurements. In a mountainous country like Switzerland ground clutter, shielding and the height dependency of the vertical radar reflectivity profile are probably the most severe error sources. Spurious radar echoes caused by topography or anomalous wave propagation (clutter) lead to overestimation of precipitation. Clutter suppression, e.g. by use of clutter maps (Galli and Joss, 1983), introduces a tendency to underestimate precipitation, since real precipitation echoes are also eliminated to some extent in the affected locations. Precipitation behind a mountain range can not be seen by the radar, an effect known as shielding. Shielded regions suffer from a serious underestimation of rain amounts. Since radar reflectivity decreases with height at an average rate of about 34%/km in summer and 86%/km in winter (Joss and Pittini, 1991), the height above ground of the lowest level visible for the radar is of crucial importance for a quantitative estimate of the precipitation reaching the surface. Mountains can increase the height of the lowest free radar beam dramatically. Galli and Joss (1989) have shown that the ratio between radar and raingauge measured precipitation amounts decreases more or less in parallel with increasing visible height above ground in Switzerland. Since no corrections for the height dependency of the radar reflectivity profile have been introduced so far, neither in Switzerland nor elsewhere, radar information is not equivalent all over the radar composite area, but its quantitative properties depend on local detectability conditions. Overall underestimation of precipitation amounts results from the implicit assumption of a height-independent reflectivity profile.

Table 3-6. Coding of precipitation rates of the Swiss weather radar

	precipitation rate ($kgm^{-2}h^{-1}$)	
pixel count	class width	class mean
1	0.32 - 1.00	0.56
2	1.00 - 3.16	1.78
3	3.16 - 10.0	5.62
4	10.0 - 31.6	17.8
5	31.6 - 100.	56.2
6	> 100.	

Despite all these caveats an attempt is undertaken to calculate a rough quantitative estimate of area average precipitation. In order to avoid the most serious problems an area north of the Swiss Alps has been chosen for which detectability conditions for the two radar stations are fairly good. Within this verification area each pixel value from the ground view is converted to a corresponding precipitation rate representative of the respective intensity class (Table 3-6). Then an area average mean value of precipitation rate is calculated. Such a reconstruction of precipitation rates is correct on average if the density of the original precipitation rates is constant on a logarithmic scale. This condition is fairly reasonably fulfilled in general. Worst case lower and upper boundaries can be deduced by attributing the smallest and largest possible value within each class to all pixels in that class. For the following studies radar data at 10 minutes or 30 minutes intervals have been used.

If area averages over model grid cells are attributed to every radar pixel within the respective cell, model grid adapted radar images can be produced (cf. e.g. Fig. 3-8c/d, Fig. 3-9) which are easily compared with pseudo-radar images of model precipitation. Model grid adapted radar images show instantaneous radar observed precipitation rates.

b.) Raingauges

It is a formidable and unresolved problem to get area average precipitation from point measurements, since precipitation is highly variable in space and time. It is very difficult to attach some measure of representativity to individual raingauge stations, since there are many factors influencing it, the nature of the precipitation event to be sampled not being the least. In addition, the geographical positioning of a model grid with respect to real orography and thus the association of surface stations with grid elements is arbitrary. For the present purpose of comparison to model data it is assumed that a simple arithmetic mean of hourly raingauge data is sufficient. In order to get an impression of the sensitivity of such a mean value to the network configuration, an additional mean value is computed by omission of the respective station measuring the largest hourly precipitation rate or the largest accumulated precipitation amount over the period of interest.

It is of interest to note that radar and raingauges have two complementary sampling modes. Radar samples an element of increasing volume and at increasing height every 10 minutes or so, thus having an effective resolution depending on distance from the radar. In contrast, raingauges sample continuously in time at fixed points in space. In the region of interest there is usually only a small number of such points, whereas radar sampling covers the whole region with high spatial and temporal resolution but under varying conditions.

3.5.2 Radar versus raingauge estimates

The verification domain used for comparison of model simulated and observed precipitation covers the part of Switzerland located north of the Alps (Fig. 3-3, page 58). The area is divided into a western and an eastern part. Good radar detectability conditions are given over the verification area. It contains 36 raingauge stations of the Swiss automatic surface network (ANETZ), where 11 and 25 stations are located in the western and eastern part respectively. In terms of HM8 (EM3) the western part contains 64 (4) model grid squares each containing 46 (764) radar pixels on average. The number of grid points for the eastern part is 96 (6).

For nine precipitation episodes accumulated area average rain amounts estimated from radar and raingauges are compared in Table 3-7. Fourteen averages belonging to the full area, the western and the eastern part are considered. Among the nine episodes two are frontal passages in winter, two are frontal passages in summer and five are convectively dominated summer situations. In only 3 cases, belonging to the summer fronts (27.8.89 and 26./27.6.91, highlighted in Table 3-7), raingauges record more precipitation than radar sees. Radar-raingauge agreement is best in frontal situations, where precipitation bands move over the whole area of interest. Structures of this type are more likely to hit all surface stations than convective clusters with arbitrary position and track through the domain.

The evolution of three episodes is given in Fig. 3-13. Accumulated area average precipitation shows excellent agreement for the frontal situation of 13 November 1987. Hourly precipitation rates from raingauges scatter around the radar time trace within the "worst case boundaries". During the main precipitation episode always more than 10, up to 26 stations out of 36 in the entire verification area record rainfall.

In contrast, on 28 May 1989 vigorous convection following the diurnal cycle was observed. Radar data reflects the episode very nicely (Fig. 3-13b). The raingauge network missed the precipitation event almost completely. Only two hours after the onset of rain the first surface station reports rainfall. After 4 (6) hours 3 (6) stations register precipitation. The readings at 15UTC suggest that one single station gives by far the largest contribution to the area average estimate. Six of the 36 stations give an average of $0.75 kgm^{-2}h^{-1}$, where

Table 3-7. Radar and raingauge estimated accumulated area average precipitation amounts

first value in each group: raingauge estimate in kgm^{-2}
second value: radar estimate in % of the raingauge estimate
third value: raingauge estimate in % of the first value excluding the most contributing station

Date	weather situation	Verification domain		
		full area	western part	eastern part
12.11.87	frontal	6.0/150/92		
13.11.87	frontal	14.3/101/94		
15.5.88	convective	4.4/205/82	4.4/252/50	4.8/169/73
28.5.89	convective	3.6/344/72		
29.5.89	convective	2.1/310/86		
30.5.89	convective	4.6/183/89		
27.8.89	frontal	17.0 /65/88		
26./27.6.91	frontal	11.6 /88/91	8.0/110/76	13.5 /83/89
6./7.7.91	convective		17.9/241/92	5.4/176/81

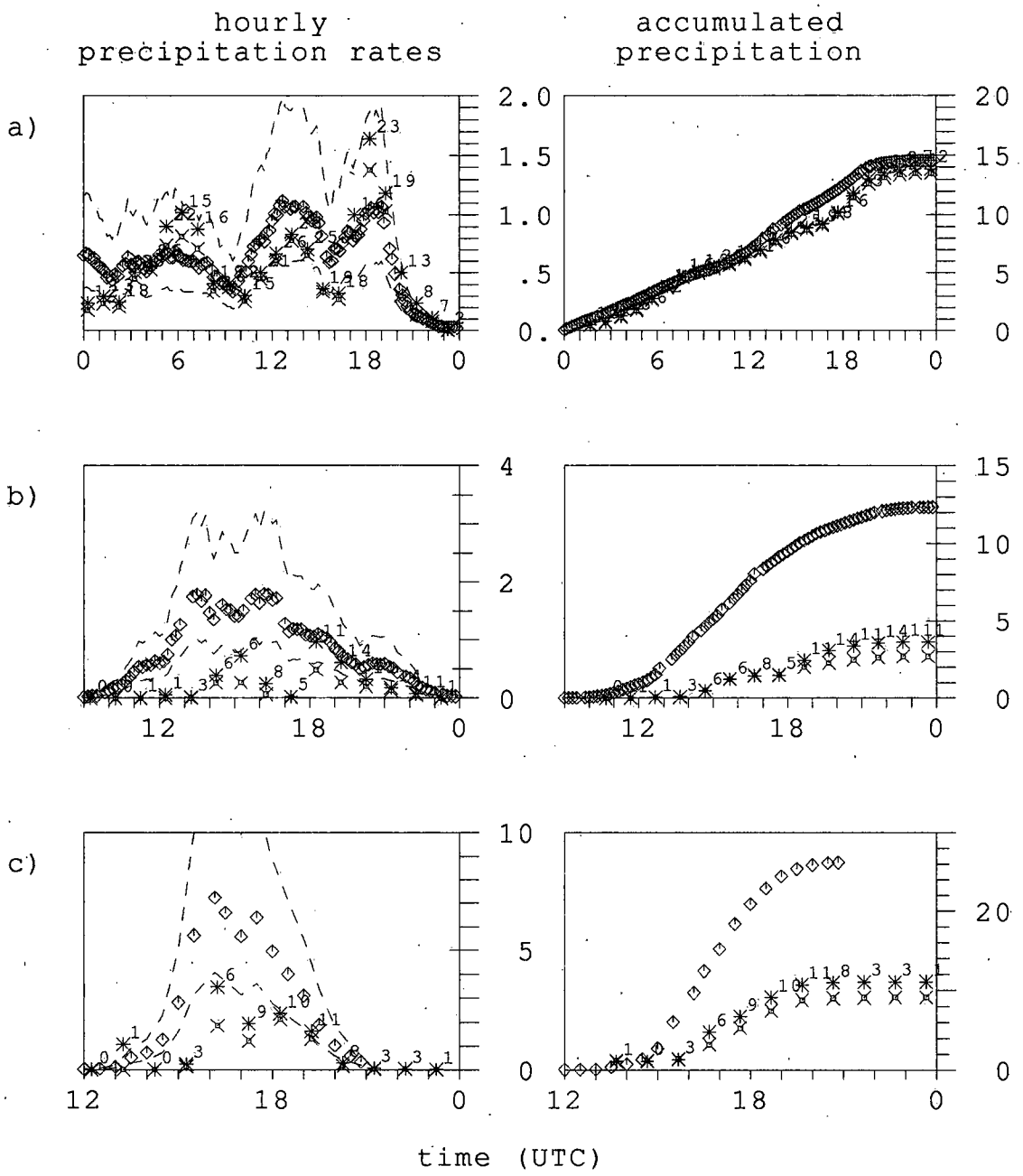

Fig. 3-13:Hourly (left panels, $kgm^{-2}h^{-1}$) and accumulated (right panels, kgm^{-2}) area average precipitation amounts from radar (squares) and raingauges (asterisks). Indicated are also the "worst case boundaries" (dashed lines) for radar and the number of stations recording precipitation. Estimates from raingauges omitting the most important station are also given (crosses).
a) 13 November 1987, full domain (36 raingauges)
b) 28 May 1989, full domain (36)
c) 7 July 1991, western part (11)

only $0.25 kgm^{-2}h^{-1}$ result when the most important station is omitted (at the same time radar estimates $1.5 kgm^{-2}h^{-1}$). These dramatic discrepancies in hourly precipitation rates finally accumulate to completely different daily sums of more than $13 kgm^{-2}$ against less than $4 kgm^{-2}$ of area average precipitation. The increasing number of stations recording light rain towards the end of the day is indicative of the stratiform character of the precipitation.

A very similar picture emerges for the convective event over the western part of Switzerland on 7 July 1991 already described in section 3.4. The eventual importance of one single surface station is apparent at 16UTC (Fig. 3-13c) where one station records the same precipitation amount as the ten remaining stations altogether (5 with and 5 without rain). Maximum precipitation rates between radar and ANETZ differ by a factor of two (16UTC) resulting in accumulated amounts of $26 kgm^{-2}$ and $10 kgm^{-2}$ respectively. Again all 11 stations receive precipitation at the end of the convective episode.

The methodological considerations in the previous subsection have suggested that radar would tend to underestimate precipitation in comparison with raingauges. As evaluated by Galli and Joss (1983), Joss and Kappenberger (1984) or Galli and Joss (1989) this is certainly true for "point intercomparison" at the location of the surface stations and for rainfall amounts accumulated over longer time ranges (sample of storms, seasons, years). Examination of single precipitation events and area averages can obviously result in a different picture.

From the present experiences it is concluded that, with respect to precipitation,

1.) in purely convective situations the raingauge network can suffer from a distinct sampling problem, and therefore

2.) basing model forecast verification exclusively on a surface network can be very misleading.

3.5.3 Simulated versus observed precipitation

Time traces and sums of area average precipitation simulated by HM8/VA for 15 May 1988 look reasonable compared to radar estimates for the large verification area (Fig. 3-14a). In this convective situation surface stations again start to record non-negligible rain only a few hours after radar detects the onset of a major rain event. ANETZ "sees" only half the amount of precipitation within the first 9 hours. The coarser model EM3 follows more the ANETZ time trace but underestimates rain even with respect to the surface network. The good result of the HM8 run is somewhat questioned when the western and eastern part of the verification domain are separately considered. In the western part of the country (Fig. 3-14b) HM8 and EM3 clearly underestimate precipitation with respect to radar. The situation at 12UTC as observed and predicted by HM8/VA is given in Fig. 3-15a/c respectively. In contrast to the former EU4/VA run (cf. Fig. 3-8b) HM8/VA does not succeed in developing orographically forced convection over the Jura mountains. In the easterly verification domain a few intensively raining grid points produce more area average precipitation than radar observations (Fig. 3-14c and Fig. 3-15c). At 16UTC wide-spread convective activity is observed over western Switzerland (Fig. 3-15b). HM8 still has some few raining grid points giving less than radar and raingauge observations. In the eastern part of the country a group of heavily raining grid points produces about the same amount

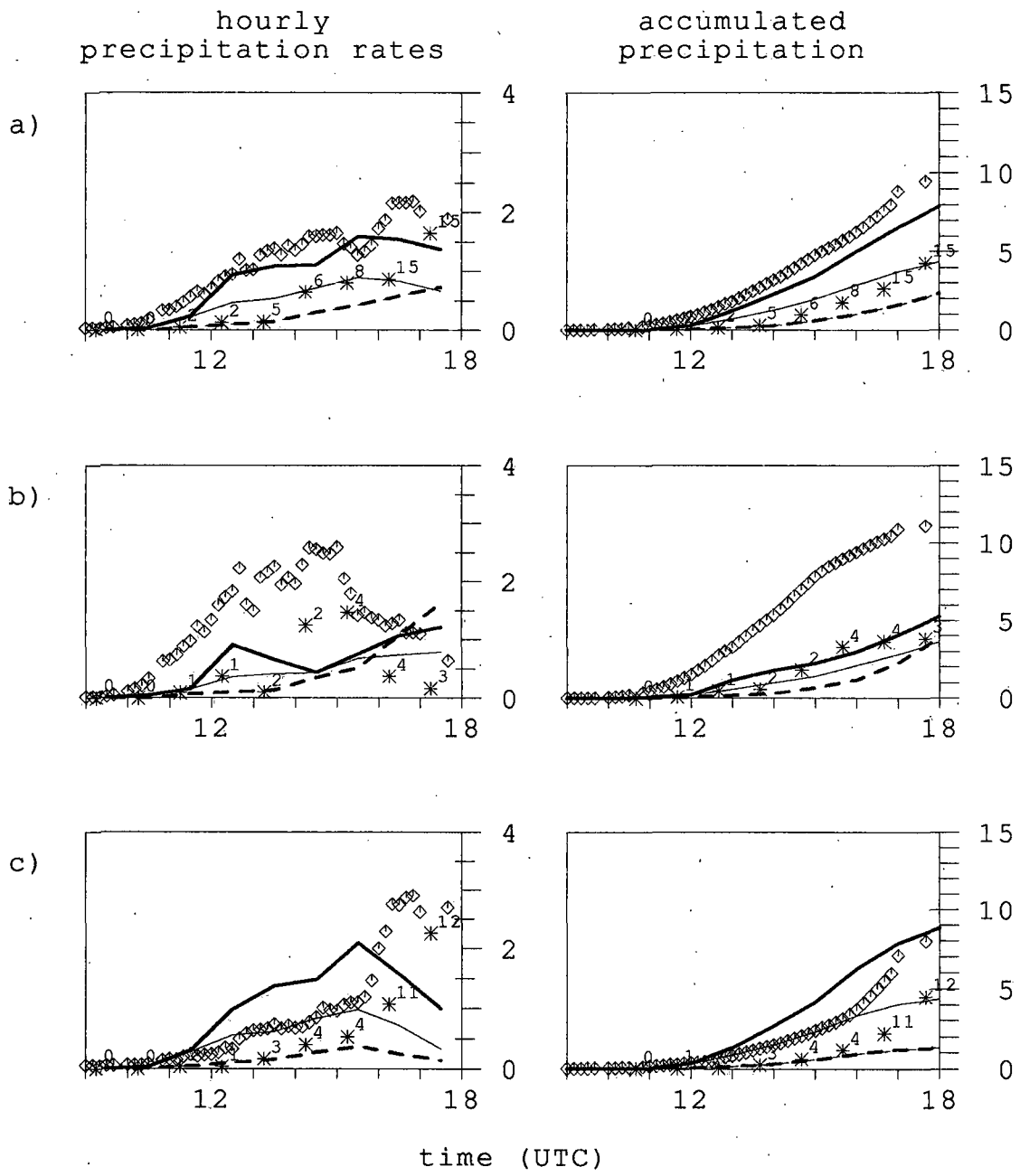

Fig. 3-14:Hourly (left panels, $kgm^{-2}h^{-1}$) and accumulated (right panels, kgm^{-2}) area average precipitation amounts from radar (squares) and raingauges (asterisks) for 15 May 1988. Model simulated values are solid (HM8/VA) and dashed (EM3/VA). Bold (thin) lines give total (convective) precipitation for the a) full verification domain, b) western part, c) eastern part.

of precipitation as observed by radar. Nonetheless the time trace of model precipitation does not correspond to the evolution indicated by radar (Fig. 3-14c).

In summary for 15 May 1988, a fair agreement between HM8/VA and radar observations for area average precipitation of the whole verification domain is found. For the western part of the domain the model does not simulate the real situation properly. Nevertheless the time trace of average precipitation follows the ANETZ curve quite closely. In the east-

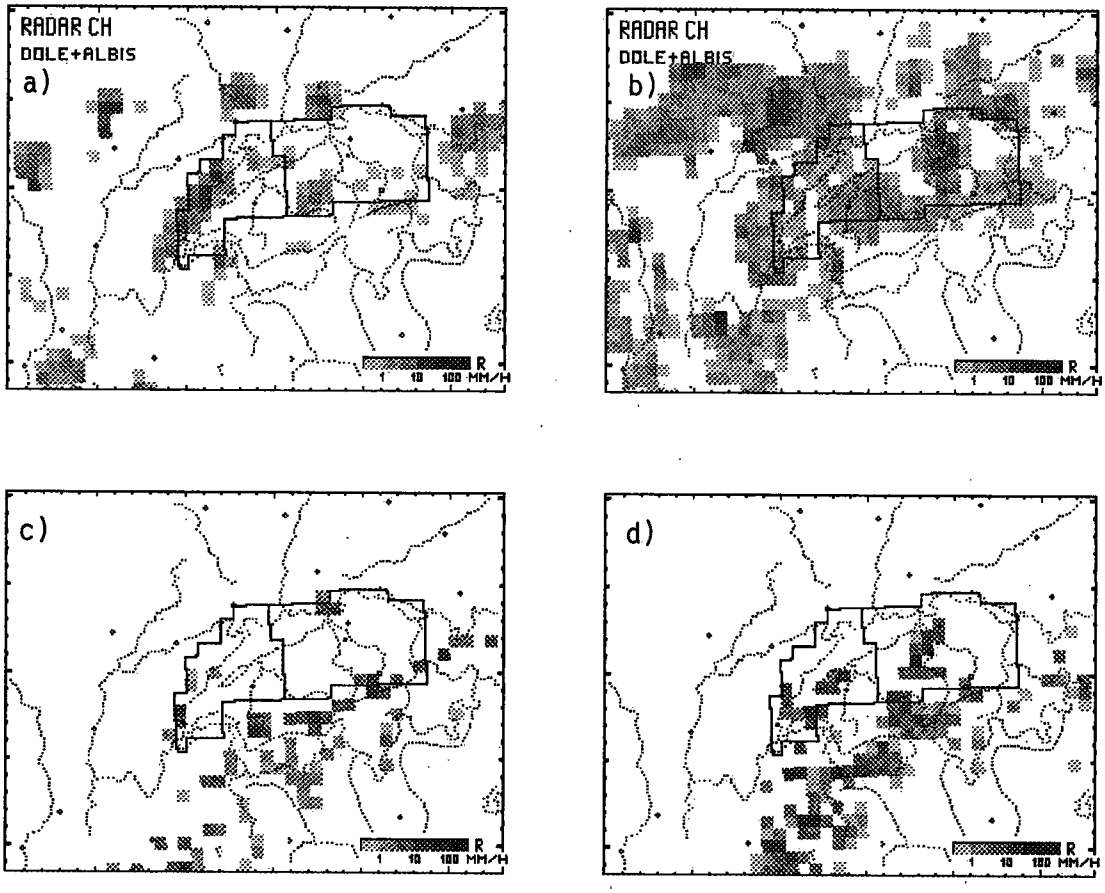

Fig. 3-15:Radar observed a), b) and HM8/VA simulated c), d) instantaneous total precipitation rates for 15 May 1988 12UTC a), c) and 16UTC b), d). Model run starts from 00UTC. The verification area is outlined.

ern part the model predicts a development of convection which is stronger than that observed. Underestimation in the western part and overestimation in the eastern part combine to a fairly good overall result. This is an indication that quantitative verification results at smaller-scales can crucially depend on configuration.

A realistic picture of the onset of convection by radiative forcing over orography was simulated by EU4/VA (Fig. 3-8b). HM8/VA did not produce the same result (Fig. 3-15c) although HM8 was brought back as far as possible to the former EUM version: – the deep-convection reference profile was exactly the same as in EUM, – the correction term for quasi-horizontal diffusion of heat and moisture was eliminated and – diffusion coefficients were calculated according to the former EUM version. Since the step from EUM to EM was accompanied by a major change of the host computer system many features of the old model version were not migrated and therefore a whole series of differences between the two model systems was impossible to be eliminated. Thus a trace back to figure out the ultimate cause for the differing results of the EU4/VA and the HM8/VA runs can not be carried out. However, the most probable explanation is the following: From inspection of the

cloud water content of the model atmosphere it is recognized that in the HM8/VA case much more clouds existed in the Alpine region during the first 12 hours of integration than in the EU4/VA case. In the very moist atmosphere present in this particular weather situation the presence or absence of clouds can depend on slight variations of the moisture field, but it has a significant impact on radiative forcing at the ground. Differences between the moisture fields can conceivably be attributed to the following changed characteristics of the two model configurations: Forecasts of limited area models are well known to be sensitive to the horizontal dimensions of the integration domain and to the specification of the boundary conditions. In fact, both these factors, the integration area (Fig. 3-2) and the boundary conditions were different in the two experiments. At the lateral boundaries EU4 was governed by analyses of the T106 model at six-hourly intervals. In contrast, boundary conditions for the HM8 run were given by forecasts of a EM3/EH simulation and were provided once per hour (Table 3-4). Initial and boundary conditions were established by two versions of the interpolation programme (cf. subsection 3.2.3). In the EU4 case the lateral boundaries were much closer to the area of interest and, very importantly, the boundary scheme did only allow for the relaxation of water *vapour* but not of *cloud* water. In contrast, the integration domain of the HM8 run was much larger and cloud water produced by the steering EM3 model was able to penetrate through the lateral boundaries. In particular, in the HM8 simulation there was no permanent spin-up of cloud water in the vicinity of the area of interest due to close lateral boundaries as in EU4. Thus it appears likely that the atmosphere was moister and that more clouds existed in the HM8 case. Taking into account that the new radiation scheme used in EM/HM is more sensitive to the presence of clouds, it is therefore concluded, that radiative forcing at the ground was stronger in the EU4 case and consequently more convection was initiated. Further non-removable differences between the old and the new model version which can influence the atmospheric moisture field directly or indirectly concern the treatment of surface evaporation and the specification of soil moisture. Certainly the changed orography has also an impact on the mesoscale structure of the moisture fields.

EM3/MX and HM8/MX runs of 26 June 1991 predict 24h accumulated precipitation amounts for the Swiss verification area which are in excellent agreement with estimates from radar *and* raingauge observations. Looking at the time variation of precipitation, it is recognized (Fig. 3-16a), that observed rain fell essentially during the passage of the front. HM8 simulated a peak rate slightly late and less intense. EM3 had even a larger phase shift. In contrast to nature model precipitation did not completely cease after the passage of the front, but there was some follow-up convective activity behind the front (note the large portion of convective rain after the main peak). In the western part (Fig. 3-16b) radar and raingauge peak rates agree very well, whilst model peak rates are much too weak. In the eastern part, on the contrary, model peak rates are similar to the ones observed, with a small time lag. Fig. 3-17a/c/e show the front as observed at 14UTC and as simulated by HM8 and EM3. In both models post-frontal "echoes" appear west of the Jura. They did not significantly move in the sequel. The front in HM8 shows the typical patchy structure. The model atmosphere was not as much stabilized by the passage of the front as in nature, since secondary maxima of convective activity appeared over the Alps in the evening (Fig. 3-17d and f). Only light, ceasing precipitation was observed by radar at that time (Fig. 3-17b).

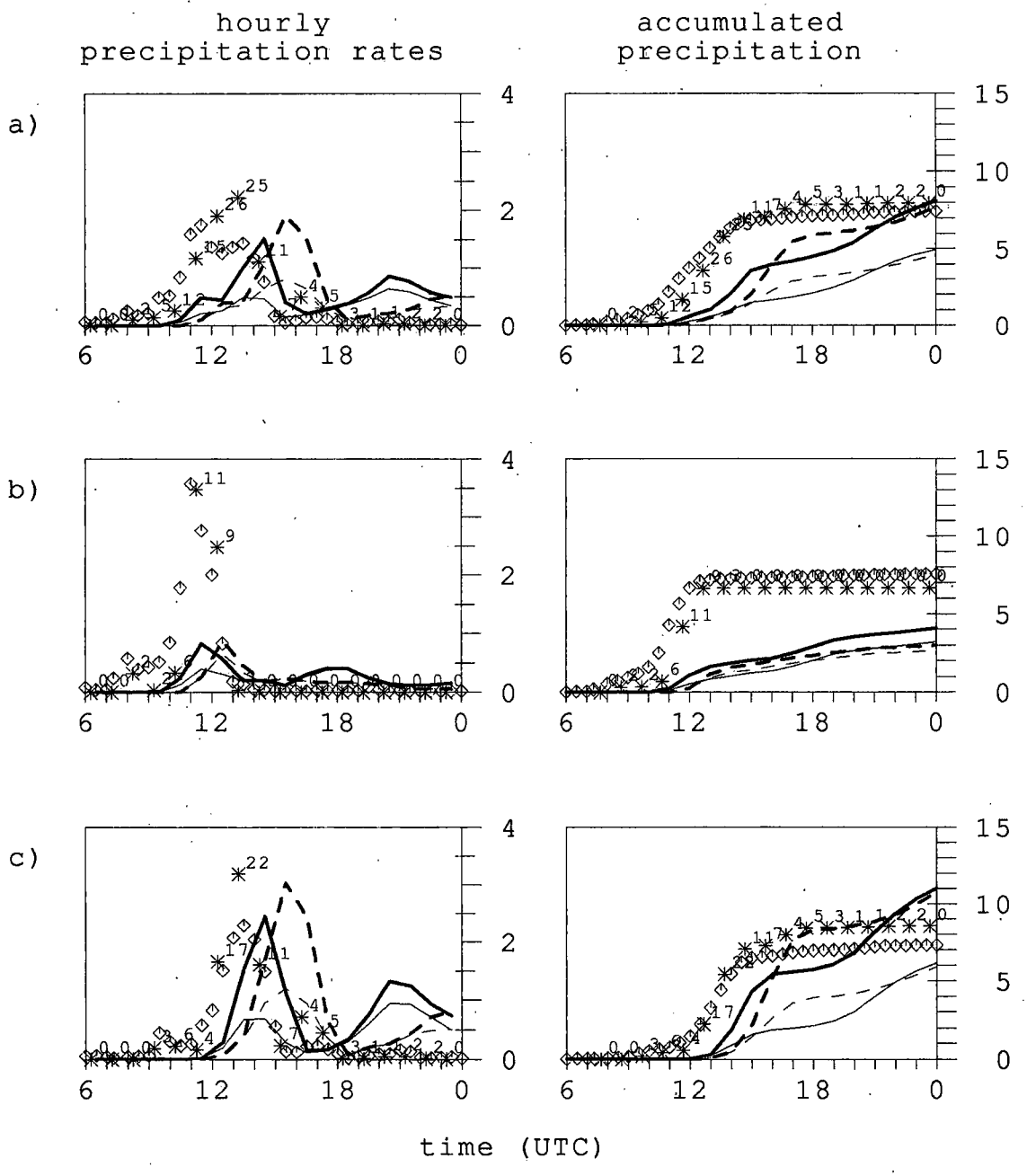

Fig. 3-16:Hourly (left panels, $kgm^{-2}h^{-1}$) and accumulated (right panels, kgm^{-2}) area average precipitation amounts from radar (squares) and raingauges (asterisks) for 26 June 1991. Model simulated values are solid (HM8/MX) and dashed (EM3/MX). Bold (thin) lines give total (convective) precipitation for the a) full verification domain, b) western part, c) eastern part.

This last example exhibits a number of unusual features at once: – agreement between radar and ANETZ is remarkable, – for the eastern verification domain raingauge peak rates as well as accumulated amounts (Table 3-7) are larger than radar estimates, – HM8 and EM3 produce quite the same precipitation amounts and – peak rates of precipitation in EM3 are not weaker than in HM8. The example also demonstrates that the evolution of precipitation events is an important aspect for verification.

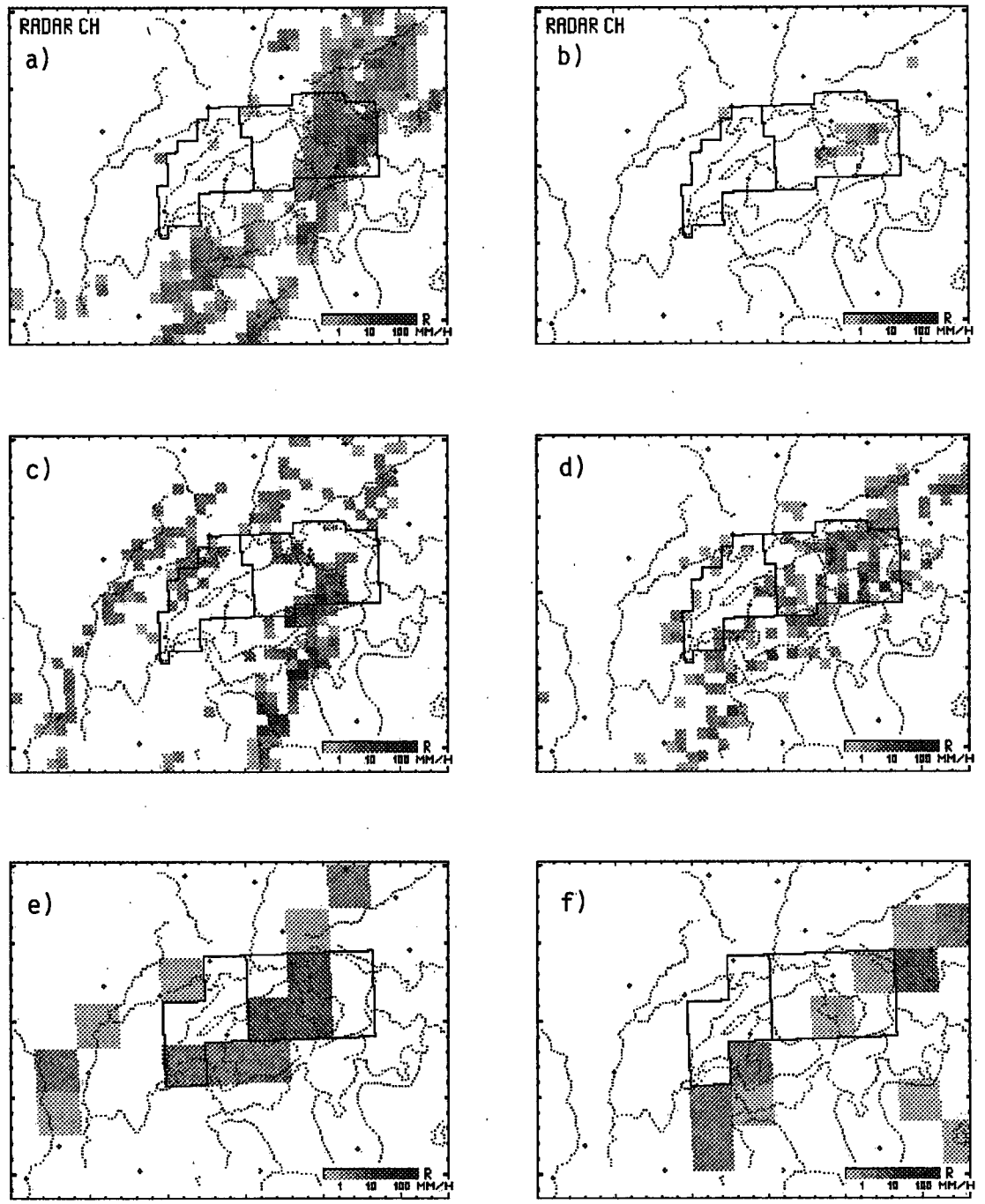

Fig. 3-17:Observed and simulated instantaneous total precipitation rates for 26 June 1991

a) radar at 14UTC, b) radar at 21UTC
c) HM8 at 14UTC (+14h) d) HM8 at 21UTC (+21h)
e) EM3 at 15UTC (+27h) f) EM3 at 21UTC (+33h)

This more illustrative section on quantitative comparison of simulated and observed precipitation has revealed some important aspects of verification of high-resolution models, in particular of precipitation forecasts:

1.) It is important to use information from as many independent sources as possible. Radar and raingauge measurements are complementary and, in combination, can enable a fairer judgement of the model than one of these sources alone.

2.) Increased temporal resolution of observational data (e.g. hourly data) allows for closer examination of model simulated systems.

3.) Comparison of observed and simulated horizontal patterns and their evolution in time provide valuable information.

4.) At high resolution verification results become more dependent on more or less arbitrary conditions such as the inclusion of a certain grid point into the verification area. Higher resolution in space and time render model verification more rigorous.

3.6 Discussion

3.6.1 Increasing precipitation amounts with increasing horizontal resolution

In common with other investigations (Zhang et al., 1988; Bougeault and Geleyn, 1989; Kristjánsson, 1991) a striking result of the mesh width experiments is the increase of area average precipitation with increasing horizontal resolution. This increase is mainly due to intensified grid-scale precipitation, whilst the convective portion is nearly unaffected. Adapting the convective adjustment time scale does not account for the full increase of total precipitation. There is always an intensification of grid-scale rain (cf. Fig. 3-4). In parallel, stronger upward velocities are found (Zhang et al., 1988; Binder and Wacker, 1990). Following a recent theoretical development of Doms (1991) the grid-scale precipitation rate in the steady state is directly proportional to the dynamical forcing and independent of the details of cloud physics parameterization. Doms (1991) considers a simplified equation for cloud water (q_c)

$$\frac{\partial q_c}{\partial t} = -cq_c + f, \tag{3-9}$$

where c represents the source and sink processes for cloud water (nucleation, autoconversion, riming, etc.) and f is the total dynamical forcing including grid-scale condensation. Defining precipitation (P_r) by

$$\frac{\partial P_r}{\partial p} = cq_c, \tag{3-10}$$

assuming linear processes in c and searching for the analytical solution in the steady state yields

$$P_r^{(s)} = f\Delta p, \tag{3-11}$$

where Δp is the depth of the layer considered. In hydrostatic models vertical velocity is directly coupled to the horizontal divergence field, which has more small-scale structures and larger amplitudes on a finer grid. Thus vertical moisture transport can significantly contrib-

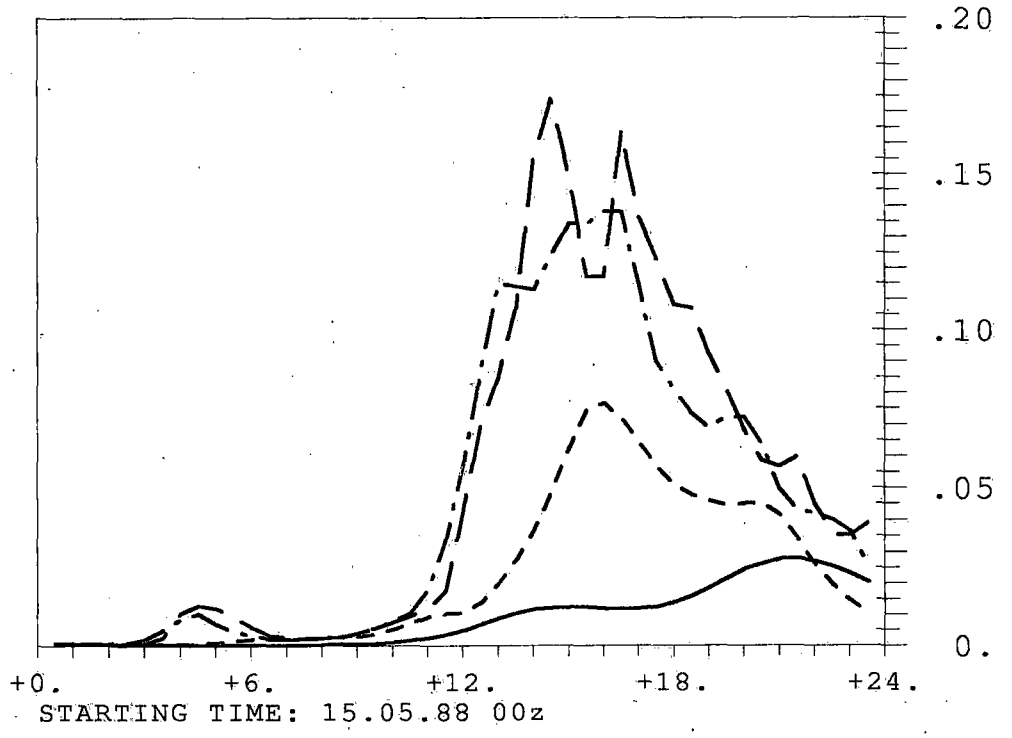

Fig. 3-18: Time trace of domain average squared vertical velocity (upward motion only) at about 550hPa. EUM/VA runs for 15 May 1988 00UTC with a horizontal mesh of 64km (solid), 32km (short dashed), 16km (long dashed) and 16km with adapted convective adjustment time τ=0.5h (dashed-dotted). Arbitrary units on the vertical axis.

ute to dynamical forcing and, in the limit, precipitation can become directly proportional to upward motion in saturated conditions.

A measure of domain averages of vertical velocity for the MAY88/EUM/VA experiment series is plotted in Fig. 3-18. In correspondence with the precipitation trace of Fig. 3-14a vertical velocity grows most significantly around noon and decays after 18UTC. The 64km model starts later, has substantially lower amplitudes and produces distinctly less rainfall. The 32km model version produces an intermediate solution.

3.6.2 On the need for cumulus parameterization in mesoscale models

A second ubiquitous problem, contributing considerably to excessive rainfall rates, are the so-called grid point storms which have also been identified by many investigators of high-resolution models (Molinari and Dudek, 1986 (Δx=0.5°); Kalb, 1987 (Δx=70km); Zhang et al., 1988 (Δx=25km,12.5km); Bougeault and Geleyn, 1989 (Δx=40km); and others). At a single grid point upward motion becomes unrealistically strong and grid-scale precipitation is very intense. This phenomenon can last for several hours with adjacent grid points remaining inconspicuous.

In a careful account Zhang et al. (1988) explain the grid point storms to be a CISK-like instability. As recognized by Kasahara (1961) the phenomenon is due to a physical instability entirely related to the grid-resolvable latent heat release. If local instabilities are generated, e.g. by transport of air with high equivalent potential temperature or by the day-

time development of the planetary boundary layer, and if mechanisms to release these instabilities are absent or ineffective, once the vertical column is saturated the shortest resolvable-scale waves start to grow exponentially. Once resolvable-scale latent heat release is initiated a mesocyclone tends to develop and then a positive feedback cycle with low-level moisture convergence is established. The term CISK-like is used because the original formulation of CISK implies a feedback with parameterized rather than grid-resolved latent heat release.

From a conceptual point of view there exist several arguments against the use of cumulus parameterization schemes in mesoscale models (here "mesoscale" has to be understood as grid spacings between 10 and 50km (Molinari and Dudek, 1992)): A fundamental requirement for the parameterizability of a physical process is the existence of a clear scale separation in space and time between the phenomena which are explicitly resolved on the grid and those to be parameterized. As the mesh size decreases in mesoscale models both the temporal and spatial scale of the grid-scale motions and the convection being parameterized become less well separated. An additional difficulty exists in establishing appropriate closure assumptions, since there are no observations available representative for that scale (Arakawa and Chen, 1987). Therefore key aspects of the parameterization remain on a rather ad hoc basis due to the lack of observational evidence. Finally, in certain conditions, namely weak rotational constraints (Frank, 1983), convective activity may no longer be controlled by grid-scale forcing, a key assumption in convective parameterization.

Explicit mesoscale model simulations (i.e. without cumulus parameterization) have been successful in certain case studies. Closer examination of these experiments reveals (Molinari and Dudek, 1992), that the success can, at least partly, be attributed to particular circumstances of the respective simulations, e.g. high initial relative humidity, strong grid-scale forcing or inclusion of stability dependent vertical diffusion. There is a series of examples, where the explicit model version provided significantly poorer results than the implicit one including cumulus parameterization (e.g. Molinari and Dudek, 1986; Kalb, 1987; Zhang et al., 1988; Cram et al., 1992a; EUM experiments). Situations with strong grid-scale forcing and relatively weak conditional instability are more favourable for simulation by the explicit approach than situations where either or both of these conditions are not fulfilled.

There exist also several arguments in favour of the parameterization of cumulus convection in mesoscale models. In nature, convective precipitation starts before an atmospheric volume corresponding to the grid element of any mesoscale model is saturated and thus a net heat source exists in that column. In addition remarkable vertical eddy transports of heat, moisture and other quantities take place. An explicit simulation, unable to account for subgrid-scale processes, will suffer from an erroneous delay in precipitation onset and miss the corresponding modification of the atmospheric thermodynamic structure. Furthermore cumulus parameterization schemes are intended to remove instability before grid-scale saturation is reached. Conditional instability of saturated model columns results in unstable growth of the vertical circulation, as described above. With the explicit approach this situation appears to be inevitable, whereas by means of cumulus parameterization there is some hope to control it, at least to a helpful extent.

Primarily based on experimental evidence, there appears to be general agreement that cumulus parameterization must be included in mesoscale models down to horizontal meshes of 10km or even smaller, although grid point storms are not always satisfactorily controlled. Cram et al. (1992b) even demonstrated the importance of a cumulus parameterization scheme for a successful simulation of a squall line by a *non-hydrostatic* model with a grid spacing of 5km! Several ways of improving parameterized convection have been proposed. Inclusion of prognostic equations for liquid and solid cloud and precipitation variables into the grid-scale prognostic system seems to be essential. Cumulus parameterization should then account for the following processes (e.g. Zhang and Fritsch, 1988a; Zhang et al., 1988):

1.) Parameterization of convective downdrafts helps to stabilize the boundary layer and can help to organize convective systems.

2.) Evaporation of rainfall cools dry boundary layers (important in dry environments).

3.) Liquid water loading reduces the buoyancy of air parcels (important in moist environments).

4.) Melting of frozen particles consumes sensible heat and modifies the vertical stability structure (Cohen and Frank, 1989; Binder, 1990).

Molinari and Dudek (1992) recommend the development of the so-called "hybrid" approach. Such a scheme (e.g. Frank and Cohen, 1987) is characterized by the inclusion of cloud and precipitation microphysics in the cumulus parameterization and the presence of convective source terms in the corresponding grid-scale prognostic equations. Unlike traditional cumulus parameterization schemes, once convective sources of condensate are determined, a fraction of this condensate is added to the grid-scale cloud and precipitation particle equations and thus a direct communication is established between parameterized and resolved processes. This concept offers the potential to simulate the mesoscale organization of major convective systems, since only the convective components need to be parameterized and the mesoscale components are resolved on the grid. It simulates particle detrainment which is a key mechanism for the development of the stratiform component fairly realistic. However, also the hybrid approach has the difficulty of choosing a closure assumption. Furthermore the possibility that convective clouds tend to grow directly on the grid scale (i.e. the existence of saturated conditionally unstable grid columns) with increasing resolution is not eliminated by this concept.

An alternative strategy towards improved mesoscale simulations is the development of cumulus parameterization schemes with prognostic equations for convective-scale quantities, such as cloud convective mass flux for instance (Bougeault and Geleyn, 1989; Chen and Bougeault, 1992 (personal communication)). Such a scheme would enable the simulation of a proper life cycle of the subgrid-scale convective clouds.

3.6.3 Synthesis

Relations between horizontal resolution and convective parameterization on one hand and characteristics of simulated precipitation on the other hand emerging from experimentation with EUM and EM and other investigators are sketched in Fig. 3-19. Increased horizontal resolution allows for intensified vertical circulation due to larger amplitude fine-scale divergence fields which might be caused by more structured external forcing (orogra-

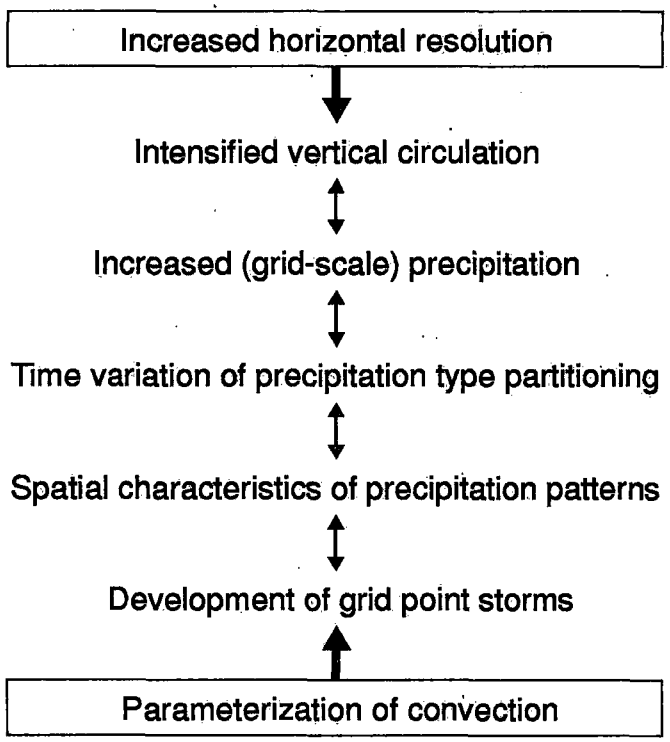

Fig. 3-19:Relations of horizontal resolution and cumulus parameterization to precipitation characteristics.

phy). Giorgi (1991) noted that grid point storms appeared most frequently over mountainous terrain. Enhanced vertical moisture transport produces more condensation, cloud water and in turn precipitation. In conditionally unstable situations the cumulus parameterization scheme acts as an alert system and starts to remove instability and moisture before grid-scale saturation is reached. If the scheme works efficiently, it can prohibit or considerably delay and reduce the development of grid point storms. An indication of the influence of the parameterization scheme on grid point storm activity can also be seen in Fig. 3-18: The 16km run using an adjustment time scale of 0.5h reduces vertical velocity peaks significantly in comparison with the 3h adjustment time step. The presence of grid point storms determines the spatial distribution of precipitation as well as the evolution of precipitation type partitioning.

Precipitation type partitioning in space and time is indicative of the model's ability to cope with convective situations. The results in this chapter suggest that EUM and EM did not manage grid point storm activity satisfactorily. Thus convective parameterization needs to be improved. On the other hand simulations presented in the literature exhibit similar features.

3.6.4 Final remarks

In section 3.4 item b.) we found an extreme sensitivity of the HM8 simulation to the specification of the deep-convection reference profile in the convective adjustment scheme. Completely different systems developed in different locations (Fig. 3-10). Bougeault and

Geleyn (1989) also noticed increasing differences between model runs with different cumulus parameterizations with increasing horizontal resolution. In fact this is the contrary of what should be expected. The finer the grid, the less differences between convective parameterization schemes should become apparent, since more features of the convective system can be resolved by the grid-scale circulations. Since this is not the case, the validity of the traditional concepts of cumulus parameterization and of the closure assumptions for the horizontal scales considered has to be questioned.

There remains a comment to be made about the similar horizontal patterns and amplitudes of convective and grid-scale precipitation in the EUM experiment using a 1-dimensional cloud model with moisture convergence closure to parameterize convection (KUO). In this case the convective precipitation microphysics are with some minor simplifications formulated the same way as the grid-scale precipitation-forming processes. This is in contrast to the adjustment scheme which essentially removes supersaturation at upper levels and allows for evaporation in unsaturated layers, but has no cloud physics. In places where grid point storms form, strong moisture convergence is present, the model atmosphere becomes saturated on the grid-scale and its vertical thermodynamic structure does probably not differ very much from the cloud sounding constructed by the convection scheme. Therefore the grid-scale precipitation scheme and the convective cloud model have the same basic state to produce precipitation. In addition, since the atmosphere is saturated in these locations, the moisture convergence closure maximizes the humidity available for cloud formation and in turn convective precipitation. It is thus conceivable that both types of precipitation reach about the same intensity.

3.7 Conclusions

The principal purpose of this chapter has been to explore the influence of increased horizontal resolution and details of the parameterization scheme of convection on the characteristics of simulated precipitation. The starting point have been two NWP model versions with grid spacings of about 60km which were gradually reduced to one half and one quarter of the original value. The convective adjustment philosophy was used to parameterize cumulus convection at all scales. Simulated precipitation features have been compared to two complementary types of observations, namely weather radar data and surface raingauge data. Weather situations with convective activity have been investigated. The main findings are as follows:

1.) The meso-β-scale models exhibit a potential for more detailed precipitation forecast in space and time. More realistically represented external forcing (e.g. orography) inducing and allowing for the development of finer-scale structures of atmospheric fields important for precipitation simulation (stability, divergence) contribute to this success.

2.) Precipitation increases with increasing horizontal resolution mainly due to enhanced grid-scale precipitation, which in turn is a consequence of intensified grid-scale circulation on the finer grid.

3.) Precipitation tends to start earlier in high-resolution models.

4.) Sensitivity of precipitation simulation to details in the cumulus parameterization scheme, namely the deep-convection reference profile in the present case, is very pronounced in high-resolution models.

5.) Grid point storm activity increases with enhanced horizontal resolution. As a consequence grid-scale precipitation becomes quantitatively more important than convective precipitation. A parameterization scheme for cumulus convection is indispensable to control these instabilities in hydrostatic models down to mesh sizes of the order of 10km.

6.) Observational data from the two sources radar and raingauge do not necessarily provide agreeing quantitative estimates of area average precipitation amounts. This has a serious impact for model verification. Whenever possible both types of observational data should be used in order to allow for a fair judgement of model results.

7.) Comparison of time traces of observed and simulated precipitation estimates is as important as examination of accumulated amounts. Model simulations can accumulate precipitation quantities similar to those observed although the time variation of the rainfall event can be completely different.

8.) Area average precipitation measures do not provide a picture of the horizontal structures producing them. Models usually simulate much narrower and more intense precipitation signatures than those observed.

9.) Partitioned simulated precipitation fields give a good impression of grid point storm activity in the model. In general precipitation type partitioning is an important aspect of the model's behaviour.

In summary, consideration of various aspects of simulated precipitation signatures is important to gain insight into model behaviour. For verification purposes different sources of observational data should be taken into account.

4 Diagnosing physical tendencies in a numerical weather prediction model

4.1 Introduction

The evolution of the idealized atmosphere in a NWP model is governed in a complex way by all explicitly formulated and parameterized, mutually interacting, physical processes represented by the model. To evaluate the model's ability to adequately represent physical processes of the real atmosphere, to quantify the influence and relative importance of every contribution made by single schemes and to gain insight into the internal interactions taking place, powerful diagnostic tools are needed. Such tools can help to detect systematic errors of an entire NWP model system or can help to investigate a single (parameterized) process in depth.

In agreement with the findings of the previous chapter, it has been recognized that there is a pronounced sensitivity of model simulations to the type of the cumulus parameterization scheme selected, at least for certain weather situations. On the one hand this dependency has been found for the choice of the parameterization scheme as a whole (e.g. Krishnamurti et al., 1980; 1983; Puri and Miller, 1990). A striking example is given by Heckley et al. (1987): The simulation of hurricane Elena (28.8.-4.9.1985 in the Gulf of Mexico) by ECMWF's T106 model using the operational Kuo scheme and the Betts-Miller adjustment scheme produced two completely different tracks of the tropical cyclone. One track compared favourably with the analysed positions whilst the other one did not at all. On the other hand model simulation results can also depend on some details of a given convective parameterization scheme (e.g. Molinari and Corsetti, 1985; Zhang and Fritsch, 1988a; Grell et al., 1991).

In the same way as cumulus convection plays a crucial role in nature, so does its representation in NWP models influence the development of the model atmosphere. Deficiencies of this representation have probably a disproportionate impact due to the pronounced sensitivity of the model to these processes. Therefore, it is important to gain a sound understanding of convection in nature on the one hand and to understand how cumulus parameterization schemes interact with other processes in numerical models and what their specific contribution to the development of the model atmosphere is on the other hand. Both the observational and the modelling point of view necessitate appropriate methodologies and diagnostic tools to meet these demands.

In this chapter a general package for comprehensive diagnostics of the full prognostic thermodynamic and moisture equations of a NWP model, namely of the Europa Modell (EM) of the Deutscher Wetterdienst (Majewski, 1991), is developed. Results for a selection of convective weather events will be presented, with special emphasis on the dependency of subgrid-scale (parameterized convection) and grid-scale (microphysics and condensation) forcing on the stage of development of the precipitation system, on horizontal resolution and on details of the parameterization of convection (deep-convection reference profile and adjustment time scale).

In the next section methods to diagnose the impact of convective systems on their environment are briefly reviewed. First the appropriate formalism for heat and moisture budgets is introduced, then pertinent results from observational studies are reported, finally different possibilities of diagnosing convection within the context of a NWP model are out-

lined. In the third section the general form of heat and moisture budgets is carefully related to the prognostic thermodynamic and moisture equations of a complete NWP model. Special reference is then made to EM in order to elaborate a diagnostic tool for physical tendencies in this model. Case studies of convective weather events simulated by various configurations of EM are presented in section 4.4. The main findings of the chapter are summarized in the final section.

4.2 Diagnosing the physics of convection

4.2.1 Heat and moisture budgets

Heat and moisture budgets are most commonly formulated in terms of the so-called apparent heat source (Q_1) and apparent moisture sink (Q_2) (Yanai et al., 1973). Q_1 and Q_2 are formally defined by Eq. (4-1) and Eq. (4-2). Here, as elsewhere, $s=c_pT+gz$ is the dry static energy, c_p the specific heat of air at constant pressure, T the temperature, g the acceleration of gravity, z the height, $\vec{v}$ the horizontal velocity, ∇ the horizontal gradient operator, ω the vertical p-velocity, p the pressure, L_v the latent heat of vaporization and q_v the specific water vapour content. $\bar{c}$ is the net condensation of water vapour and Q_R is the heating by radiation.

$$Q_1 := \frac{d\bar{s}}{dt} = \frac{\partial \bar{s}}{\partial t} + \bar{\vec{v}} \bullet \nabla \bar{s} + \bar{\omega}\frac{\partial \bar{s}}{\partial p} = -\nabla \bullet \overline{\vec{v}'s'} - \frac{\partial}{\partial p}(\overline{\omega' s'}) + L_v \bar{c} + Q_R \quad (4\text{-}1)$$

$$-\frac{Q_2}{L_v} := \frac{d\overline{q_v}}{dt} = \frac{\partial \overline{q_v}}{\partial t} + \bar{\vec{v}} \bullet \nabla \overline{q_v} + \bar{\omega}\frac{\partial \overline{q_v}}{\partial p} = -\nabla \bullet \overline{\vec{v}'q'_v} - \frac{\partial}{\partial p}(\overline{\omega' q'_v}) - \bar{c} \quad (4\text{-}2)$$

These definitions are based on the conservation of dry static energy (s) under dry adiabatic processes and moisture conservation expressed in terms of specific water vapour content (q_v). In addition, atmospheric variables are split into a (large-scale) horizontal average part (denoted by an overbar) and a portion representing deviations therefrom (denoted by a prime), i.e. $\psi = \bar{\psi} + \psi'$.

Eq. (4-1) shows that the apparent heat source (Q_1) of the large-scale motion system consists of horizontal convergence of horizontal eddy transports, vertical convergence of vertical eddy transports, latent heating by net condensation (i.e. including evaporation of cloud water) and heating due to radiation. The apparent moisture sink (Q_2) is given by horizontal convergence of horizontal turbulent transports, vertical convergence of vertical turbulent transports and net condensation. Often the horizontal eddy terms are neglected.

Summation of Eq. (4-2) and Eq. (4-1) yields an expression for moist static energy $h_p=c_pT+L_vq_v+gz$ which is approximately conserved under moist adiabatic processes:

$$Q_1 - Q_2 = \frac{\partial \overline{h_p}}{\partial t} + \bar{\vec{v}} \bullet \nabla \overline{h_p} + \bar{\omega}\frac{\partial \overline{h_p}}{\partial p} = -\nabla \bullet \overline{\vec{v}'h'_p} - \frac{\partial}{\partial p}(\overline{\omega' h'_p}) + Q_R \quad (4\text{-}3)$$

Moving Q_R to the left hand side of the equation and neglecting horizontal turbulent transports, only the vertical flux convergence of moist static energy remains on the right hand side. Thus vertical turbulent transport $\overline{\omega' h'_p}$ of moist static energy can be considered as a measure of convective activity. An important point is that in Eq. (4-3) condensation no longer appears.

Vertical integration of Eqs. (4-1) and (4-2) from the earth surface (p_0) to some pressure level p_T where vertical velocity and vertical turbulent fluxes are assumed to be zero yields

$$\frac{1}{g}\int_{p_T}^{p_0} Q_1 dp = \frac{1}{g}\int_{p_T}^{p_0} \left(\frac{\partial \bar{s}}{\partial t} + \bar{\vec{v}} \bullet \nabla \bar{s}\right) dp = L_v P_0 + S_0 + \frac{1}{g}\int_{p_T}^{p_0} Q_R dp \qquad (4\text{-}4)$$

$$\frac{1}{g}\int_{p_T}^{p_0} Q_2 dp = \frac{-L_v}{g}\int_{p_T}^{p_0} \left(\frac{\partial \overline{q_v}}{\partial t} + \bar{\vec{v}} \bullet \nabla \overline{q_v}\right) dp = L_v (P_0 - E_0) \qquad (4\text{-}5)$$

where P_0 is the total precipitation (the vertical integral over $\bar{c}$), S_0 and E_0 are the supply of sensible heat from the earth surface and evaporation from the earth surface respectively. From these expression it can be seen that precipitation amounts can be determined as residuals from the budgets, if some estimates of radiation and surface heat and moisture fluxes are available.

4.2.2 The observational point of view

The above budget formalism has been used extensively to investigate the effect of cumulus activity on its larger-scale environment. Observed estimates of the horizontal and vertical advection of thermodynamical and moisture quantities in combination with corresponding local time tendencies can be used to evaluate the left hand side of Eqs. (4-1) and (4-2) in order to obtain vertical profiles of the apparent heat source and moisture sink (Reed and Recker, 1971; Yanai et al., 1973; Johnson, 1976; Thompson et al., 1979; and others). Most often upper air data from a sounding station network is used for this purpose and large-scale vertical motion is evaluated by some kinematic method. If it is assumed that the terms on the right hand side of Eqs. (4-1) and (4-2) are primarily due to the cumulus activity, then vertical profiles of cloud mass fluxes, vertical transports and condensational heating can be diagnosed if a hypothetical cloud model is imposed (e.g., Yanai et al., 1973; Ogura and Cho, 1973; Houze et al., 1980). From Q_1, Q_2 and estimates of diabatic heating by radiation, of surface sensible heat flux and of surface evaporation the precipitation from a vertical column can be diagnosed as a residual (Thompson et al., 1979; Pedigo and Vincent, 1990; Vincent et al., 1991). In fact two independent residuals can be calculated from the heat and moisture budgets (Eqs. (4-4) and (4-5)). Vincent et al. (1991) use a large dataset of global ECMWF analyses to compile a precipitation climatology of the tropical belt. Such precipitation fields can constitute a valuable complement to satellite estimates and the sparse surface observations in these regions. Shay-el and Alpert (1991) compute heat and moisture budgets as residuals from initialized ECMWF analyses to diagnose diabatic heating and net condensation rates over the Mediterranean and surrounding area.

The organization of tropical cloud clusters, squall-type and non-squall-type, into isolated deep precipitating convective cells and wide-spread cloud shields with stratiform rain has well been documented in the GATE experiment (see review by Houze and Betts, 1981). The convective-scale cumulus towers contain non-hydrostatic buoyant updrafts and negatively buoyant downdrafts and produce heavy rainfall. The mesoscale up- and downdrafts of the stratiform region are wide-spread, gentle and hydrostatic, produce lighter but wide-

spread precipitation and, in contrast to the convective updrafts which root in the boundary layer, are fed by mid-level convergence. Therefore, these two components make distinct contributions to the large-scale heat and moisture budget.

A set of equations for a spectral population of model clouds that have both convective and mesoscale vertical circulations was introduced by Houze et al. (1980) to diagnose the relative contributions of the various scales of up- and downdrafts to the large-scale vertical motion. In addition to the synoptic approach which uses radiosonde data to specify the left hand side of the heat and moisture budget equations, characteristics of precipitation patterns derived from weather radar and raingauge data are used as input to these equations in order to diagnose the mass transport spectrum, bulk mass and heat fluxes and the heat budget of the cloud ensemble. The radar approach constitutes an independent observational evaluation of the budgets. The sensitivity of the Houze et al. (1980) cloud population model to various parameters has been examined in a series of follow-up studies. The mass and heat fluxes associated with the convective-scale drafts are most sensitive to the definition of the cloud size – entrainment rate relationship assumed and the thermodynamic conditions at the updraft base (Cheng and Houze, 1980). The inclusion of mesoscale vertical air motion significantly influences the massflux characteristics of the entire system: The cloud ensemble mass flux at low levels is reduced in the presence of a mesoscale downdraft (Leary and Houze, 1980). Total mass fluxes are more dependent on the inclusion of mesoscale circulations than heat fluxes (Houze and Cheng, 1981). Gamache and Houze (1982) definitively confirmed the existence of the mesoscale updraft in which about 25% to 40% of the condensate of the anvil cloud is produced by condensation. Horizontal transfer of condensate from the convective region accounts for the remaining 60% to 75%. Composited fields of wind, vertical motion and humidity and the use of radar and satellite information established this water budget for the convective and stratiform regions from observations (Gamache and Houze, 1983). An important component of this budget is the transfer of ice particles detrained or left aloft by the deep convective towers to the stratiform cloud where they grow through deposition of water vapour condensed in the mesoscale updraft (seeder-feeder mechanism between convective and mesoscale components).

Houze (1982) designed a conceptual model which splits the *right* hand side of the heat budget equation into terms associated with convective and mesoscale updraft condensation and downdraft evaporation, heat fluxes by convective and mesoscale up- and downdrafts, melting of precipitation particles in the anvil region and radiation. Estimates of these terms are made by use of simple models for the drafts and hence vertical profiles of the contributions of the convective and mesoscale components of the cloud clusters to the heat budget are derived. It turns out that heating is determined primarily by the condensation and evaporation associated with the vertical air motions in both regions. The organization into a convective and a stratiform region has been found for a variety of mesoscale convective systems in tropical oceanic, tropical continental, subtropical oceanic and mid-latitude continental environments (Houze, 1989). The degree of organization reaches from the "classical" leading line, trailing stratiform squall line to chaotic arrangements (Houze et al., 1990).

Using radiosonde data Johnson and Young (1983) confirmed the vertical structure of the apparent heat source and apparent moisture sink of the mesoscale component of meso-

scale convective complexes suggested by the conceptual model of Houze (1982). Using the mesoscale profiles of Johnson and Young (1983) and assuming that 20% of total precipitation are falling from the mesoscale region, Johnson (1984) partitioned the heat and moisture budgets of Yanai et al. (1973) into convective-scale and mesoscale contributions. This method can be understood as partitioning the left hand side of Eqs. (4-1) and (4-2) into two parts without utilizing assumptions related to a cloud model. Partitioned heat and moisture budgets from radiosonde data have also been presented recently (Gallus and Johnson, 1991; Johnson and Bresch, 1991).

Provided appropriate data quality, consistent and simultaneous derivation of the thermodynamic (temperature and pressure) and microphysical variable fields (e.g., water vapour, cloud water and rain water) is possible through variational analysis of the whole set of the governing momentum, thermodynamic and microphysical equations with the wind field specified by dual-Doppler radar observations (Hauser et al., 1988). Given the fact that many squall line systems are almost steady state translation systems three-dimensional thermodynamic and water substance fields can even be derived from single-Doppler radar measurements (Roux and Sun, 1990). These methods have been developed and refined by studying squall lines observed during COPT81 over continental tropical Africa. Model derived radar reflectivity fields, low-level temperature perturbations and surface rainfall compare favourably with observations. The retrieved detailed kinematic, thermodynamic and microphysical fields can then be used to determine apparent heat source and apparent moisture sink of the entire system as well as contributions of the system's components, i.e. the convective-scale leading line and the mesoscale trailing stratiform region, and of the physical processes like latent heat release by water phase changes and vertical eddy transports (Chong and Hauser, 1990).

In summary, the partitioning of mesoscale convective systems into convective-scale and mesoscale components with distinct dynamical features has turned out to be essential for diagnostic studies. The formal framework of apparent heat source and apparent moisture sink provides a useful concept for diagnosing the effects of convective activity on its environment. Quantitative diagnostics have been derived from radiosonde data, aircraft data, conventional and Doppler radar data. Conceptual ideas about cloud ensemble models in combination with observed input data allow for the derivation of cumulus-scale and mesoscale vertical mass, heat and moisture transports.

The findings of these diagnostic studies have implications for the cumulus parameterization problem. Since the mesoscale circulation contributes significantly to total rainfall of mesoscale convective systems, the portion being dependent on the geographical region and the life history of the system, a cumulus parameterization scheme should in fact be able to properly determine the contributions to total heating from the cumulus-scale and the mesoscale components of the convective system (Johnson, 1984). A consequence of the mesoscale circulation features is warming, i.e. $\frac{\partial}{\partial t}\bar{s} > 0$, due to the mesoscale downdraft in the lower troposphere in contrast to the negative apparent heat source, i.e. $Q_1 < 0$, dominated by hydrometeor melting and evaporation. If the parameterization scheme does not correctly represent heating rates, resulting temperature fields can be in error (Johnson, 1986). In parallel to the diagnostic models of Yanai et al. (1973) and Ogura and Cho (1973) early

parameterization schemes using spectral cloud ensembles tend to represent only convective-scale clouds (Arakawa and Schubert, 1974).

4.2.3 The context of numerical weather prediction

In principal, there are three different ways of using observational data to test cumulus parameterization schemes: the purely diagnostic approach, the semi-prognostic and the fully prognostic approach.

Variants of the purely diagnostic approach have been described in the previous subsection. In a first approach observations are used to calculate the left hand side of Eqs. (4-1) and (4-2). Vertical profiles of warming and drying, of vertical eddy fluxes, of condensation and evaporation rates can be deduced through the cumulus parameterization on the right hand side of the budget equations from Q_1 and Q_2 together with estimates of the surface heat and moisture fluxes and the heating rate due to radiation. Since temperature and moisture tendencies have already been used for the determination of Q_1 and Q_2, this procedure is not capable of verifying the prognostic value of a parameterization scheme. Observations can also be used to determine the components of the parameterization scheme (vertical turbulent mass and heat fluxes, condensation and evaporation) as done by Houze (1982). Q_1 and Q_2 are then the result of the evaluation of the parameterization scheme and can be compared to independent observations.

In the semi-prognostic approach (Lord, 1982), advection terms, surface fluxes and radiative heating deduced from observations are used to make a one-step forecast which provides instantaneous values of Q_1 and Q_2. This approach does not use a NWP model explicitly and is therefore free from errors other than those of the parameterization scheme or observations. In contrast to the purely diagnostic approach, here calculated and observed Q_1 and Q_2 are not constrained to agree. The semi-prognostic study does not march in time and absolute statements about the validity of the parameterization scheme are therefore not possible. This method has extensively been used e.g. by Krishnamurti et al. (1980, 1983), Lord (1982), Kuo and Anthes (1984b), Bougeault (1985), Grell et al. (1991), among others. It is noteworthy that the semi-prognostic method tends to exaggerate the deficiencies of adjustment schemes, since the one-time-step procedure gives only the initial adaptation process.

Both the purely diagnostic and the semi-prognostic approach assume that convection is by far the most important source term on the right hand side of the budget equations.

For the fully prognostic approach the cumulus parameterization scheme is used within the framework of a complete prediction model. Observations are used to define an initial condition. Precipitation rates, heat and moisture budgets can then be derived at each model time step of the model integration. The performance of the parameterization scheme is assessed by comparison of instantaneous or time averaged values of precipitation, heat and moisture budgets to observations. It is difficult or even impossible to isolate errors caused by the convective parameterization scheme from errors caused by other components of the model (parameterization schemes of other physical processes, initialization, numerical methods). It has to be borne in mind that the different parameterization schemes also interact.

The so-called single column test (Betts and Miller, 1986; Tiedtke, 1989) combines features of the semi-prognostic and the fully prognostic approaches. In this case, adiabatic tendencies, surface heat and moisture fluxes and radiative heating is specified as in the semi-prognostic tests, but the numerical model is integrated in time, i.e. the cumulus parameterization scheme is allowed to modify the temperature and moisture field through heating and moistening. The examination of the evolution of the vertical thermodynamic structure in the column ("model sounding") is of particular interest, since it reflects the time averaged effect of heating and moistening. These profiles as well as model derived apparent heat source and moisture sink can be compared to observations.

The essence of the diagnostic procedure introduced in the present study is to calculate the value of each individual term in the thermodynamic and moisture equation right after the prognostic step. This allows to determine classical heat and moisture budgets in a fully prognostic mode on one hand, on the other hand the influence of every process active in the model can be diagnosed. There is no a priori restriction to convectively dominated situations and no simplifying assumptions are required. Examination of the relative importance of the physical tendencies in the prognostic equations reveals which processes contribute the most to the development of the model atmosphere. This way, the impact of changes to the parameterization of convection can be monitored and the interaction with other parameterization schemes becomes apparent.

An interesting aspect of establishing heat and moisture budgets of a NWP model is to partition Q_1/Q_2 into contributions from subgrid-scale (i.e. cumulus parameterization) and grid-scale precipitation formation processes ($Q_{1/2}^{cum}$ and $Q_{1/2}^{grid}$). Comparison with observed structures of $Q_{1/2}^{conv}$ and $Q_{1/2}^{meso}$ would be indicative of the correspondence between observed convective-scale and parameterized subgrid-scale processes on one hand and observed mesoscale and parameterized grid-scale processes on the other hand. E.g. it could be figured out whether the cumulus parameterization scheme has a similar influence on the model atmosphere as the convective scale processes in a real convective system have on the real atmosphere, and analogously for the stratiform precipitation part.

4.3 Application to a NWP model

Some more formal considerations are necessary in order to properly elaborate the heat and moisture budgets of a NWP model. Applying the budget concept on a NWP model enables the comparison of model results with observations. In this section the appropriate formalism with respect to the Europa Modell (EM) of the Deutscher Wetterdienst (Majewski, 1991) is developed. The resulting diagnostic tool will later be applied to investigate aspects of the convective parameterization scheme embedded in this model.

4.3.1 Heat and moisture budgets of a NWP model

For a NWP model the grid-scale properties of a meteorological variable ψ can be defined by the following averaging operator (Reynolds averaging)

$$\overline{\psi}(x,y) = \frac{1}{\Delta x \Delta y} \int_{(x-0.5\Delta x)}^{(x+0.5\Delta x)} \int_{(y-0.5\Delta y)}^{(y+0.5\Delta y)} \psi dx dy, \tag{4-6}$$

where Δx and Δy are the averaging intervals in the x and y directions and are taken to be the mesh size of the model (Anthes, 1977). $\overline{\psi}$ is a "running" mean in space and varies continuously from point to point. The subgrid-scale deviation from $\overline{\psi}$ is denoted by ψ', so that

$$\psi(x,y) = \overline{\psi}(x,y) + \psi'(x,y) \text{ and } \overline{\psi'} = 0 \text{ by definition.} \tag{4-7}$$

Strict application of these definitions to the prognostic thermodynamic and moisture equations formulated in temperature (T) and specific water vapour mixing ratio (q_v) yields

$$\frac{Q_1}{c_p} = \frac{\partial \overline{T}}{\partial t} + \overline{\vec{v}} \bullet \nabla \overline{T} + \overline{\dot{\eta}} \frac{\partial \overline{T}}{\partial \eta} - \frac{\overline{\alpha\omega}}{c_p} = -\nabla \bullet \overline{\vec{v}'T'} - \frac{\partial}{\partial \eta}(\overline{\dot{\eta}'T'}) + \frac{L_v}{c_p}\bar{c} + \frac{\overline{\alpha'\omega'}}{c_p} + \frac{Q_R}{c_p} \tag{4-8}$$

$$-\frac{Q_2}{L_v} = \frac{\partial \overline{q_v}}{\partial t} + \overline{\vec{v}} \bullet \nabla \overline{q_v} + \overline{\dot{\eta}} \frac{\partial \overline{q_v}}{\partial \eta} = -\nabla \bullet \overline{\vec{v}' q'_v} - \frac{\partial}{\partial \eta}(\overline{\dot{\eta}' q'_v}) - \bar{c} \tag{4-9}$$

where a hybrid vertical coordinate η has been used. The individual terms on the left hand side of the equations stand for local time tendency (also referred to as Eulerian tendency or storage term), horizontal advection, vertical advection and the adiabatic energy conversion term $\alpha\omega$ in the thermodynamic equation ($\alpha = RT_v/p$, where R is the gas constant for dry air, T_v is the virtual temperature and p is pressure, ω is the vertical p-velocity). Note that the energy conversion term is not present in the thermodynamic equation if potential temperature, dry or moist static energy is used as prognostic variable (cf. Eq. (4-1)). On the right hand side we have horizontal convergence of horizontal eddy fluxes, vertical convergence of vertical eddy fluxes, net (grid-scale) condensation, and for the thermodynamic equation the energy conversion of eddy vertical fluxes and radiative heating. Since the mean quantities $\overline{\psi}$ slightly vary over the averaging area, mixed terms of the form $-\nabla \overline{\vec{v}'\psi}$, e.g., are not exactly zero, but are most often neglected (Anthes, 1977).

In diagnostic studies or investigations concentrating on the cumulus parameterization problem, horizontal eddy flux terms on the right hand side are generally ignored be-

cause the covariances between the perturbations of the temperature and moisture field on one hand and the velocity fluctuations on the other hand are assumed to be small. Vertical eddy transports, condensation and energy conversion are then fully attributed to the cumulus activity. In agreement with the observational finding that mesoscale convective systems consist of a cumulus-scale convective part and a mesoscale stratiform part vertical transports and net condensation rates could be separated into parts corresponding to these distinct features.

Addition of Eqs. (4-8) and (4-9) gives an equation for total enthalpy $h=c_pT+L_vq_v$:

$$Q_1 - Q_2 = \frac{\partial \bar{h}}{\partial t} + \bar{\vec{v}} \bullet \nabla \bar{h} + \bar{\dot{\eta}} \frac{\partial \bar{h}}{\partial \eta} - \bar{\alpha}\bar{\omega} = -\nabla \bullet \overline{\vec{v}'h'} - \frac{\partial}{\partial \eta}(\overline{\dot{\eta}'h'}) + \overline{\alpha'\omega'} + Q_R \quad (4\text{-}10)$$

Most important is the elimination of the condensation term in Eq. (4-10). In contrast to Eq. (4-3) the energy conversion terms are retained.

Next, prognostic equations for T and q_v are written in a manner that conforms to a NWP model:

$$Q_1 =$$

$$c_p\left(\frac{\partial \bar{T}}{\partial t} + \bar{\vec{v}} \bullet \nabla \bar{T} + \bar{\dot{\eta}} \frac{\partial \bar{T}}{\partial \eta}\right) - \bar{\alpha}\bar{\omega} = F_s^H - g\frac{\partial \eta_s}{\partial p} + \left.\frac{\partial s}{\partial t}\right|_{cum} + \left.\frac{\partial s}{\partial t}\right|_{grid} + L_v S_{COND} + \left.\frac{\partial s}{\partial t}\right|_{rad} \quad (4\text{-}11)$$

$$-\frac{Q_2}{L_v} =$$

$$\frac{\partial \overline{q_v}}{\partial t} + \bar{\vec{v}} \bullet \nabla \overline{q_v} + \bar{\dot{\eta}} \frac{\partial \overline{q_v}}{\partial \eta} = F_{q_v}^H - g\frac{\partial \eta_{q_v}}{\partial p} + \left.\frac{\partial q_v}{\partial t}\right|_{cum} + \left.\frac{\partial q_v}{\partial t}\right|_{grid} - S_{COND} \quad (4\text{-}12)$$

The left hand sides correspond exactly to Eqs. (4-8) and (4-9). Source terms on the right hand side are horizontal diffusion, vertical diffusion, local tendencies due to subgrid-scale cumulus convection, grid-scale parameterized cloud physics, grid-scale condensation (S_{COND}) and radiation in the thermodynamic equation (limited area models also have a boundary relaxation term which is not indicated here). For reasons which will become apparent in the next subsection, the grid-scale condensation rate is explicitly written and not included in the cloud physics parameterization. Assuming that diffusion and the other physical processes do not modify the geopotential field directly it is often more convenient to formulate the source terms on the right hand side of the thermodynamic equation in terms of a conserved quantity like dry static energy (s). Comparison of the general budget equations (4-8) and (4-9) with the NWP equations (4-11) and (4-12) suggests the following correspondence between terms on the right hand side and their association with physical processes:

1.) Horizontal convergence of subgrid-scale horizontal eddy fluxes can be associated with horizontal diffusion in the NWP model.

2.) The cumulus parameterization scheme in general simulates vertical eddy transports and condensation which both modify the temperature and moisture structure. Only the bulk effect is transmitted to the prognostic model equations. Interference with the vertical diffusion scheme is probable. It is therefore argued that vertical eddy flux divergence in the budget equations is partly represented by the parameterized convection scheme and partly by the vertical diffusion scheme of the model. A strict separation is impossible.

3.) If only subgrid-scale convection were active, the effect of condensation on the temperature and moisture field would be fully represented by the convective parameterization term. The cloud physics term is reserved to represent precipitation-forming processes on the grid scale, excluding phase transitions between water vapour and cloud water. In the budget equations the net condensation rate should be split into contributions from cumulus convection and stratiform condensation as suggested by the circulation features of mesoscale convective complexes. Cloud physics can also incorporate ice phase processes and a wealth of conversion rates which can be introduced into the budget equations by additional source terms (e.g., Houze, 1982; Johnson and Young, 1983; Gallus and Johnson, 1991).

4.) The correspondence of the radiation term in the thermodynamic equations is obvious.

From these considerations it appears natural to partition the model budgets into subgrid-scale contributions $Q_{1/2}{}^{\mathrm{cum}}$ defined by the cumulus parameterization tendencies and grid-scale contributions $Q_{1/2}{}^{\mathrm{grid}}$ defined by the cloud physics processes and grid-scale condensation.

Adding Eq. (4-12) to Eq. (4-11) yields a prognostic equation for total enthalpy (h) corresponding to the budget equation (4-10):

$$Q_1 - Q_2 =$$

$$\frac{\partial \bar{h}}{\partial t} + \bar{\vec{v}} \bullet \nabla \bar{h} + \bar{\dot{\eta}} \frac{\partial \bar{h}}{\partial \eta} - \bar{\alpha}\bar{\omega} = F^{\mathrm{H}}_{h_p} - g \frac{\partial \eta_{h_p}}{\partial p} + \left.\frac{\partial h_p}{\partial t}\right|_{\mathrm{cum}} + \left.\frac{\partial h_p}{\partial t}\right|_{\mathrm{grid}} + \left.\frac{\partial h_p}{\partial t}\right|_{\mathrm{rad}} \qquad (4\text{-}13)$$

On the right hand side, which is expressed in moist static energy (h_p), the grid-scale local tendency only represents ice phase processes, since conversion rates connected to the latent heat of vaporization (L_v) do not affect the total enthalpy content of an air parcel. For the same reason no grid-scale condensation term occurs. In parallel with Eq. (4-10) and in contrast to Eq. (4-3) the $\alpha\omega$-term is present on the left hand side. It is worth noting that each term in Eqs. (4-11)- (4-13) has to be represented in a form which allows for linear combination of two of the three variables T (s), q_v and h (h_p) in order to provide a physically correct and consistent representation.

Eq. (4-13) is the thermodynamic prognostic equation of EM. The associated prognostic moisture equation is formulated in specific total water content (q_{vc}), which is the sum of specific water vapour content (q_v) and specific cloud (liquid) water content (q_c), i.e. $q_{vc}=q_v+q_c$. The corresponding prognostic equation reads

$$\frac{\partial}{\partial t}\overline{q_{vc}}+\bar{\vec{v}}\bullet\nabla\overline{q_{vc}}+\bar{\dot{\eta}}\frac{\partial}{\partial\eta}\overline{q_{vc}} \quad =F^{H}_{q_{vc}}-g\overline{\frac{\partial\eta_{q_{vc}}}{\partial p}}+\overline{\frac{\partial q_{vc}}{\partial t}}\Big|_{cum}+\overline{\frac{\partial q_{vc}}{\partial t}}\Big|_{grid} \tag{4-14}$$

Again, condensation of water vapour and evaporation of cloud water do not change the total specific water content and therefore the grid-scale condensation term is absent.

A schematic representation of the grid-scale precipitation-forming processes used in EM is given in Fig. 3-1 and the corresponding thermodynamic and moisture tendencies for the prognostic (h, q_{vc})-equations are given in Eqs. (3-5) and (3-6). We now write the grid-scale tendencies for the prognostic equations of the budget variables and include the net condensation rates to get the grid-scale partition of the apparent heat source and moisture sink:

$$Q_1^{grid}=\overline{\frac{\partial s}{\partial t}}\Big|_{grid}+L_v\bar{c}=$$

$$L_v\,(S_{DEP}-S_{EVAP})+L_f\,(S_{DEP}+S_{RIM}+S_{NUC}-S_{MELT})+L_v S_{COND} \tag{4-15}$$

$$Q_2^{grid}=-L_v\,(\overline{\frac{\partial q_v}{\partial t}}\Big|_{grid}-\bar{c})=-L_v\,(-S_{DEP}+S_{EVAP}-S_{COND}) \tag{4-16}$$

where the S-terms represent rates of deposition (DEP), evaporation of rain drops (EVAP), riming (RIM), nucleation (NUC), melting of frozen particles (MELT) and condensation/ evaporation of vapour/cloud water (COND). L_v and L_f are latent heats of vaporization and fusion.

Given the convective adjustment scheme of EM, the subgrid-scale partition of the apparent heat source and moisture sink are defined by

$$Q_1^{cum} = \frac{1}{\tau}c_p\Delta T^{cum} \tag{4-17}$$

$$Q_2^{cum} = \frac{1}{\tau}(-L_v)\,\Delta q_v^{cum} \tag{4-18}$$

where τ is the convective adjustment time scale and ΔT^{cum} and Δq_v^{cum} are the differences of the temperature and humidity structures between the reference state and the actual state.

4.3.2 A note on condensation rates

There exists a fundamental difference in handling condensation rates between prognostic systems formulated in thermodynamic and moisture variables which are unaffected by phase changes of water between vapour and liquid like h, h_p, θ_e, q_{vc} and systems which use variables like T, s, θ, q_v, q_c. For convenience the first category is called (h, q_{vc})-systems and the second category (T, q_v)-systems.

The prognostic equations of EM belong to the (h, q_{vc})-family and therefore do not contain condensation terms (Eqs. (4-13) and (4-14)). The phase transition between water vapour and cloud water is an internal process in the (h, q_{vc})-system. During the integration of the (h, q_{vc})-equations a condensation rate has never to be explicitly calculated. The common meteorological variables temperature, specific water vapour and cloud water content can be diagnosed from h and q_{vc} with the use of the water vapour saturation criterion, i.e. assuming that clouds only exist, when the air is saturated at the corresponding temperature. Hence the resulting temperature and humidity fields are a priori balanced with respect to water vapour saturation.

In contrast, integration of a (T, q_v)-set of equations does not yield balanced temperature and moisture fields in general. Rather a first guess pair of values (T^{*n+1}, q_v^{*n+1}) is obtained by a prognostic step (n+1 denotes the time level). Adjustment increments have then to be computed in order to get balanced fields with respect to water vapour saturation (Haltiner and Williams, 1980):

$$q_v^{*n+1} + \delta q_v = q_{v,s}^{n+1}(T^{*n+1} + \delta T, p) = q_{v,s}^{n+1}(T^{n+1}, p) \text{ and} \tag{4-19}$$

$$(-L_v)\,\delta q_v = c_p \delta T \tag{4-20}$$

Subscript "s" denotes water vapour saturation. Thus in a moist atmosphere, one is forced to calculate condensation rates as adjustment increments in a (T, q_v)-system in order to maintain a balanced state with respect to temperature and humidity. This adjustment procedure does not allow the determination of the process (or processes) responsible for condensation, since the predicted first guess values (T^{*n+1}, q_v^{*n+1}) are already the result of all processes active in the model. In general, it is impossible to attribute a certain part of the overall condensation rate to, e.g., vertical advection or convective mixing. It is worth noting that the problem cannot be circumvented by procedures like multiple execution of the prognostic step, once using the full prognostic equation and then cyclically omitting one single term. Partial condensation rates calculated this way do not sum up to the total condensation rate. However, (T, q_v)-systems allow for so-called "no latent heat" experiments, in which supersaturation is determined with respect to the first guess temperature value T^{*n+1} and condensate is removed, but the temperature field remains unaffected.

The very elegant, implicit treatment of condensation in (h, q_{vc})-systems renders budget considerations in terms of apparent heat source and apparent moisture sink, where condensation plays a crucial role, more difficult. Whilst computation of condensation is necessary in a (T, q_v)-system, special measures have to be taken to retrieve it from a (h, q_{vc})-system. "No latent heat" runs for (h, q_{vc})-systems are not trivial at all.

4.3.3 Formal aspects of heat and moisture budgets from EM

Consideration of heat and moisture budgets of EM which is formulated as a (h, q_{vc})-system first necessitates the computation of condensation/evaporation rates. This can be achieved with the following procedure:

1.) Integrate EM for one time step.

2.) Diagnose (T^{n+1}, q_v^{n+1}) from (h^{n+1}, q_{vc}^{n+1}).

3.) Insert (T^{n+1}, q_v^{n+1}) into the auxiliary (T, q_v)-set of prognostic equations which has to be discretized identically to the (h, q_{vc})-set of EM. Thus the magnitude of each term in the (T, q_v)-equations is determined.

4.) Compute S_{COND} as a residual of the (T, q_v)-equations.

The rationale for the above method is as follows: Integration of the prognostic EM equations (4-13) and (4-14) for one time step yields a pair of values (h^{n+1}, q_{vc}^{n+1}) which, by construction, solves the discretized form of these equations in a numerically exact sense. The variables (T^{n+1}, q_v^{n+1}) are diagnosed from (h^{n+1}, q_{vc}^{n+1}) and are adjusted with respect to water vapour saturation. They solve the Eqs. (4-11) and (4-12) in a numerically exact sense, if the same numerical discretization is used. The (T, q_v)-set of equations can be conceived as a linear decomposition of the h-equation. Thus the condensation rate S_{COND} can be computed as a residual from Eq. (4-11) and Eq. (4-12) independently, if all the other terms in the equations are diagnostically calculated after the prognostic step. Comparison of the S_{COND}-residuals from the T- and the q_v-equation allows for an accuracy check of the calculation.

This rather expensive method to retrieve condensation rates from a (h, q_{vc})-system at the same time provides a powerful and complete diagnostic tool for the examination of the evolution of the model atmosphere, since the amplitudes of all processes, including advection, diffusion and all physical parameterizations are computed. In fact, as soon as an implicit time integration scheme is chosen for any term in the prognostic equation (most often used for vertical advection and vertical diffusion), the diagnostic reconstruction of the prognostic equation is the only way of monitoring all processes, even in a (T, q_v)-system. Once S_{COND} is computed, it could be subtracted from T^{n+1} in order to get a "no latent heat value" T^{*n+1} in the (h, q_{vc})-system. In practice, the method is probably too costly in terms of computer memory and time to reconstruct the prognostic equations in the whole integration domain after each time step in order to carry out real "no latent heat" runs.

Since condensation rates emerge as residuals of a highly complex numerical procedure, careful examination of the computational accuracy and the correctness of the code are essential. In the (h, q_{vc})-system or at grid points where no condensation takes place vanishing residuals have to be expected. But calculation of small differences of large numbers causes loss of significance in computational procedures and therefore non-vanishing residuals will result. Therefore, checking the significance of residuals in the above method is important. A convenient relation for testing the significance of residuals is given by

$$\Delta(\text{o.m.}) := \log_{10}\left(\frac{\max\left(|\psi|, |\text{expression}\ (\psi)|\right)}{|\text{residual}\ (\psi)|}\right) > \mathcal{N} \qquad (4\text{-}21)$$

where $\mathcal{N}$ is the number of significant decimals defined by the internal representation of floating point numbers (e.g., $\mathcal{N}$=15 for the 48-bit mantissa in Cray machines). Expression (4-21) describes the difference in orders of magnitude (Δ(o.m.)) between the largest value or expression occurring in the ψ-equation and the residual obtained for that equation, where ψ stands for h, q_{vc}, T or q_v. For instance, if h is O(5) and $\mathcal{N}$=15 then residuals smaller than O(-10) are insignificant.

Diagnostic numerically exact reconstruction of the model equations requires that the time stepping procedure has strictly to be followed. The time stepping procedure of EM consists of four steps (n-1, n, n+1 denote the respective time levels, Δt is the time step):

1.) Explicit step (without boundary relaxation):

$$\psi_{ex}^{n+1} = \psi^{n-1} + A(\hat{\psi}^{n})\,2\Delta t + B(\psi^{n-1}, \psi_{ex}^{n+1})\,2\Delta t + C(\psi^{n-1})\,2\Delta t \qquad (4\text{-}22)$$

where
A: horizontal advection, horizontal diffusion, geostrophic adjustment (momentum equation)
B: vertical advection, vertical turbulent transport
C: parameterized convection, cloud physical terms and radiation

2.) Semi-implicit correction:

$$\tilde{\psi}^{n+1} = \psi_{ex}^{n+1} + (\Delta\psi)_{SI} \qquad (4\text{-}23)$$

3.) Boundary relaxation:

$$\hat{\psi}^{n+1} = (1-\alpha_\mu)\,\tilde{\psi}^{n+1} + \alpha_\mu \bar{\psi}^{n+1}, \text{ where } \alpha_\mu = \frac{2\Delta t \mu_R}{1 + 2\Delta t \mu_R} \qquad (4\text{-}24)$$

$\bar{\psi}^{n+1}$ is the boundary value and μ_R the boundary relaxation coefficient.

4.) Asselin time filter:

$$\psi^{n} = \hat{\psi}^{n} + \gamma(\hat{\psi}^{n+1} - 2\hat{\psi}^{n} + \psi^{n-1}), \quad \text{where } \gamma \text{ is the filter constant.} \qquad (4\text{-}25)$$

In particular, the semi-implicitly corrected values after step 2 do not satisfy the discretized explicit equations. Running the model in an explicit mode, i.e. choosing a smaller time step and omitting step 2, shows that postponed boundary relaxation (step 3 after step 1) and simultaneous boundary relaxation are not identical. Simultaneous boundary relaxation is defined by including the boundary relaxation term in the equations of step 1 (EUM scheme, Müller et al., 1987). A condensation rate, conceived as the adjustment increment to balance T- and q_v-values with respect to water vapour saturation, can be attributed to the explicit prediction step, the semi-implicit correction and the boundary relaxation step. Whether all of them are significant contributions to the heat and moisture budgets will be answered by the experiments.

4.3.4 The complete diagnostic procedure

Having solved the formal and technical problems to retrieve condensation rates from a (h, q_{vc})-system we are now in the position to set up the complete diagnostic procedure to build heat and moisture budgets for events simulated by the numerical model.

In general, potentially interesting (precipitation) systems move through the model domain changing their shape continuously. In order to establish meaningful heat and moisture budgets from such systems a tracking mechanism must be available. The following procedure has been implemented:

For any time step during a model run a rectangular frame encompassing the meteorological system of interest can be defined, within which all quantities necessary for the computation of the budgets are calculated and stored. Before post-processing a grid point mask for each of these frames can be set up depicting the points selected for further evaluation. For this set of grid points vertical interpolation (linear or spline) from hybrid to pressure levels is applied prior to horizontal averaging.

In summary, the following steps have to be carried out:

1.) First EM run: basic prediction (the operational forecast, e.g.).

2.) Selection of time steps and subdomains containing the "event of interest" (a convective complex, e.g.).

3.) Second EM run: diagnostic computation of all terms of the prognostic equations at all grid points defined by step 2.

4.) Definition of grid point masks within the diagnosed subdomains: any selection criteria can be introduced to establish a mask, e.g. grid points with a certain minimum rainfall rate.

5.) Calculation of quantities deduced from the terms of the equation grid point by grid point (e.g. budget quantities from Eqs. (4-11), (4-12), (4-15), (4-16), (4-17), (4-18)).

6.) Vertical interpolation of all quantities at each grid point on pressure or height levels.

7.) Horizontal averaging over the masked grid points on pressure or height levels.

This procedure constitutes a versatile and powerful tool to monitor the evolution of the model atmosphere by determining the contributions of all dynamical and physical processes in the prognostic thermodynamic and moisture equation.

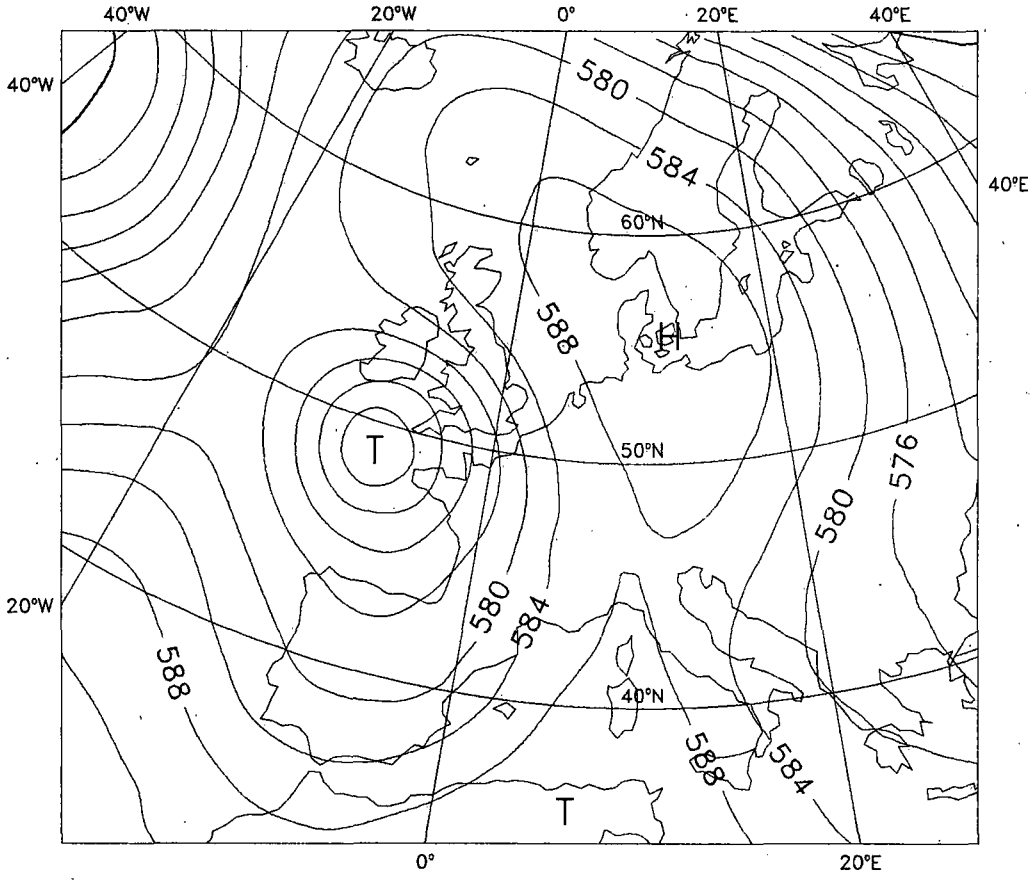

Fig. 4-1: 500hPa geopotential height field simulated by JUL91/EM3/EH 6 July 1991 12UTC +6h.The isoline interval is 4 geopotential decameters.

4.4 Case studies of precipitation events: Scale and parameterization dependencies of physical tendencies

After the formal development and the discussion of some technical aspects of the diagnostic tool, results of its application to model simulations will be presented in this section. Emphasis is put on the scale and parameterization dependency of the tendencies of convective activity and grid-scale precipitation-forming processes, but since the diagnostic tool allows the monitoring of the full prognostic equations, the discussion is not confined to heat and moisture budgets. We will primarily concentrate on the weather situation of 6/7 July 1991, aspects of which have already been discussed in the previous chapter.

The present study contrasts in several aspects to most studies of convective systems reported in the literature. No special analyses based on enhanced observational networks and/or special observational equipment as operated in field experiments are available to accurately describe real atmospheric conditions for the cases presented. In section 3.4 it has been recognized that the numerical simulations of the JUL91 case were not particularly successful and depended strongly on the convective parameterization scheme used (see Fig. 3-10). Therefore, the main interest of this study is directed towards the investigation of the internal development of the model atmosphere in relation to its dependency on the particular parameterization scheme used and, in addition, on horizontal grid distance.

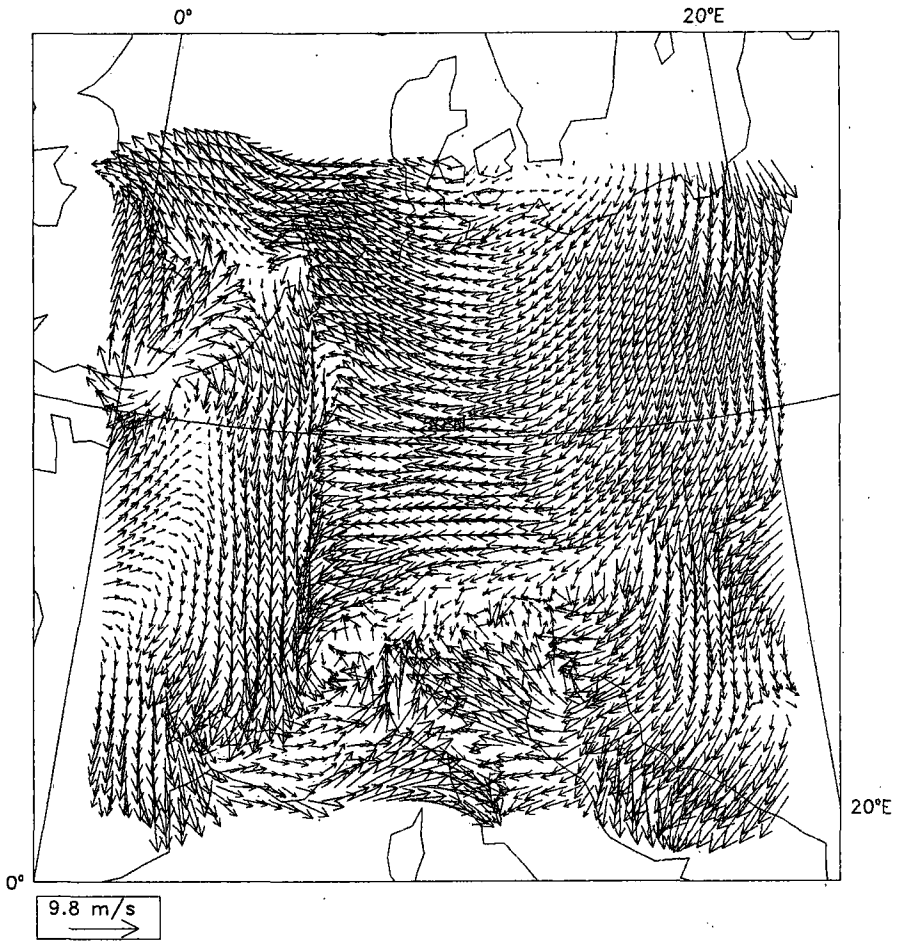

Fig. 4-2: Wind field on the lowest model level simulated by JUL91/HM8/MX 6 July 1991 12UTC +6h. Arrows are plotted every second model grid point.

4.4.1 Parameterization dependency of the vertical structure of partitioned heat and moisture budgets: Aspects of the life cycle

First an examination is undertaken of the principal features of the life cycle of convective precipitation systems simulated by the HM8 high-resolution model configuration. The experiments JUL91/HM8/MX and JUL91/HM8/EH are compared. Refer to Table 3-4 and the associated references for the detailed specification of these model runs.

The prevailing Ω-pattern of the 500hPa geopotential height field on 6 July 1991 18UTC becomes apparent in Fig. 4-1. The Alps are located in the weak gradient region at the southern exit of the Ω. The surface wind field exhibits a rather complex pattern as revealed by the JUL91/HM8/MX run after +6 hours simulation time (Fig. 4-2). Generally weak winds prevail over the Alps. North of the Alps there is a distinct easterly flow in the boundary layer. A northerly airstream flows from the Dutch coast to the Gulf of Lyon, leading to strong horizontal shear with the easterly flow over eastern France. In addition, strong vertical shear exists between the northerly low-level and the southerly upper-level flow (Fig. 4-1).

Both high-resolution experiments, JUL91/HM8/**MX** and JUL91/HM8/**EH**, simulated convective systems during the evening of 6 July 1991, although the timing and position-

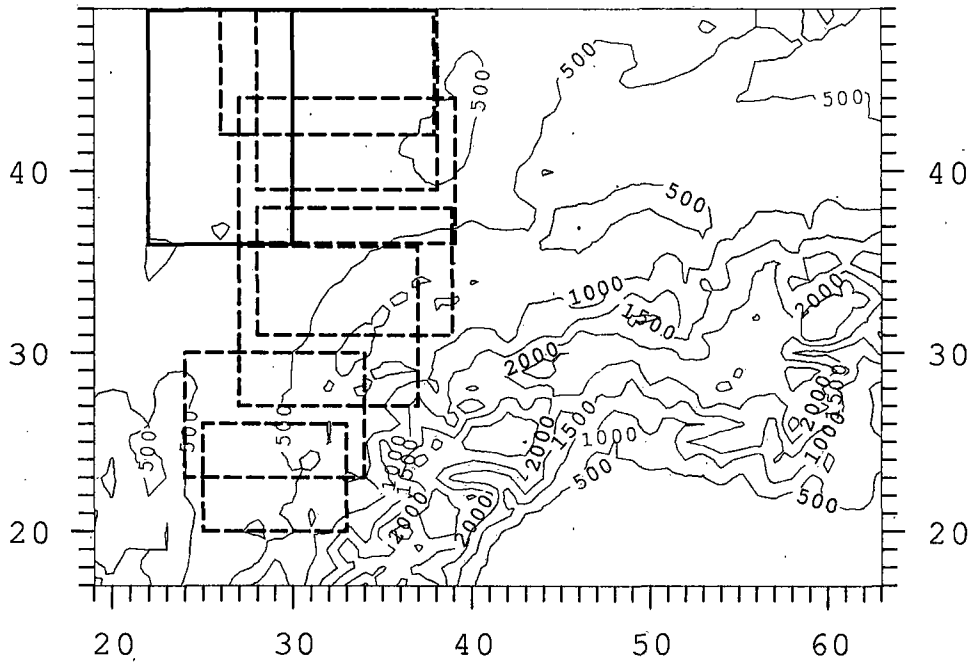

Fig. 4-3: Window of the HM8 integration domain with an indication of the local orography. The solid and dashed frames encompass the area where the convective system of the JUL91/HM8/MX and JUL91/HM8/EH runs occurred respectively. The second system moved through the domain. Frames are plotted at one hourly intervals. Grid point numbering is indicated on the axes.

ing of the convection was different for the two runs. In the MX experiment a convective system occurred in the north-western part of the region outlined in Fig. 4-3 after about +8 hours of simulation time. This system did not move appreciably but rather remained within the top-left frame in Fig. 4-3 for the next few hours. In the EH run convection developed in a more southerly position soon after the start of the integration at 6 July 1991 12UTC. This system moved northwards as time went on. The series of encompassing frames used to track the system is displayed in Fig. 4-3 as well. The first and southern most frame corresponds to +2 hours simulation time, the last and northern most frame to +9 hours simulation time.

The vertical thermodynamic structure of the model atmosphere at the early stage of the respective convective systems is given by the soundings in Fig. 4-4, which represent area averages over the grid points of the first frames indicated in Fig. 4-3. There are several common features to be recognized: The atmosphere below 750hPa is dry. The mean sounding associated with the MX run exhibits a stable layer just below 825hPa. Solar heating at the surface established a well mixed layer up to about 900hPa. In contrast, the dry adiabatic lapse-rate extends from the surface up to about 800hPa in the EH experiment (in a different location of the integration domain!). In both simulations the sharp wind shear appears at 825hPa, turning from northerly directions below to southerly directions above. The MX atmosphere has highest relative humidity between 500hPa and 600hPa where some clouds exist. This cloud layer is almost 200hPa lower in the EH case. Above the cloud layer the model atmosphere is very dry in both simulations. Above the level with maximum vertical

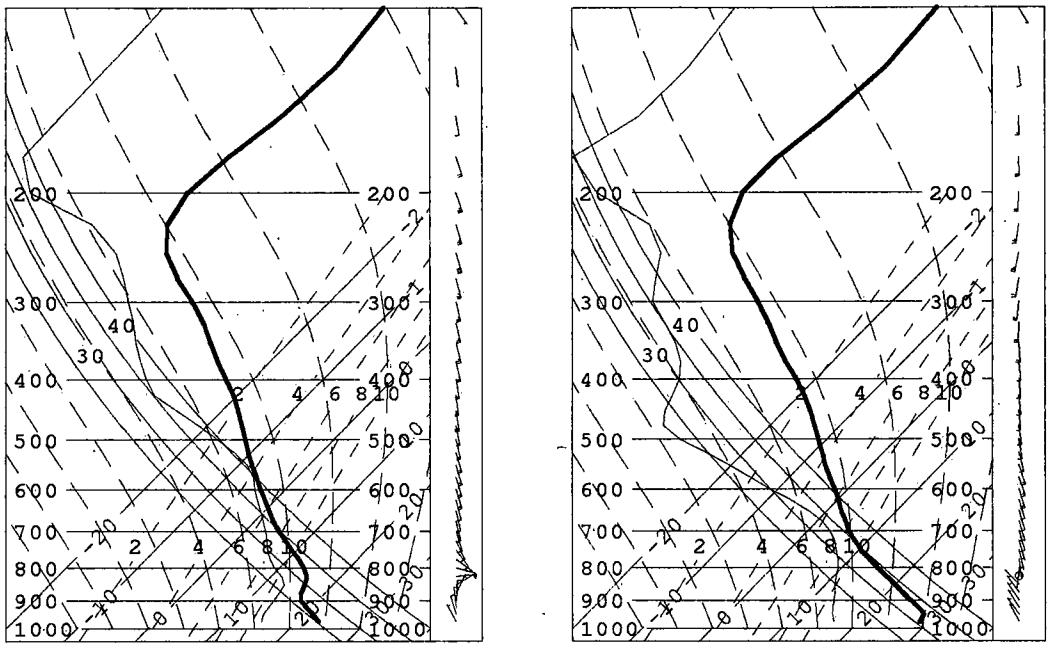

Fig. 4-4: Area average soundings in the early stage of the convective events in the experiments JUL91/HM8/MX (left) and JUL91/HM8/EH (right): Temperature (bold) and dew point soundings (thin) are plotted on a skew *T-log(p)* diagram which contains lines of constant pressure, temperature, potential temperature (dry adiabats), equivalent potential temperature (pseudoadiabats) and lines of constant water vapour mixing ratio. Each full barb of the wind flag represents $10 m s^{-1}$.

wind shear a deep layer with an unstable lapse-rate with respect to the pseudoadiabat is found in both experiments.

a.) Early stage

In the early stage of convective activity, the apparent heat source and apparent moisture sink are dominated by the temperature and moisture tendencies produced by the convective parameterization scheme. Fig. 4-5 shows the "event-average" vertical budget profiles for the MX experiment at simulation time +8h. The "event average" is calculated over all grid points within the tracking frame where the instantaneous precipitation rate exceeds $0.3 kg m^{-2} h^{-1}$ which corresponds to the first radar intensity level (cf. Table 3-6). At that time only convective rain precipitates ($0.7 kg m^{-2} h^{-1}$) and convective overturning takes place in the layer between 775hPa and 350hPa. In the convection domain the apparent heat source (Q_1) is almost completely determined by the subgrid-scale contribution. Only in the cloud layer around 550hPa grid-scale condensation adds a little bit of latent heating. Radiative cooling (not shown) reduces heating in this layer. Net heating prevails in the convection domain except in the layer at the very bottom and at the top. It is noteworthy that with the adjustment type scheme of convective parameterization contributions of convective condensation and vertical eddy transport can not be distinguished. Below the base of the convection domain cooling is mainly due to evaporation of convective rain in the dry boundary layer (cf. Fig. 4-4). The apparent moisture sink exhibits drying in the lower part and moistening in the upper part of the convection domain (Fig. 4-5). Again the Q_2 profile

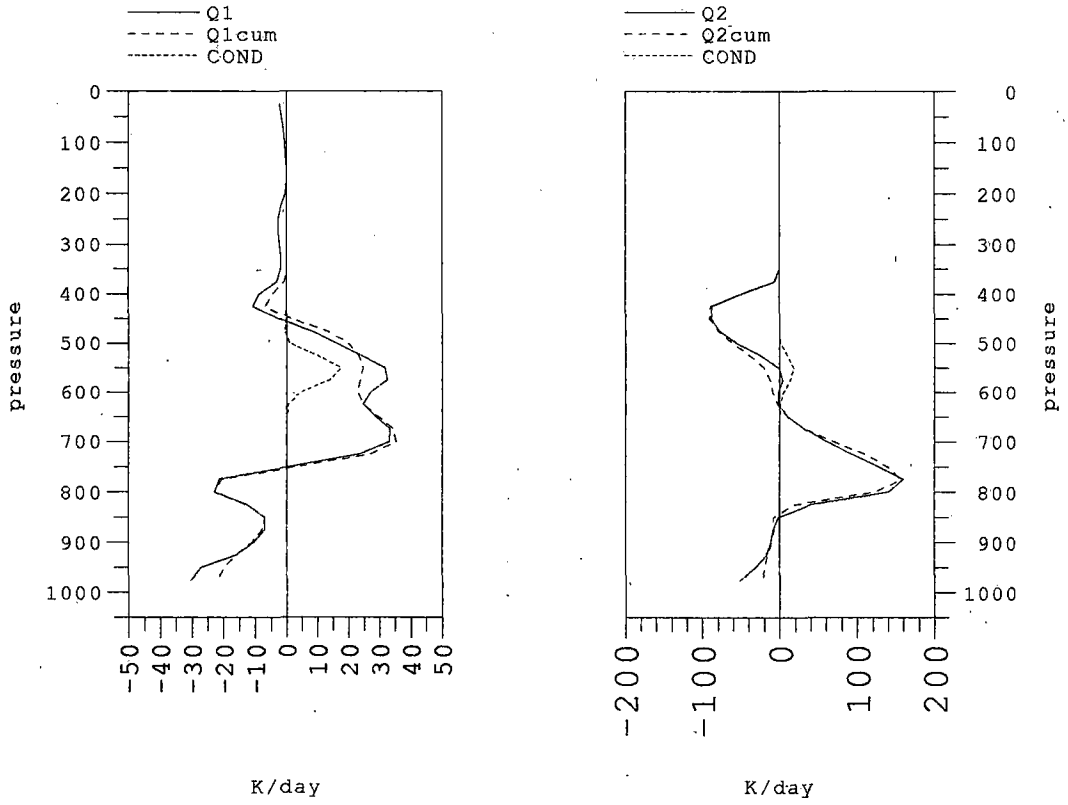

Fig. 4-5: Early stage apparent heat source (left panel) and apparent moisture sink of JUL91/HM8/MX at simulation time +8h (verification time 6 July 1991 20UTC). Solid: budget quantities; long dashed: contributions from convective parameterization; short dashes: grid-scale condensation rate. Note the different scaling. The convection domain extends from approximately 775hPa to 350hPa.

is essentially determined by the contribution of the convection scheme. Apparent heating and moistening rates of the order of $10^2 K day^{-1}$ are very large values. But if they are normalized to 1cm precipitation per day, as is usually done in the literature, we get for the peak rate in the moisture budget about $10 K day^{-1}/(cm day^{-1})$, which is well within the range of published values. The point is that the basic values used to build the ratio are much larger than those obtained from larger-scale studies. As noted by Kuo and Anthes (1984a) in their mesoscale observational study, the amplitudes of the budget quantities increase with decreasing spatial and temporal scale. In the present study instantaneous grid point values of a model with approximately 14km horizontal resolution and a time step of 75s are considered. The resulting values can not be directly compared to values reported in the literature, which most often examine budgets averaged over several tens of kilometers and several hours duration. Therefore more emphasis will be put on the vertical structures rather than on absolute values.

Approximately the same amount of precipitation as in the MX experiment is falling after +2h simulation time in the JUL91/HM8/EH experiment ($0.8 kg m^{-2} h^{-1}$). The convection domain extends from 800hPa to 425hPa. The main contribution to the apparent heat source and apparent moisture sink are also provided by the developing convective activity

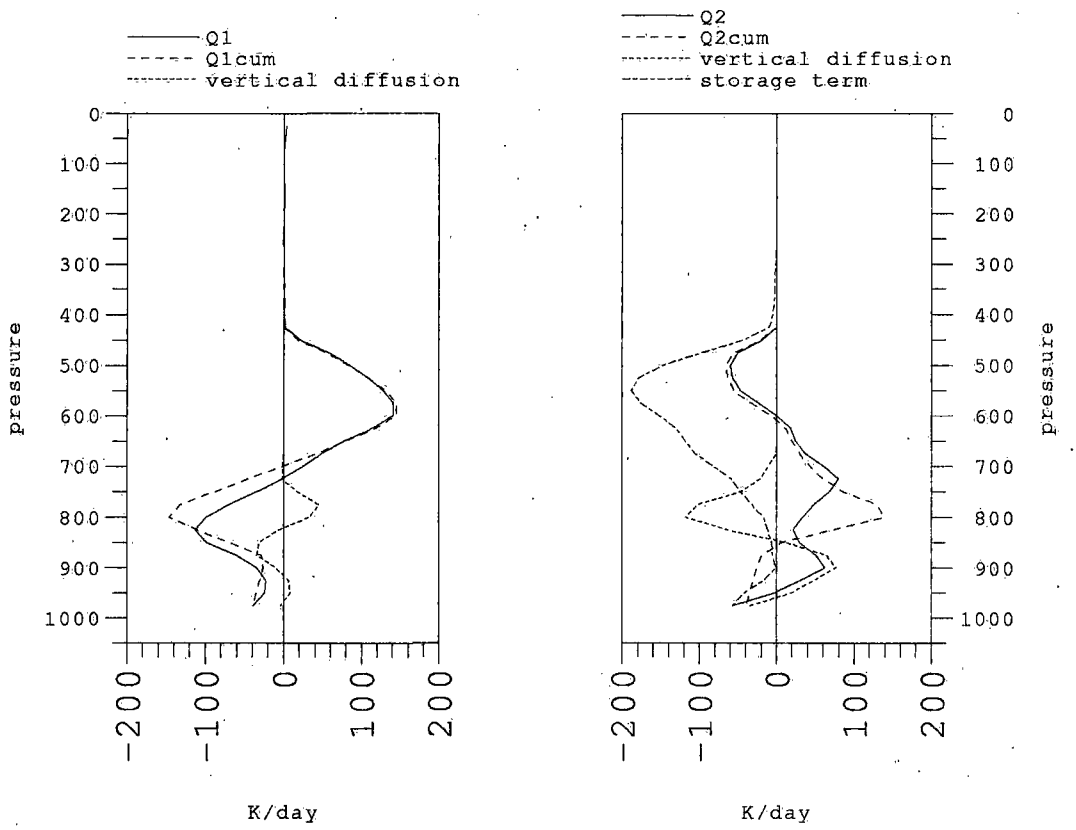

Fig. 4-6: Early stage apparent heat source (left panel) and apparent moisture sink of JUL91/HM8/EH at simulation time +2h (verification time 6 July 1991 14UTC). Solid: budget quantities; long dashed: contributions from convective parameterization; short dashes: vertical diffusion of s and q_v respectively; unevenly dashed: storage term of the moisture budget. Convection domain: 800hPa to 425hPa.

(Fig. 4-6). The vertical profile of Q_1 differs considerably from the one of the MX simulation. A dipole structure with cooling in the lower part and heating in the upper part of the convection domain with much larger amplitudes is found in the EH case. At the base of the convection domain vertical eddy sensible heat transport compensates the strong convective cooling to some extent. In addition, weak grid-scale condensation occurs in the cloud layer around 725hPa (not shown). Turbulent vertical moisture transport considerably modifies the structure of the apparent moisture sink across the lower boundary of the convection domain. The loss of moisture by convective overturning at the bottom of the convection domain is partly compensated by the vertical eddy moisture flux which in turn dries the boundary layer. Thus the total moisture sink extends from near the surface to about 600hPa. Above, the troposphere is moistened. In contrast to Q_2, the Eulerian tendency (or storage term, $-L_v \frac{\partial}{\partial t}(\overline{q_v})$) of the moisture budget equation indicates moistening over the whole depth of the troposphere. This case illustrates the two different points of view of the budget quantity and the local time tendency at the grid point: Q_2 describes the development of the air mass characteristics with a moisture sink in the lower troposphere, where the storage term indicates an increase of water vapour content at the grid point, representative of the modification of the environmental moisture field by the precipitation system.

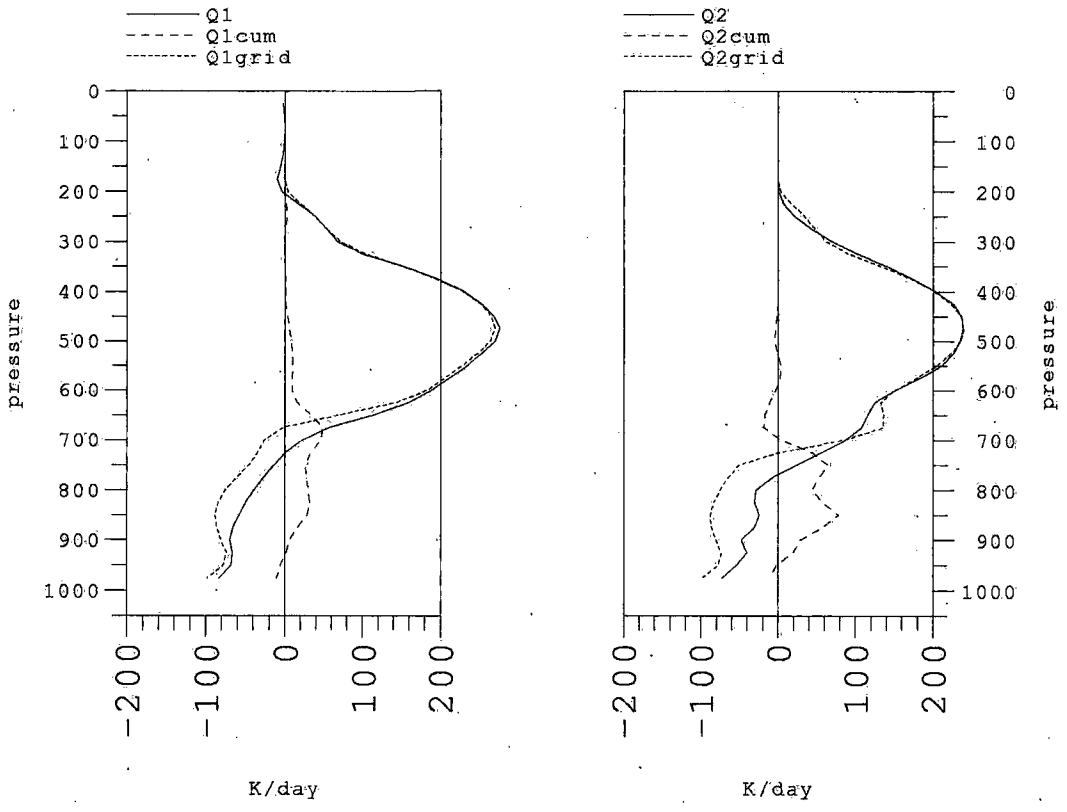

Fig. 4-7: Mature stage apparent heat source (left panel) and apparent moisture sink of JUL91/HM8/MX at simulation time +31h (verification time 7 July 1991 19UTC). Solid: budget quantities; long dashed: contributions from convective parameterization; short dashes: grid-scale contributions. Convection domain: 900hPa to 400hPa.

Comparison of Fig. 4-5 and Fig. 4-6 indicates that the two deep-convection reference profiles used in the MX and EH schemes give raise to very different vertical structures of the "event-average" apparent heat source and moisture sink.

b.) Mature stage

For the characterization of mature convective systems two events occurring in the late afternoon of 7 July 1991 are chosen. The system in the top left position clearly visible in Fig. 3-11d is selected from the MX run. The EH system considered is the cluster displayed in Fig. 3-10c. Simulation times are +31h and +30h for the MX and the EH experiment respectively. As for the early stage only grid points with precipitation rates exceeding $0.3\,kg\,m^{-2}h^{-1}$ were taken into account for the calculation of the event-average budgets. The associated ratios of convective to grid-scale precipitation are 1.0/3.5 and 1.0/4.9 where the total rainfall in the MX experiment ($10.8\,kg\,m^{-2}h^{-1}$) is more than twice as intense as in the EH run. It is a well known fact that simulations using the MX reference profile produce more precipitation than those with the EH profile (cf. Fig. 3-4 and Table 3-5). In both simulations the convection domain reaches from 900hPa to about 400hPa and clouds exist between 750hPa and 200hPa. The "event-average" soundings reflect the characteristics of the respective deep-convection reference profiles: the MX simulation tends towards the "on-

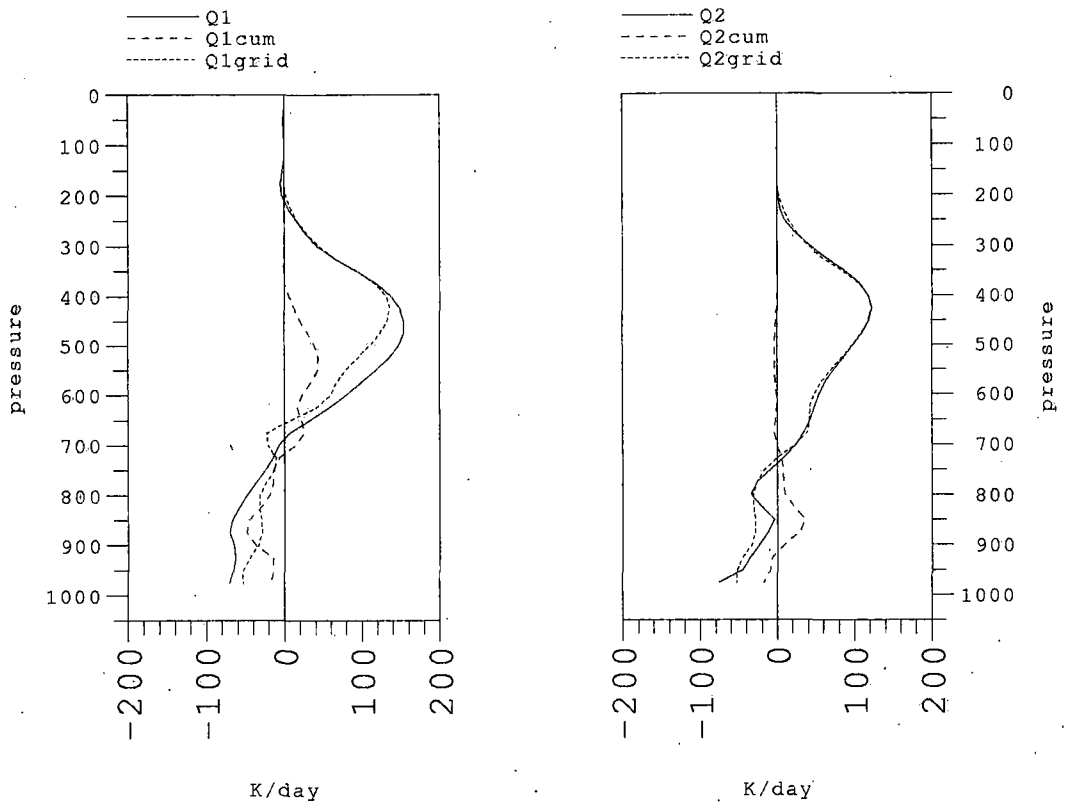

Fig. 4-8: Mature stage apparent heat source (left panel) and apparent moisture sink of JUL91/HM8/EH at simulation time +30h (verification time 7 July 1991 18UTC). Solid: budget quantities; long dashed: contributions from convective parameterization; short dashes: grid-scale contributions. Convection domain: 900hPa to 400hPa.

ion-shape" sounding with a saturated atmosphere above 650hPa, whereas the EH run tends to maintain an unsaturated atmosphere in the upper part of the convection domain. With respect to the temperature structure the early-stage soundings for the two clusters discussed here were very similar to the one of the EH simulation displayed in Fig. 4-4, but they were significantly moister in the upper part of the troposphere. The vertical grid-scale circulation exhibits a distinct feature in all systems examined: in the mature to late stage of convective systems a layer of downward motion is developed below 750hPa and upward motion is found above. In connection with the grid point storm problem (cf. chapter 3) upward velocities can be very strong. In the MX run an "event-average" minimum of -227hPa/h was reached, a value which is not uncommon in hydrostatic high-resolution NWP models. Zhang et al. (1988) found "event-average" minima of -576hPa/h with their 12.5km model and even values as large as -850hPa/h in the 25km simulation without convective parameterization scheme. Zhang and Fritsch (1988b, mesh size 25km) claim a value of -500hPa/h near 300hPa to be consistent with observations in a mesoscale convective complex. Values of this order of magnitude were diagnosed by Smull and Houze (1987) for major individual up- and downdrafts in the convective part of a mid-latitude squall line.

In the mature stage vertical Q_1 and Q_2 profiles are entirely dominated by the grid-scale precipitation-forming processes and condensation as displayed in Fig. 4-7 for the MX

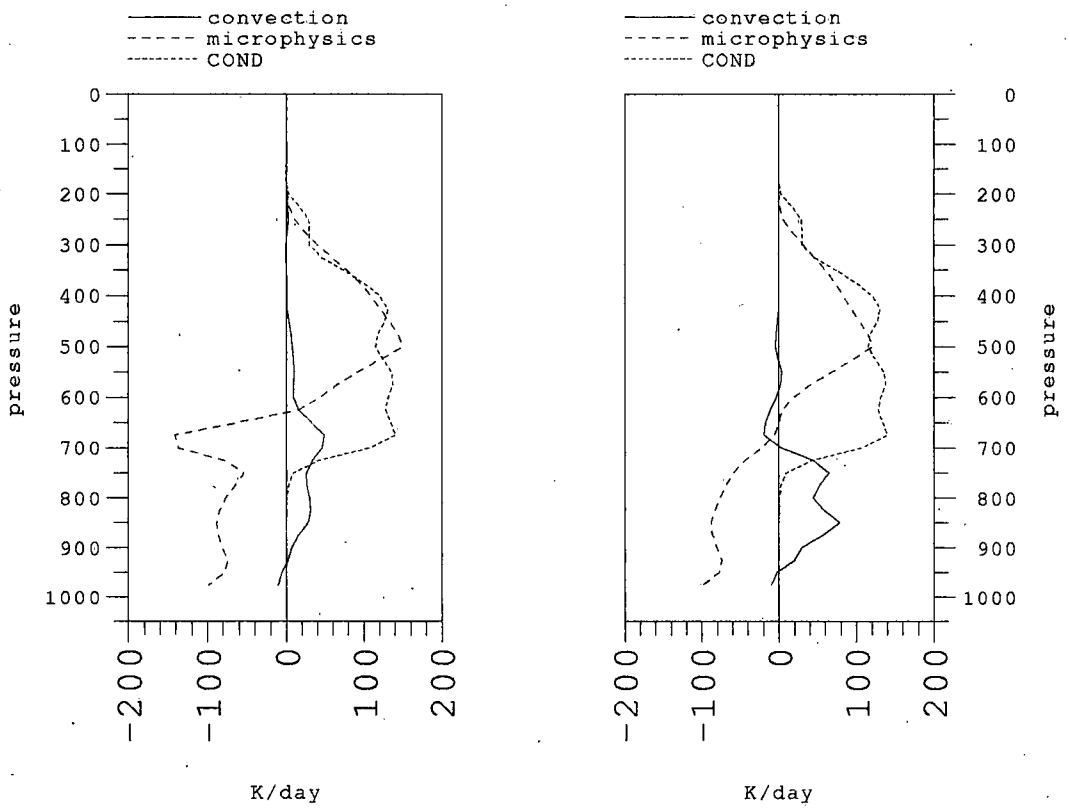

Fig. 4-9: Contributions to apparent heat source (left panel) and moisture sink for JUL91/HM8/MX at simulation time +31 h (verification time 7 July 1991 19UTC) by parameterized convection (solid), microphysics parameterization (long dashed) and grid-scale condensation (short dashed). The 0°C-level is at about 650hPa.

experiment and in Fig. 4-8 for the EH experiment. Total heating is strongest at about the height of maximum upward motion. The general structure of the subgrid-scale apparent heat source is still the same as in the initial stage: In the MX case convective heating is present throughout the convection domain, in the EH case the lower part of the convection domain is cooled and the upper part heated. The convective parameterization scheme still dries the lower part of the convection domain, but in the mature stage only weak moistening of the upper part is possible, since the atmosphere has become much moister aloft during the development of the precipitating system, also via grid-scale vertical moisture advection.

It is of interest to split the grid-scale contributions to the budgets into the parts due to microphysics parameterization and grid-scale condensation. According to Eq. (4-16) only deposition/sublimation and evaporation of rainwater and grid-scale condensation affect the specific water vapour content. The respective contributions to the apparent moisture sink of the MX run are displayed in Fig. 4-9. Above 650hPa, which is approximately the height of the melting level, deposition removes water vapour in favour of ice phase precipitation, below that level evaporation of falling precipitation adds water vapour to the unsaturated atmosphere. Condensation forced by the grid-scale upward motion increases cloud water content in the layer between 750hPa and 200hPa. The maximum deposition

rate is found at 500hPa where deposition and condensation have approximately the same amplitude. Removal of water vapour by convective processes takes place below 700hPa and is less important than moistening by the evaporation of rain (cf. Fig. 4-7).

Additional microphysical processes contribute to the grid-scale partition of the heat budget (cf. Eq. (4-15)): In addition to deposition, nucleation and riming provide latent heat of freezing above the 0°C-level. Comparison of the "event-average" microphysics profile of the heat budget with that one of the moisture budget (Fig. 4-9) reveals that deposition is by far the most important process in the negative temperature region. The pronounced cooling peak due to melting of frozen precipitation particles in the layer below the melting level almost balances the latent heat release by grid-scale condensation in the same layer. Because of this local compensation, the change from cooling to heating in Q_1^{grid} is at a level about 50hPa higher up than the change from moistening to drying in Q_2^{grid} (Fig. 4-7). Heating by parameterized convection plays a minor role compared to the grid-scale processes.

Examination of the remaining individual terms of the budget equations (Eqs. (4-11) and (4-12)) enables the following insights to be gained: If the vertical grid-scale circulation is well developed (mature stage), vertical temperature advection and adiabatic energy conversion are by far the largest terms, but they cancel each other to a large extent. In the JUL91/HM8/MX +31h case the difference is about a factor 5 smaller than the original terms. This difference is balanced by the moist grid-scale processes (condensation plus microphysics): Strong upward motion forces grid-scale condensation, cloud water is used to form precipitation which grows in the ice phase by water vapour deposition and riming. Except within the planetary boundary layer, the storage term, the horizontal and vertical diffusion terms and the radiative heating term are unimportant with respect to the above mentioned terms. Temperature increments due to the semi-implicit correction step (Eq. (4-23)) and the lateral boundary relaxation (Eq. (4-24)) and eventual associated condensation adjustments are negligible in the situations considered. In the water vapour equation there is no analogue to the adiabatic energy conversion term of the temperature equation. This adiabatic term in fact is a compensation mechanism directly linked to the magnitude of upward motion. In the water vapour equation primarily grid-scale condensation and microphysics balance the vertical moisture advection.

In the early stage of convective development, tendencies of parameterized convection have about the same amplitude as the vertical advection and adiabatic terms. At the bottom of the convection domain vertical turbulent transports of heat and moisture are also important and they depend on the deep-convection reference profile used. Horizontal advection and diffusion as well as radiation terms are small and therefore the storage term in both the thermodynamic and moisture equation can be of similar magnitude as the other dominating terms.

c.) Discussion

In the early stage of the development of convective systems heat and moisture budgets are largely dominated by the contributions Q_1^{cum} and Q_2^{cum} of the convective parameterization scheme. "Event averages" were calculated over a small number (5 and 12 for the MX and EH case respectively) of grid points where only convective precipitation was falling at a rate exceeding $0.3\,kg\,m^{-2}h^{-1}$. The vertical structure of the apparent heat source and

apparent moisture sink depends crucially on the deep-convection reference profile imposed in the convective adjustment scheme. In this early stage grid-scale moisture processes and thus their latent heating effects play a minor role. The vertical profile of Q_1^{cum} from the MX simulation indicating net heating throughout (with the exception of the lowest level) the depth of the convection domain (775hPa to 350hPa) (Fig. 4-5) carries some resemblance with the structures proposed by Houze (1982) and observed by Chong and Hauser (1990). Cooling in the planetary boundary layer by evaporation of convective rain also corresponds to the finding of Chong and Hauser (1990) for a continental environment with a deep subsaturated layer near the earth surface. With the adjustment type scheme for the parameterization of convection neither the contributions of condensation/evaporation to convective heating/cooling and drying/moistening can be distinguished nor is an ice phase included. The cooling in the lower part of the convection domain in the EH case (Fig. 4-6) is a consequence of the specific construction of the EH reference profile and not a consequence of evaporation.

Both the MX and the EH simulations produce a vertical structure of the apparent moisture sink with drying in the lower part and moistening in the upper part of the convection domain (Fig. 4-5 and Fig. 4-6). In contrast to the general assumption that the moisture sink extends throughout the troposphere, in the weather situation discussed here the upper level moistening might be due to the very dry initial conditions in the upper troposphere (cf. average initial soundings in Fig. 4-4). In the EH experiment vertical diffusion at the bottom of the convection domain and in the boundary layer plays an important role. It significantly modifies the total budget profiles (Fig. 4-6).

From examination of the early stage it is seen that the MX deep-convection reference profile being phenomenologically more realistic than its EH counterpart (see section 2.5, item f.)) produces vertical heating and moistening profiles more consistent with observations. It has also been recognized that the MX experiment had a better, though not entirely satisfactory, overall performance in the JUL91 case (cf. Fig. 3-10). Thus a realistic specification of the deep-convection reference profile (cf. section 2.4) in convective adjustment schemes appears to be an important ingredient for successful simulations.

In the mature stage convective and grid-scale precipitation is falling at the same grid points simultaneously as exemplified by the MX experiment (see the top-left system in Fig. 3-11d). The grid-scale precipitation is much more intense (factor of 3.5). Again "event-average" quantities are calculated over the group of grid points with rain rates larger than $0.3 kg m^{-2} h^{-1}$ (19 and 30 grid points are taken into account for the MX and EH case respectively). As pointed out earlier, the mature system is too concentrated in space and in particular the lateral spread-out of the stratiform portion is not adequately simulated by the model (section 3.4 item c.)).

In the mature stage grid-scale moisture processes, i.e. condensation and microphysics parameterization, dominate the apparent heat source and apparent moisture sink (Fig. 4-7 and Fig. 4-8). In accordance with e.g. Chong and Hauser (1990) the heating and drying peaks of the "stratiform" processes are at higher levels than those of the convective circulation. Melting of frozen precipitation particles makes a very distinct contribution to the heat budget at and in the layer below the 0°C-level (Fig. 4-9). Cooling by melting compensates heating by condensation to a large extent. Evaporation of grid-scale precipitation

in the dry sub-cloud layer still leads to net cooling and moistening in the lower part of the troposphere. Convection is not very important at this stage though it is still active. Microphysics parameterization makes important contributions to the total heat and moisture budgets (Fig. 4-9).

The development of a layer with downward motion in the lower troposphere above the surface during the mature to late stage of the convective system resembles the circulation features of the mesoscale or stratiform part of convective precipitation systems (Houze et al., 1980; Chong and Hauser, 1990). Again it has to be noted that vertical motion associated with the convective circulation represented by the convective parameterization scheme can not be isolated in the convective adjustment scheme. The grid-point vertical velocity incorporates contributions from the convective and mesoscale component of the precipitation system which can not be separated within one grid element. It has been argued (e.g. Gallus and Johnson, 1991) that the horizontal eddy transport (i.e. horizontal diffusion in the context of a NWP model) may not be negligible for the transfer of hydrometeors from the convective to the mesoscale region. This transfer process would essentially take place within one grid element in a NWP model with a mesh width of about 15km and would therefore not appear in the horizontal diffusion term.

In agreement with the mesoscale observational budget study of Kuo and Anthes (1984a) the individual terms of the thermodynamic equation have different orders of magnitude, the contributions of vertical advection and adiabatic energy conversion having largest amplitudes where grid-scale vertical motion is well developed. Since there is no other term apart from vertical advection directly linked to vertical motion in the moisture equation, individual terms may be of similar magnitude. In contrast, as discussed above, the storage term is the most important component of the apparent heat source and moisture sink in the early stage of development and it reflects the structure of the subgrid-scale processes. Significant modifications due to vertical diffusion can appear (Fig. 4-6).

4.4.2 Dependency of partitioned heat and moisture budgets on horizontal resolution and adjustment time scale

The vertical "event-average" structures of partitioned heat and moisture budgets of convective precipitation systems simulated by HM8 and HM4 are examined. In addition, the adjustment time scale of the HM4 simulation is varied. It is worth noting that even small changes, e.g. the doubling of the adjustment time, can have an influence on the occurrence and the development of the precipitation event. In particular, the positioning and grouping of the grid points where convective precipitation is produced depends on the parameter set chosen. Differences between simulations with different mesh widths are even greater. For the present purpose, convective precipitation systems which are as similar as possible with respect to position, stage of development and occurrence in the different model runs are selected for comparison.

First, the early stage (+27h) of the system examined at its mature stage (+31h) in the previous subsection (cf. Fig. 4-7 and Fig. 3-11d) is considered, i.e. JUL91/HM8/MX+27h. The adjustment time for the HM8 simulation is 30 minutes. Analogous precipitation systems occur at +28h in JUL91/**HM4**/MX runs, henceforth denoted as MX30 and MX60, with adjustment time scales of 30 and 60 minutes respectively. The convective domains for

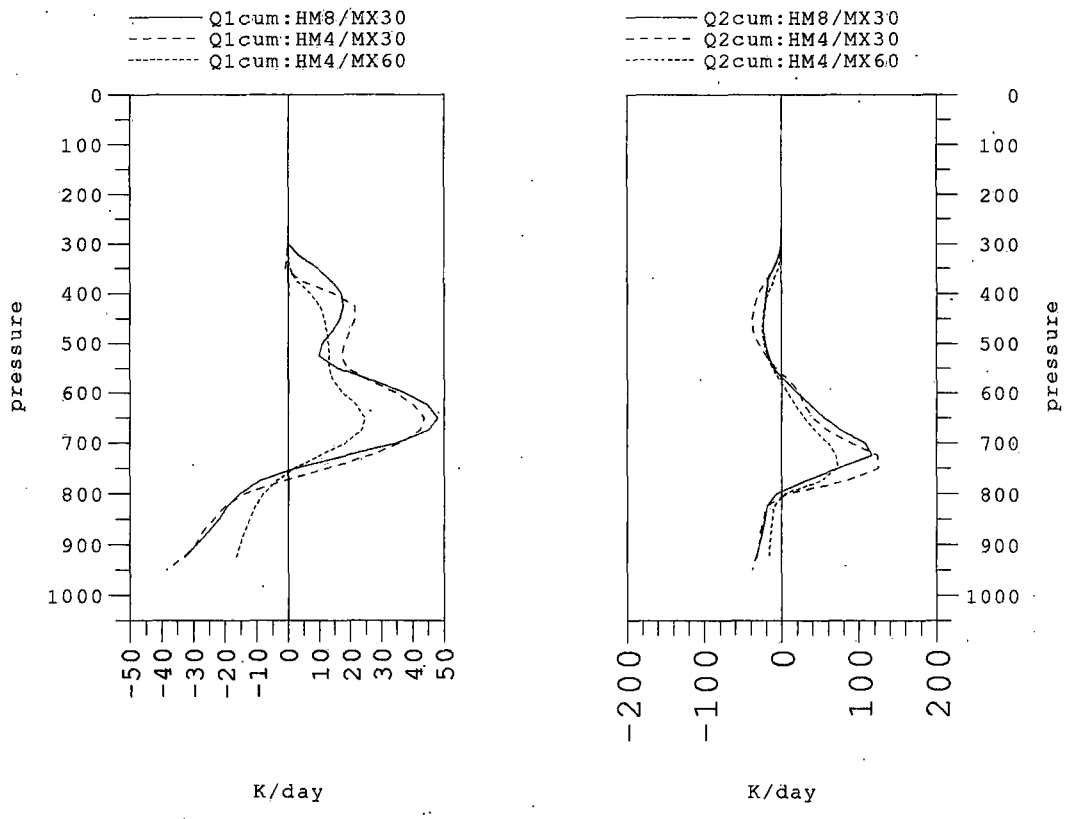

Fig. 4-10: Subgrid-scale contributions by convection Q_1^{cum} to the heat (left panel) and Q_2^{cum} to the moisture budget in the early stage of a precipitation system in the following simulations (the scaling of the horizontal axes differs by a factor 4):

solid:	JUL91/HM8/MX30 +27h
dashed:	JUL91/HM4/MX30 +28h
short dashed:	JUL91/HM4/MX60 +28h

all three systems extend between about 750hPa and 300hPa. "Event-average" soundings exhibit a very dry atmosphere below 750hPa, a moist layer with clouds between 600hPa and 400hPa and subsaturation above. At this stage of development only convective precipitation is falling. Grid-scale precipitation-forming processes and condensation are also active, but all precipitation is evaporated in the dry boundary layer before reaching the ground. "Event-average" contributions of the convective parameterization scheme to the heat and moisture budget are displayed in Fig. 4-10. The HM8/MX30 and HM4/MX30 systems have very similar vertical structures and amplitudes. Corresponding instantaneous convective precipitation rates are $1.5\,kgm^{-2}h^{-1}$ and $1.3\,kgm^{-2}h^{-1}$. Since the construction of convective tendencies only takes static properties of the atmosphere into account and since the model atmospheres in the HM8 and HM4 case have very similar thermodynamic and humidity structures, this result is to be expected. Accordingly, convective tendencies are inversely proportional to the adjustment time scale (cf. Eqs. (4-17) and (4-18)). Therefore the HM4/MX60 simulation produces only half the amplitudes of the HM4/MX30 run and a convective precipitation rate of $0.7\,kgm^{-2}h^{-1}$. The ratio between the maximum amplitudes of the two HM4 runs is 1.9/1.0 and 1.75/1.0 for the heat and moisture budget respectively.

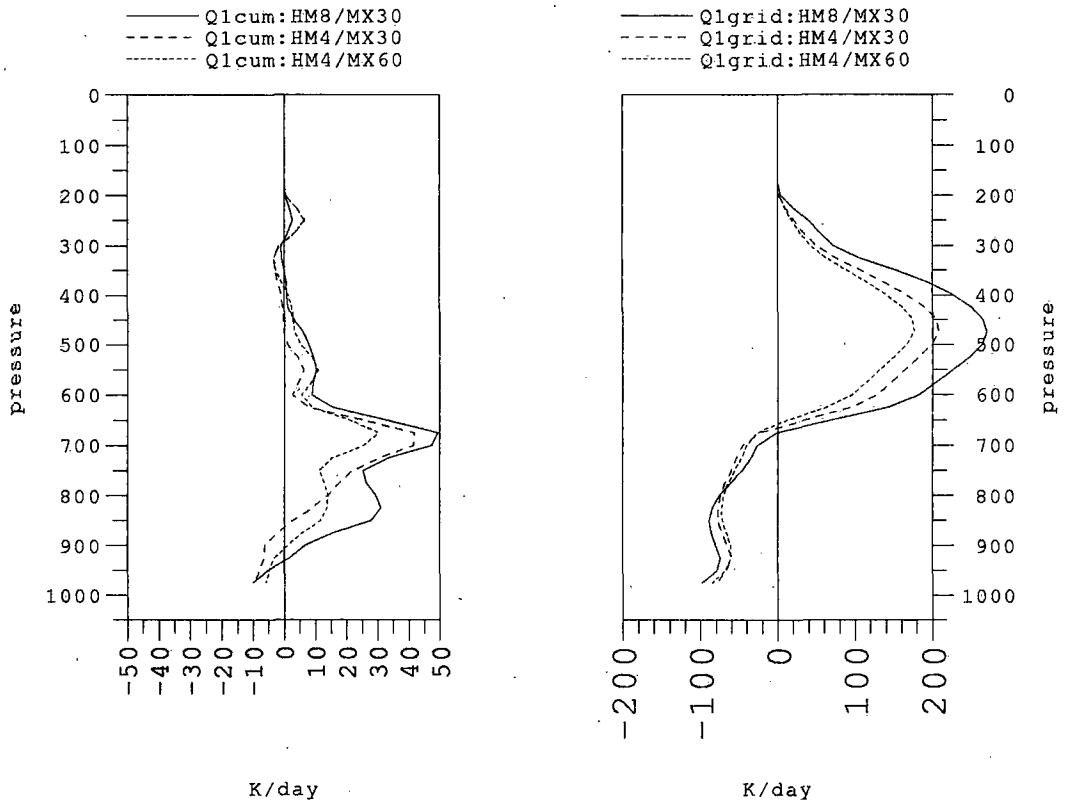

Fig. 4-11: Q_1^{cum} (left panel) and Q_1^{grid} in the mature stage of a precipitation system in the following simulations (the scaling of the horizontal axes differs by a factor 4):

solid:	JUL91/HM8/MX30 +31h
dashed:	JUL91/HM4/MX30 +32h
short dashed:	JUL91/HM4/MX60 +32h

It is more difficult to find corresponding mature stages of the precipitation systems in the three simulations, since total precipitation rates depend on the mesh width and convective to grid-scale precipitation rate ratios depend on both, the mesh width and the adjustment time scale. Simulation time +32h of the HM4 experiments has been found to best match the mature stage of the precipitation system in the HM8 run at +31h. From Table 3-5 we have seen that in general the adjustment time scale does not significantly influence the total precipitation amount accumulated over one day or more and averaged over a domain of several thousands square-kilometers. The only notable exception was the JUL91 case where reduced adjustment time scales increased convective as well as total precipitation. The same trend is found for the individual precipitation systems considered here with HM4/MX60 precipitating the least and HM8/MX30 raining the most. At +32h the HM4/MX60 simulation produced instantaneous convective and grid-scale precipitation rates of 1.48kgm^{-2}h^{-1} and 3.60kgm^{-2}h^{-1} respectively. The corresponding values for the HM4/MX30 run are 1.66kgm^{-2}h^{-1} and 4.30kgm^{-2}h^{-1}, for the HM8/MX30 experiment at +31h 2.40kgm^{-2}h^{-1} and 8.40kgm^{-2}h^{-1} are found. The intensified grid-scale precipitation is due to increasing amplitudes of the grid-scale contributions to the heat budget (Fig. 4-11). From Fig. 4-7 and Fig. 4-8 it is known that the structure of the grid-scale contribution to

the moisture budget in the mature stage does not differ principally from the structure of the heat budget, with the exception of the melting layer. Intensified grid-scale condensation and microphysics are supported by enhanced vertical velocities: Minimum vertical velocities were -147hPa/h at 425hPa (HM4/MX60), -175hPa/h at 450hPa (HM4/MX30) and -227hPa/h at 425hPa (HM8/MX30) respectively. As noted earlier, horizontal resolution has a strong impact on the magnitude of vertical velocity. Thus it appears natural that the amplitudes of grid-scale moist processes due to precipitation systems simulated at different mesh widths differ more than those due to different adjustment time scales at the same horizontal resolution (Fig. 4-11). In contrast, the convective adjustment scheme only "sees" the thermodynamic structure of the model atmosphere and does not take any dynamical features into account. Since the model soundings are similar in all three simulations, the amplitudes of the convective parameterization scheme primarily depend on the adjustment time scale as seen in Fig. 4-11, at least for the maximum amplitudes at the bottom of the convection domain. Nevertheless, the different "histories" of the precipitating systems in each model run have led to small differences which in turn can have a non-negligible impact on temperature and water vapour increments in a nearly saturated or saturated atmosphere. Therefore the inverse proportionality between adjustment time scale and convective increments is not so obvious and might be disturbed in the mature stage.

4.5 Summary

Generalizations, simplifications and approximations have to be adopted in order to represent the wealth of dynamical and physical processes and their interaction on various space and time scales going on in the real atmosphere. Comprehensive diagnosis of the influence of the explicit and parameterized processes on and the contributions to the development of the model atmosphere is an essential task in order to gain insight into the correspondence between modelled and real atmospheric processes. The current chapter has been devoted to the formal and technical development of such a diagnostic tool. Some examples of its application within the framework of high-resolution versions of the Europa Modell (EM) on case studies of convective precipitation events have been given.

Emphasis is put on the diagnosis of convection. Many observational studies have revealed the organization of major convective systems in two circulation regimes of different scale: A cumulus-scale component with associated vigorous up- and downdrafts producing heavy convective precipitation and a mesoscale component with gentler vertical upward motion in the upper and downward motion in the lower part of the troposphere generating stratiform precipitation. These two components make distinct contributions to the system's heat and moisture budgets. The most commonly used framework to explore the effect of convection on its larger-scale environment introduced by Yanai et al. (1973) has therefore been extended in order to account for partitioned heat and moisture budgets as well as ice phase processes.

The purely diagnostic, the semi-implicit and the fully prognostic approach as well as single column tests have been used for testing cumulus parameterization schemes in comparison with observations. Most often the fully prognostic approach consists in the comparison of results of multiple model runs using variants of a parameterization scheme. With this procedure it is difficult, if not impossible, to isolate errors due to the scheme under con-

sideration, since deficiencies of other model components or distorted interactions can also influence the model results.

The diagnostic tool presented in this study allows for inspection of all processes active in the model simultaneously by determination of all individual terms of the prognostic model equations. It can be flexibly applied to subdomains containing events of interest moving through the model integration domain. Absolute and relative importance of the modelled processes can be estimated.

A careful derivation of the budget formalism for a NWP model has been carried out identifying the correspondence between real and model-represented processes. The peculiarity of EM, i.e. the formulation of the prognostic equations in terms of total enthalpy and total specific water content, poses the formally and technically non-trivial problem of retrieving condensation rates which are important contributions to heat and moisture budgets. The problem has been solved by diagnostic reconstruction of the individual terms of a (T, q_v)-set of equations which can be conceived as a linear decomposition of the prognostic h-equation. Condensation appears as a residual after each step forward in time.

Examination of convective precipitation events simulated by model versions with different deep-convection reference profiles for the convective adjustment scheme and at different horizontal resolution revealed the following insights: In the early stage of development of the precipitation system tendencies provided by the cumulus parameterization schemes dominate. The vertical structure of "event-average" subgrid-scale contributions to the heat and moisture budget depends crucially on the reference profile used. In the mature stage the grid-scale precipitation-forming processes (microphysics parameterization) and grid-scale condensation overwhelm the influence of the convective parameterization scheme. Grid-scale moisture processes are strongly linked to vertical velocity which tends to increase with enhanced horizontal resolution. Tendencies from a convective adjustment scheme are primarily defined by the static properties of the model atmosphere and are therefore inversely proportional to the adjustment time scale. In contrast, vertical circulation characteristics strongly determine the tendencies from grid-scale moisture processes which are therefore primarily dependent on horizontal resolution. The fact that the convective adjustment scheme does not inherently account for horizontal scale nor any dynamical features might be one of the causes of occasional inappropriate development of the model atmosphere in convectively unstable regions (grid point storms).

The relative importance of the individual processes in the model has turned out to be the following: In the convective weather situations considered here, vertical circulation plays an important role. Therefore vertical advection tends to have large amplitudes in the middle to upper troposphere where vertical velocity is largest. In the thermodynamic equation this amplitude is offset to a large extent by the adiabatic energy conversion term. In the mature stage of development these two terms have by far the absolutely largest values. Grid-scale condensation and microphysics tendencies are the second but most important processes and largely compensate the difference of the first two terms. These two processes also balance the strong vertical advection in the moisture equation where no other term directly linked with vertical velocity exists. In the early stage of development parameterized convection dominates the thermodynamic and moisture equation. Depending on the reference profile used, vertical diffusion can be significant in the boundary layer and the lowest

part of the convection domain. Local time tendencies are largest in the boundary layer and in the very early stage of development, when they have to balance the convective tendencies. Horizontal advection, horizontal diffusion and radiation are always of minor importance in the cases examined. The semi-implicit correction and eventual associated condensation is also negligible.

To conclude we return to the subdivision of major convective systems into cumulus-scale and mesoscale components. In NWP models with mesh widths between 5 and 20km its appears necessary to parameterize the convective component. In contrast, the mesoscale circulations can be, at least partly, simulated. The findings of this chapter suggest that the model indeed captures, to some extent, both components. The grid-scale circulation exhibits some characteristics of the mesoscale circulation. The dominance of grid-scale precipitation and the split into upward and downward motion branches in the mature stage are noteworthy in this respect. However, parameterized convection has a strong impact on the evolution of the precipitation systems and its representation has to be carefully accounted for.

5 Summary of main conclusions

Starting from an up-to-date operational hydrostatic NWP model with a grid distance of about 60km experiments with reduced mesh widths of 30km and 15km have been carried out to examine the capabilities and limitations of the various model configurations. Special attention has been paid to the simulation of (convective) precipitation events. Aspects of primary interest are the dependency of the results on *horizontal resolution* and on *cumulus parameterization*. To assess the simulation results in comparison to observations appropriate *data* and *evaluation methods* are required. A *powerful diagnostic tool* is needed for incisive analysis of model internal processes in order to gain insight into the causes of the specific simulation results.

a.) Scale dependency

The first important finding is that mesh width reduction of a hydrostatic model to a grid size of the order of 10km is a feasible approach to develop a meso-β-scale model. The two principal results of the mesh width experiments are:

1.) High-resolution meso-β-scale models have a potential to improve precipitation forecasts in space and time.

2.) Precipitation amounts and intensities increase with increasing horizontal resolution.

The more detailed representation of external forcing on the finer grid contributes to both these effects. Finer-scale orography, e.g., allows for the development of more structured and thus more realistic horizontal and vertical circulation features. The systematic increase of precipitation amounts and intensities is firstly attributable to the increase of grid-scale precipitation, which is a consequence of the intensified vertical circulation, and secondly to the increase of convective precipitation due to the required reduction of the adjustment time scale in convective adjustment schemes.

b.) Parameterization dependency

First it is recognized that

3.) Cumulus parameterization is needed for hydrostatic meso-β-scale NWP models with a grid distance of the order of 10km.

Until recently this issue was open to question for meso-β-scale models. The parameterization of convection is needed for a timely initiation of convection, thus for the removal of instability and moisture prior to grid-scale saturation and hence to control the occurrence of unhealthy overdeveloped grid-scale vertical circulation features (grid point storms).

The impact of the adjustment scheme for cumulus parameterization was investigated in more detail. It turns out that

4.) Precipitation simulation is sensitive to details of the parameterization of convection (deep-convection reference profile and adjustment time scale).

The deep-convection reference profile is decisive in defining the location and intensity of convection. Furthermore

5.) Deep-convection references profiles used in convective adjustment schemes crucially determine the vertical structure of convective heating and moistening.

A phenomenologically realistic representation of the post-convective atmosphere by the reference profile proves to have a beneficial impact on the model simulation (cf. better performance of the MX versus the EH simulation of the JUL91 case). It is thus of interest that

6.) The thermodynamic structure of the convectively adjusted atmosphere of the mid-latitude continental environment can be inferred from observations and can be described by a set of a few parameters, as originally proposed by Betts (1986) for the tropics.

Appropriate parameter values have been derived from a set of upper air ascents of the sounding station Payerne in Switzerland.

c.) High-resolution model verification

Especially in convectively dominated weather situations rain gauge networks can suffer from a distinct sampling problem.

7.) Area-covering weather radar data are an important complement to surface rain gauge measurements. They provide valuable qualitative and quantitative information for comparison with model simulations.

It is worth noting that most commonly the verification of precipitation simulated by operational NWP models exclusively relies on rain gauge data and often considers only accumulated amounts over twelve hours or more. To verify meso-β-scale NWP models dense observational data in space and time are needed. It has been recognized that

8.) Time sequences and the development of horizontal patterns of precipitation (partitioned into its convective and grid-scale part) are important aspects of the examination of model results.

Utilizing a convective adjustment scheme, convective precipitation dominates in the first phase of the developing precipitation event and reaches its peak rate earlier than the grid-scale precipitation. This is a realistic feature. With a Kuo-type convection scheme, convective and grid-scale precipitation develop much in parallel. Horizontal patterns also show the overconcentrated grid-scale precipitation in the mature and late stage of the life cycle of the simulated convective systems.

NWP model verification is rendered more difficult and rigorous at smaller scales, since

9.) High-resolution verification results are more dependent on more or less arbitrary conditions such as the specific number and arrangement of grid points included in the verification area.

d.) Diagnosis of model internal physical tendencies

The diagnostic tool which has been developed allows for the inspection of all processes represented in the prediction model's prognostic equations for the thermodynamic and moisture variables. Investigation of precipitating convective weather events at different stages of the life cycle provides the following insights:

10.) Heat and moisture budgets of simulated convective precipitation systems are largely determined by the contributions of parameterized convection in the early stage of de-

velopment and by grid-scale precipitation-forming processes (grid-scale condensation and parameterized microphysics) in the mature stage.

Thus in case of a convective adjustment scheme the specification of the deep-convection reference profile largely determines the vertical structure of total heating and moistening in the early stage.

11.) Heating / cooling and drying / moistening profiles due to grid-scale precipitation forming processes (grid-scale condensation and cloud microphysics) look rather realistic.

Condensation, deposition of water vapour on ice, melting of ice particles and evaporation of rain water have the largest thermodynamic impact. Despite the reasonable structures of heat sources and moisture sinks, which carry resemblance with observed features, the life cycle of convective precipitation systems, in particular the spatial development of the mesoscale (stratiform) component, is not properly simulated. Improved cumulus parameterization might help to cure this problem.

Since the adjustment type scheme for the parameterization of convection takes only static properties of the model atmosphere into account and grid-scale precipitation intensity crucially depends on vertical circulation features, it turns out that

12.) The amplitudes of the convective tendencies occurring in the prognostic model equations primarily depend on the adjustment time (in convective adjustment schemes). Tendencies due to precipitation formation and non-convective condensation strongly depend on the mesh size.

e.) Perspective

Finally it is concluded from the various aspects of the present study that the meso-β-scale model offers promising perspectives for operational NWP, though specific improvements, particularly with respect to cumulus parameterization, are needed.

6 Final remarks

Due to its importance on the global scale, much effort has been devoted to the investigation of tropical convection. In mid-latitudes, well organized forms of major convective systems such as squall lines, mesoscale convective complexes and supercell thunderstorms, primarily over the North American Great Plains, have received the most attention. These systems have served as prototypes for the design of many cumulus parameterization schemes. Therefore it might be suspected that some characteristics of such parameterization schemes are specific to the systems they are based on. For Central Europe, and in particular for the Alpine region which is of special interest here, no systematic investigations of the nature of convective systems are available. Certainly some types of convective organization hardly ever occur (squall lines) and other types are rarely observed. Probably due to different environmental conditions, i.e. large-scale synoptic situation and complex lower boundary condition (orography), more chaotic arrangements seem to prevail. More statistically significant information about the predominant characteristics of convection in this region and in particular on the environmental conditions initiating it (trigger mechanism) would be very helpful for a more specific adaptation of cumulus parameterization to local conditions. Since the "perfect" parameterization scheme, capable of representing all kinds of convection, does not (currently) exist, it appears justifiable in a pragmatic approach to impose "local characteristics" on such a scheme, although atmospheric convection as a physical process relies always on the basic principles of buoyancy and turbulence. Derivation of the adjustable parameters in the Betts representation of the convectively adjusted atmosphere can be regarded as an example for this kind of approach.

The examination of only a small number of meteorological events might constitute a major limitation of the present investigations. For instance it would be inappropriate to consider the simulated cases as a basis for an optimal tuning of the cumulus parameterization scheme. Observational and modelling case studies are intended to provide insights which would be difficult, if not impossible, to be gained from a statistical ensemble. But rigorous testing of a NWP model in a large number of weather situations is essential to explore the potential of the model. However, appropriate strategies and diagnostic tools as developed here are indispensable to examine the model's behaviour and to verify its results.

In the context of operational weather forecasting rigorous time constraints have to be respected. The shorter the forecast range the less time is available to produce the numerical prediction. Despite the steady increase of computer power, computational efficiency of the numerical procedures and parameterization schemes implemented in NWP models will remain an important requirement. Additional computer resources can easily be offset by an extension of the forecast area, enhanced horizontal and vertical resolution or improved and more detailed representation of atmospheric processes. Further sophistication and increased complexity of cumulus parameterization has to be expected, e.g. by inclusion of more detailed microphysics with several precipitation stages or the implementation of prognostic approaches. Given the aforementioned constraints, more expensive schemes will have to demonstrate their definite superiority to simpler schemes prior to their introduction into routine operation.

Since the forecast range of meso-β-scale limited area models is rather short, say 24 to 36 hours, a significant spin-up phase should be avoided. Particularly critical in this re-

spect is the specification of the initial atmospheric moisture field. The inclusion of information about clouds and eventually existing precipitation systems and associated (vertical) circulation features should be included in the initial conditions. To put it differently, initial conditions for the NWP model should be specified in such a way, that the model is in the position to produce the correct cloud and precipitation patterns right from the beginning of the integration.

Efforts in this direction have already been undertaken either by means of appropriate initialization techniques (Donner, 1988) or by relaxation procedures. In the latter method supplementary forcings, e.g. latent heating rates of a convective precipitation system, characteristic of the process to be represented are imposed on the model equations. This method has proved to be potentially successful in several preliminary case studies (Molinari, 1982; Ueno et al., 1987; Wang and Warner, 1988). A major problem is the derivation of the information needed by the numerical model from the observations available. Radar data for instance indicate the location of precipitation is space, but do not allow for the derivation of the vertical structure of latent heating and cooling, moistening and drying. In fact it is necessary to specify a three- or, even better, four-dimensional heating and moistening function. In addition, the forcing function imposed must have a model compatible structure, that is to say correspond to circulation features which are consistent with the model dynamics (Koss, 1976; Davies, 1987). If this is not the case, the model will experience the forcing as a noisy perturbation and will try to get rid of it. Furthermore, even an "optimal" forcing will only be successful if it is supported by the environmental conditions of the model atmosphere, i.e. if the temperature and moisture field and the pre-existing vertical circulation support the development of a precipitation system.

In order to meet these requirements all available routine observations have to be exploited to provide optimally analysed meteorological fields and appropriate forcing functions. Satellite data provides information about cloud cover and precipitable water content. Rainfall rates are observed by weather radar and surface rain gauge networks. Knowledge about the vertical heating profiles preferred by the model can be derived from either theoretical considerations, diagnostic studies or first guesses from a preliminary model integration step (Turpeinen et al., 1990).

It might be argued that the Swiss mesoscale routine observations provided by the weather radar network and the automatic surface station network, both reporting at 10 minutes intervals, in conjunction with the understanding of the model precipitation generation mechanisms gained by the investigations carried out in the work presented here offer an opportunity to envisage diabatic initialization procedures for the NWP model under development.

7 References

Akmaev, R.A., 1991: A direct algorithm for convective adjustment of the vertical temperature profile for an arbitrary critical lapse-rate.
Mon. Weather Rev., **119**, 2499-2504.

Anthes, R.A., 1977: A cumulus parameterization scheme utilizing a one-dimensional cloud model. Mon. Weather Rev., **105**, 270-286.

Anthes, R.A., Y.-H. Kuo, D.P. Baumhefner, R.M. Errico and T.W. Bettge, 1985: Predictability of mesoscale atmospheric motion.
Advances in Geophysics, **28**, Academic Press, 159-202.

Arakawa, A., and W.H. Schubert, 1974: Interaction of a cumulus cloud ensemble with the large-scale environment. Part I. J. Atmos. Sci., **31**, 674-701.

Arakawa, A., and J.-M. Chen, 1987: Closure assumptions in the cumulus parameterization problem. In Short- and Medium- Range Numerical Weather Prediction, T. Matsuno Ed., Collection of papers presented at the WMO/IUGG NWP symposium, Tokyo, 4-8 August 1986, 107-131.

Austin, P.M., and R.A. Houze, 1973: A technique for computing vertical transports by precipitating cumuli. J. Atmos. Sci., **30**, 1100-1111.

Barnes, G.M., and K. Sieckman, 1984: The environment of fast- and slow-moving tropical mesoscale cloud lines. Mon. Weather Rev., **112**, 1782-1794.

Bengtsson, L., 1991: Advances and prospects in numerical weather prediction.
Quart. J. Roy. Meteor. Soc., **117**, 855-902.

Betts, A.K., 1974: Further comments on "A comparison of equivalent potential temperature and the static energy". J. Atmos. Sci., **31**, 1713-1715.

Betts, A.K., 1982: Saturation point analysis of moist convective overturning.
J. Atmos. Sci., **39**, 1484-1505.

Betts, A.K., 1986: A new convective adjustment scheme. Part I: Observational and theoretical basis. Quart. J. Roy. Meteor. Soc., **112**, 677-691.

Betts, A.K., and M.J. Miller, 1986: A new convective adjustment scheme. Part II: Single column tests using GATE wave, BOMEX, ATEX and arctic airmass data sets. Quart. J. Roy. Meteor. Soc., **112**, 693-709.

Betts, A.K., and M.J. Miller, 1992: The Betts-Miller scheme. To appear in Meteor. Monographs of the Amer. Meteor. Soc.

Binder, P., 1990: On the parametric representation of the tropospheric thermodynamic structure for mid-latitude convective situations.
Quart. J. Roy. Meteor. Soc., **116**, 1349-1357.

Binder, P., and U. Wacker, 1990: Mesoscale numerical weather prediction: Dependencies of precipitation simulations on orography and horizontal resolution. Proc. ITAM-90, 21. Internationale Tagung für Alpine Meteorologie, Engelberg, 17.-21. September 1990, Veröffentlichungen der Schweiz. Meteorol. Anstalt, Nr. 48, 1990, 115-119.

Bjerknes, V., 1904: Das Problem der Wettervorhersage, betrachtet vom Standpunkte der Mechanik und der Physik. Meteorol. Z., **39**, 1-7.

Bolton, D., 1980: The computation of equivalent potential temperature. Mon. Weather Rev., **108**, 1046-1053.

Bougeault, P., 1985: A simple parameterization of the large-scale effects of cumulus convection. Mon. Weather Rev., **113**, 2108-2121.

Bougeault, P., and J.-F. Geleyn, 1989: Some problems of closure assumption and scale dependency in the parameterization of moist deep convection for numerical weather prediction. Meteorol. Atmos. Phys., **40**, 123-135.

Bougeault, P., 1992: Current trends and achievements of limited area modelling. WMO programme on weather prediction research, PWPR report series No. 1, WMO/TD No. 479, Appendix 6, pp. 19.

Bushby, F.H., and M.S. Timpson, 1967: A 10-level atmospheric model and frontal rain. Quart. J. Roy. Meteor. Soc., **93**, 1-17.

Chen, D.-H., and P. Bougeault, 1992: A simple prognostic closure assumption to deep convective parameterization. personal communication.

Cheng, C.-P., and R.A. Houze, 1980: Sensitivity of diagnosed convective fluxes to model assumptions. J. Atmos. Sci., **37**, 774-783.

Chong, M., and D. Hauser, 1990: A tropical squall line observed during the COPT 81 experiment in West Africa. Part III: Heat and moisture budgets. Mon. Weather Rev., **118**, 1696-1706.

Cohen, C., and W.M. Frank, 1989: A numerical study of lapse-rate adjustment in the tropical atmosphere. Mon. Weather Rev., **117**, 1891-1905.

Cram, J.M., R.A. Pielke and W.R. Cotton, 1992a: Numerical simulation and analysis of a prefrontal squall line. Part I: Observations and basic simulation results. J. Atmos. Sci., **49**, 189-208.

Cram, J.M., R.A. Pielke and W.R. Cotton, 1992b: Numerical simulation and analysis of a prefrontal squall line. Part II: Propagation of a squall line as an internal gravity wave. J. Atmos. Sci., **49**, 209-225.

Davies, H.C., 1976: A lateral boundary formulation for multilevel prediction models. Quart. J. Roy. Meteor. Soc., **102**, 405-418.

Davies, H.C., 1987: On the assimilation of cloud condensational heating in prediction models. In Short- and Medium- Range Numerical Weather Prediction, T. Matsuno Ed., Collection of papers presented at the WMO/IUGG NWP symposium, Tokyo, 4-8 August 1986, 585-594.

Dell'Osso, L., 1984: High-resolution experiments with the ECMWF model: A case study. Mon. Weather Rev., **112**, 1853-1883.

Doms, G., 1990a: Some physical/numerical aspects of the Europa Modell. LAM Newsletter No. 19, December 1990, 187-199.

Doms, G., 1990b: Numerisch-physikalische Aspekte des EM. DWD-SMA Rundbrief Nr. 5 (Hochauflösendes Regionalmodell), Teil II.

Doms, G., 1991: Zur Parametrisierung der stratiformen Wolken- und Niederschlagsbildung im EM und HRM. DWD-SMA Rundbrief Nr. 6 (Hochauflösendes Regionalmodell), Teil II.

Donner, L.J., 1988: An initialization for cumulus convection in numerical weather prediction models. Mon. Weather Rev., **116**, 377-385.

Emanuel, K.A., and D.J. Raymond, 1992: Report from a workshop on cumulus parameterization, Key Biscayne, Florida, 3-5 May 1991.
Bull. Amer. Meteor. Soc., **73**, 318-325.

Frank, W.M., 1977: The structure and energetics of the tropical cyclone. Part I: Storm structure. Mon. Weather Rev., **105**, 1119-1135.

Frank, W.M., 1983: The cumulus parameterization problem.
Mon. Weather Rev., **111**, 1859-1871.

Frank, W.M., and C. Cohen, 1987: Simulation of tropical convective systems. Part I: A cumulus parameterization. J. Atmos. Sci., **44**, 3787-3799.

Fritsch, J.M., and C.F. Chappell, 1980: Numerical prediction of convectively driven mesoscale pressure systems. Part I: Convective parameterization.
J. Atmos. Sci., **37**, 1722-1733.

Galli, G., and J. Joss, 1983: Errors in measuring rain amounts with operational radars at long ranges in the Swiss Alps using projections of maximum reflectivity.
Preprints 21st Conference on Radar Meteorology, September 1983, Edmonton, Canada, Amer. Meteor. Soc., 699-706.

Galli, G., 1984: Generation of the Swiss radar composite. Preprints 22nd Conference on Radar Meteorology, September 1984, Zürich, Switzerland, Amer. Meteor. Soc., 208-209.

Galli, G., and J. Joss, 1989: Using and adjusting conventional radar reflectivity data for estimation of precipitation: Past, present and future studies in Switzerland. Paper F1, Int. Symp. on Hydrological Applications of Weather Radar, August 1989, Salford, UK.

Gallus, W.A., and R.H. Johnson, 1991: Heat and moisture budgets of an intense midlatitude squall line. J. Atmos. Sci., **48**, 122-146.

Gamache, J.F., and R.A. Houze, 1982: Mesoscale air motions associated with a tropical squall line. Mon. Weather Rev., **110**, 118-135.

Gamache, J.F., and R.A. Houze, 1983: Water budget of a mesoscale convective system in the tropics. J. Atmos. Sci., **40**, 1834-1850.

Geleyn, J.-F., C. Girard and J.-F. Louis, 1982: A simple parameterization of moist convection for large-scale atmospheric models. Beitr. Phys. Atmosph., **55**, 325-334.

Geleyn, J.-F., 1985: On a simple parameter-free partition between moistening and precipitation in the Kuo scheme. Mon. Weather Rev., **113**, 405-407.

Giorgi, F., 1991: Sensitivity of simulated summertime precipitation over the western United States to different physics parameterizations.
Mon. Weather Rev., **119**, 2870-2888.

Grell, G.A., Y.-H. Kuo and R.J. Pasch, 1991: Semiprognostic tests of cumulus parameterization schemes in the middle latitudes. Mon. Weather Rev., **119**, 5-31.

Haltiner, G.J., and R.T. Williams, 1980: *Numerical prediction and dynamic meteorology.* 2nd edition, John Wiley & Sons, pp. 477.

Hauser, D., F. Roux and P. Amayenc, 1988: Comparison of two methods for the retrieval of thermodynamic and microphysical variables from Doppler radar measurements: Application to a case of a tropical squall line. J. Atmos. Sci., **45**, 1285-1303.

Heckley, W.A., M.J. Miller and A.K. Betts, 1987: An example of hurricane tracking and forecasting with a global analysis-forecasting system. Bull. Amer. Meteor. Soc., **68**, 226-229.

Holton, J.R., 1979: *An introduction to dynamic meteorology.* International Geophysics Series, Vol 23, 2nd edition, Academic Press, pp. 391.

Houghton, D.D., R.L. Wobus and R.A. Petersen, 1991: Spatial resolution impacts on national weather service nested grid model simulations. Preprints 9th Conference on Numerical Weather Prediction, October 1991, Denver, Colorado, 225-228.

Houze, R.A., C.-P. Cheng, C.A. Leary and J.F. Gamache, 1980: Diagnosis of cloud mass and heat fluxes from radar and synoptic data. J. Atmos. Sci., **37**, 754-773.

Houze. R.A., and A.K. Betts, 1981: Convection in GATE. Rev. Geophys. Space Phys., **19**, 541-576.

Houze, R.A., and C.-P. Cheng, 1981: Inclusion of mesoscale updrafts and downdrafts in computations of vertical fluxes by ensembles of tropical clouds. J. Atmos. Sci., **38**, 1751-1770.

Houze, R.A., 1982: Cloud clusters and large-scale vertical motions in the tropics. J. Meteor. Soc. Japan, **60**, 396-409.

Houze, R.A., and P.V. Hobbs, 1982: Organization and structure of precipitating cloud systems. Advances in Geophysics, **24**, Academic Press, 225-315.

Houze, R.A., 1989: Observed structure of mesoscale convective systems and implications for large-scale heating. Quart. J. Roy. Meteor. Soc., **115**, 425-461.

Houze, R.A., S.A. Rutledge, M.I. Biggerstaff and B.F. Smull, 1989: Interpretation of Doppler weather radar displays of mid-latitude mesoscale convective systems. Bull. Amer. Meteor. Soc., **70**, 608-619.

Houze, R.A., B.F. Smull and P. Dodge, 1990: Mesoscale organization of springtime rainstorms in Oklahoma. Mon. Weather Rev., **118**, 613-654.

Imbard, M., A. Craplet, P. Degardin, Y. Durand, A. Joly, N. Marie and J.-F. Geleyn, 1988: Fine-mesh limited area forecasting with the French operational "Péridot" system. Proc. ECMWF seminar/workshop on the nature and prediction of extra-tropical weather systems, Vol II, September 1987, 231-269.

Johnson, R.H., 1976: The role of convective-scale precipitation downdrafts in cumulus and synoptic scale interactions. J. Atmos. Sci., **33**, 1890-1910.

Johnson, R.H., and G.S. Young, 1983: Heat and moisture budgets of tropical mesoscale anvil clouds. J. Atmos. Sci., **40**, 2138-2147.

Johnson, R.H., 1984: Partitioning tropical heat and moisture budgets into cumulus and mesoscale components: implications for cumulus parameterization. Mon. Weather Rev., **112**, 1590-1601.

Johnson, R.H., 1986: Lower-tropospheric warming and drying in tropical mesoscale convective systems: Implications for the problem of cumulus parameterization. J. Meteor. Soc. Japan, **64**, 721-726.

Johnson, R.H., and J.F. Bresch, 1991: Diagnosed characteristics of precipitation systems over Taiwan during May-June 1987 TAMEX. Mon. Weather Rev., **119**, 2540-2557.

Jordan, C.L., 1958: Mean soundings for the West Indies area. J. Meteor., **15**, 91-97.

Joss, J., and G. Kappenberger, 1984: Quantitative measurement of precipitation with radar in an alpine country. Preprints 22nd Conference on Radar Meteorology, September 1984, Zürich, Switzerland, Amer. Meteor. Soc., 270-275.

Joss, J., and A. Pittini, 1991: Real-time estimation of vertical profile of radar reflectivity to improve the measurement of precipitation in an alpine region. Meteorol. Atmos. Phys., **47**, 61-72.

Kalb, M.W., 1987: The role of convective parameterization in the simulation of a Gulf coast precipitation system. Mon. Weather Rev., **115**, 214-234.

Kasahara, A., 1961: A numerical experiment on the development of a tropical cyclone. J. Meteor., **18**, 259-282.

Koss, W.J., 1976: Linear stability analysis of CISK-induced disturbances: Fourier component eigenvalue analysis. J. Atmos. Sci., **33**, 1195-1222.

Kreitzberg, C.W., and D.J. Perkey, 1976: Release of potential instability. Part I: A sequential plume model within a hydrostatic primitive equation model. J. Atmos. Sci., **33**, 456-475.

Krishnamurti, T.N., and W.J. Moxim, 1971: On the parameterization of convective and nonconvective heat release. J. Appl. Meteor., **10**, 3-13.

Krishnamurti, T.N., Y. Ramanathan, H.-L. Pan, R.J. Pasch and J. Molinari, 1980: Cumulus parameterization and rainfall rates I. Mon. Weather Rev., **108**, 465-472.

Krishnamurti, T.N., S. Low-Nam and R.J. Pasch, 1983: Cumulus parameterization and rainfall rates II. Mon. Weather Rev., **111**, 815-828.

Kristjánsson, J.E., 1991: Cloud parametrization at different horizontal resolutions. Quart. J. Roy. Meteor. Soc., **117**, 1255-1280.

Kuo, H.L., 1965: On formation and intensification of tropical cyclones through latent heat release by cumulus convection. J. Atmos. Sci., **22**, 40-63.

Kuo, H.L., 1974: Further studies of the parameterization of the influence of cumulus convection on large-scale flow. J. Atmos. Sci., **31**, 1232-1240.

Kuo, Y.-H., and R.A. Anthes, 1984a: Mesoscale budgets of heat and moisture in a convective system over the Central United States. Mon. Weather Rev., **112**, 1482-1497.

Kuo, Y.-H., and R.A. Anthes, 1984b: Semiprognostic tests of Kuo-type cumulus parameterization schemes in an extratropical convective system. Mon. Weather Rev., **112**, 1498-1509.

Leary, C.A., and R.A. Houze, 1980: The contribution of mesoscale motions to the mass and heat fluxes of an intense tropical convective system. J. Atmos. Sci., **37**, 784-796.

Lord, S.J., 1982: Interaction of a cumulus cloud ensemble with the large-scale environment. Part III: Semi-prognostic test of the Arakawa-Schubert parameterization. J. Atmos. Sci., **39**, 88-103.

Madden, R.A., and F.E. Robitaille, 1970: A comparison of the equivalent potential temperature and the static energy. J. Atmos. Sci., **27**, 327-329.

Majewski, D., 1985: Balanced initial and boundary values for a limited area model. Beitr. Phys. Atmosph., **58**, 147-159.

Majewski, D., 1990: On the influence of lateral boundary values on limited area forecasts. LAM Newsletter No. 19, December 1990, 200-206.

Majewski, D., 1991: The Europa Modell of the Deutscher Wetterdienst. Proc. ECMWF Seminar on numerical methods in atmospheric models, Vol II, September 1991, 147-191.

Manabe, S., J. Smagorinsky and R.F. Strickler, 1965: Simulated climatology of a general circulation model with a hydrological cycle. Mon. Weather Rev., **93**, 769-798.

Molinari, J. 1982: Numerical hurricane prediction using assimilation of remotely-sensed rainfall rates. Mon. Weather Rev., **110**, 553-571.

Molinari, J., 1982: A method for calculating the effects of deep cumulus convection in numerical models. Mon. Weather Rev., **110**, 1527-1534.

Molinari, J., and T. Corsetti, 1985: Incorporation of cloud-scale and mesoscale downdrafts into a cumulus parameterization: Results of one- and three-dimensional integrations. Mon. Weather Rev., **113**, 485-501.

Molinari, J., and M. Dudek, 1986: Implicit versus explicit convective heating in numerical weather prediction models. Mon. Weather Rev., **114**, 1822-1831.

Molinari, J., and M. Dudek, 1992: Parameterization of convective precipitation in mesoscale numerical models: A critical review. Mon. Weather Rev., **120**, 326-344.

Müller, E., D. Frühwald, I. Jacobsen, A. Link, D. Majewski, J.-U. Schwirner and U. Wacker, 1987: Results and prospects of mesoscale modelling at the Deutscher Wetterdienst. In Short- and Medium- Range Numerical Weather Prediction, T. Matsuno Ed., Collection of papers presented at the WMO/IUGG NWP symposium, Tokyo, 4-8 August 1986, 533-546.

Müller, E., and U. Wacker, 1988: Simulation of frontal clouds and precipitation using a mesoscale weather prediction model. Preprints 10th International Cloud Physics Conference, August 1988, Bad Homburg, FRG, IAMAP, 532-534.

Ogura, Y., and H.-R. Cho, 1973: Diagnostic determination of cumulus cloud populations from observed large-scale variables. J. Atmos. Sci., **30**, 1276-1286.

Orlanski, I., 1975: A rational subdivision of scales for atmospheric processes. Bull. Amer. Meteor. Soc., **56**, 527-530.

Pedigo, C.B., and D.G. Vincent, 1990: Tropical precipitation rates during SOP-1, FGGE, estimated from heat and moisture budgets. Mon. Weather Rev., **118**, 542-557.

Persson, P.O.G., and T.T. Warner, 1991: Model generation of spurious gravity waves due to inconsistency of the vertical and horizontal resolution. Mon. Weather Rev., **119**, 917-935.

Puri, K., and M.J. Miller, 1990: Sensitivity of ECMWF analyses-forecasts of tropical cyclones to cumulus parameterization. Mon. Weather Rev., **118**, 1709-1741.

Quiby, J., F. Schubiger et P. Binder, 1988: Le programme MESOMOD de l'ISM (Développment d'un modèle numérique de prévision à méso-échelle). Rapport de travail de l'Institut Suisse de Météorologie, no. 150, Octobre 1988, pp. 40.

Reed, R.J., and E.E. Recker, 1971: Structure and properties of synoptic-scale wave disturbances in the equatorial western Pacific. J. Atmos. Sci., **28**, 1117-1133.

Ritter, B., and J.-F. Geleyn, 1992: A comprehensive radiation scheme for numerical weather prediction models with potential applications in climate simulations. Mon. Weather Rev., **120**, 303-325.

Roux, F., and J. Sun, 1990: Single-Doppler radar observations of a West African squall line on 27-28 May 1981 during COPT 81: Kinematics, thermodynamics and water budget. Mon. Weather Rev., **118**, 1826-1854.

Schubiger, F., and G. de Morsier, 1992: Erstellung von Anfangs- und Randdaten für das hochauflösende Regionalmodell (HRM) und zugehörige Experimente. Arbeitsbericht der Schweiz. Meteorologischen Anstalt Nr. 169, pp. 34.

Schüepp, 1979: *Witterungsklimatologie. Klimatologie der Schweiz*, Band III (in German). (Available from Swiss Meteorological Institute, 8044 Zürich, Switzerland)

Shay-el, Y., and P. Alpert, 1991: A diagnostic study of winter diabatic heating in the Mediterranian in relation to cyclones. Quart. J. Roy. Meteor. Soc., **117**, 715-747.

Simpson, J., and V. Wiggert, 1969: Models of precipitating cumulus towers. Mon. Weather Rev., **97**, 471-489.

Smull, B.F., and R.A. Houze, 1987: Dual-Doppler radar analysis of a midlatitude squall line with a trailing region of stratiform rain. J. Atmos. Sci., **44**, 2128-2148.

Sundqvist, H., E. Berge and J.E. Kristjánsson, 1989: Condensation and cloud parameterization studies with a mesoscale numerical weather prediction model. Mon. Weather Rev., **117**, 1641-1657.

Thompson, R.M., S.W. Payne, E.E. Recker and R.J. Reed, 1979: Structure and properties of synoptic-scale wave disturbances in the intertropical convergence zone of the eastern Atlantic. J. Atmos. Sci., **36**, 53-72.

Tiedtke, M., 1988: Parameterization of cumulus convection in large-scale models. In Physically-based modelling and simulation of climate and climatic change – Part I, M. Schlesinger Ed., Kluwer Academic Publishers, 375-431.

Tiedtke, M., 1989: A comprehensive mass flux scheme for cumulus parameterization in large-scale models. Mon. Weather Rev., **117**, 1779-1800.

Turpeinen, O.M., L. Garand, R. Benoit and M. Roch, 1990: Diabatic initialization of the Canadian regional finite-element (RFE) model using satellite data. Part I: Methodology and application to a winter storm.
Mon. Weather Rev., **118**, 1381-1395.

Ueno, M., R. Taira and T. Kudo, 1987: A dynamic assimilation method for a mesoscale model using observed rainfall rates. In Short- and Medium- Range Numerical Weather Prediction, T. Matsuno Ed., Collection of papers presented at the WMO/IUGG NWP symposium, Tokyo, 4-8 August 1986, 573-584.

Vincent, D.G., K.H. North, R.A. Velasco and P.G. Ramsey, 1991: Precipitation rates in the tropics based on the Q_1-budget method: 1 June 1984 - 31 May 1987.
J. Climate, **4**,1070-1086.

Vukicevic, T., and R.M. Errico, 1990: The influence of artificial and physical factors upon predictability estimates using a complex limited area model.
Mon. Weather Rev., **118**, 1460-1482.

Wang, W., and T.T. Warner, 1988: Use of four-dimensional data assimilation by Newtonian relaxation and latent-heat forcing to improve a mesoscale-model precipitation forecast: A case study. Mon. Weather. Rev., **116**, 2593-2613.

Xu, K.-M., and K.A. Emanuel, 1989: Is the tropical atmosphere conditionally unstable?
Mon. Weather Rev., **117**, 1471-1479.

Yanai, M., S. Esbensen and J.-H. Chu, 1973: Determination of bulk properties of tropical cloud clusters from large-scale heat and moisture budgets.
J. Atmos. Sci., **30**, 611-627.

Yessad, K., 1992: The "permanent spin-up" in the Péridot limited area model operational at Météo France. (submitted to Contrib. Atmos. Phys.)

Zhang, D.-L., and J.M. Fritsch, 1988a: Numerical sensitivity experiments of varying model physics on the structure, evolution and dynamics of two mesoscale convective systems. J. Atmos. Sci., **45**, 261-293.

Zhang, D.-L., and J.M. Fritsch, 1988b: A numerical investigation of a convectively generated, inertially stable, extratropical warm-core mesovortex over land. Part I: Structure and evolution. Mon. Weather Rev., **116**, 2660-2687.

Zhang, D.-L., E.-Y. Hsie and M.W. Moncrieff, 1988: A comparison of explicit and implicit predictions of convective and stratiform precipitating weather systems with a meso-β-scale numerical model. Quart. J. Roy. Meteor. Soc., **114**, 31-60.

Zhang, G.J., and N.A. McFarlane, 1991: Convective stabilization in midlatitudes.
Mon. Weather Rev., **119**, 1915-1928.

Zipser, E.J., 1977: Mesoscale and convective-scale downdrafts as distinct components of squall-line structure. Mon. Weather Rev., **105**, 1568-1589.

Acknowledgements

This work would not have been possible without the friendly agreement between and the generous support of the three institutions involved: The Swiss Meteorological Institute (SMI), the Laboratory for Atmospheric Physics of the ETH Zurich (LAPETH) and the Deutscher Wetterdienst (DWD) in Offenbach. First I want to express my gratitude to the SMI, especially to Dr. Th. Gutermann, head of the research and applications division, and to Jean Quiby, head of the numerical meteorology section, for offering me the opportunity to carry out this work within the framework of one of SMI's major projects (MESOMOD).

I am greatly indebted to Prof. H.C. Davies, LAPETH, and Prof. R.A. Houze, University of Washington, Seattle, for their scientific guidance. Huw Davies substantially contributed to this work by his expert advice and his excellent capability to point out the most interesting and decisive aspects of a problem. My attention was drawn to the various budget studies on convection during the weekly meetings with Bob Houze, when he spent his sabbatical year in Zurich. The work presented in chapter 4 is based on these encouraging discussions.

Jean Quiby is especially thanked for providing me with optimum conditions to accomplish this work, in particular during the final phase. I appreciate very much the friendly atmosphere in our section and the constructive collaboration with my colleagues Francis Schubiger and Guy de Morsier. I thank Dr. Jürg Joss, head of the cloud physics section, for introducing me to the Swiss radar data and for his steady interest in my work with this kind of data. Gianmario Galli solved many data collection, archiving and transmission problems in order to make radar data available for me.

The colleagues of the research division of DWD introduced us to the Europa Modell system and generously supported us with their know-how and allowed us to utilize all their facilities. We greatly profited from their expertise. I gratefully acknowledge the numerous discussions on technical and scientific subjects with Detlev Majewski, Günter Doms, Erdmann Heise, Ulrike Wacker, and Ingo Jacobsen. Most computations were performed at the European Centre for Medium Range Weather Forecasts (ECMWF). Norbert Kreitz supported me with advice and actions in favour of improved efficiency for member state users, especially for those "under pressure".

Last but not least I thank my wife and my children for creating an eventful and stimulating environment. Beatrice provided me with steady and invaluable support. Julia, Christa, Martina and Johanna induced me to think about countless non-meteorological, most exciting and important aspects of life.

Corresponding author's address:

Dr. P. Binder
Swiss Meteorological Institute
Krähbühlstrasse 58
CH - 8044 Zürich

Nr. 1a Uttinger H., Die Niederschlagsstunden in Zürich.
22 Seiten, 1962

Nr. 1b Ambrosetti Fl., Die Niederschlagsstunden in Locarno-Monti.
12 Seiten, 1965

Nr. 2 Thams J.C., unter Mitarbeit von A. Aufdermaur, P. Schmid und E. Zenone.
Die Ergebnisse des Grossversuches III zur Bekämpfung des Hagels im Tessin in den Jahren 1957–1963.
32 Seiten, 1966 (vergriffen)

Nr. 3 Grütter M., Die bemerkenswertesten Niederschläge der Jahre 1948–1964 in der Schweiz.
20 Seiten, 1966

Nr. 4 Schram K. und Thams J.C., [Redaktion], 9. Internationale Tagung für Alpine Meteorologie in Brig und Zermatt, 14.–17. September 1966.
366 Seiten, 1967

Nr. 5 Ambrosetti Fl. und Thams J.C., Die direkte Sonnenstrahlung auf die Flächen eines nach Süden orientierten Würfels ohne Grundfläche in Locarno-Monti.
16 Seiten, 1967

Nr. 6 Schram K. und Thams J.C., Der Tagesgang der Abkühlungs- und Aufwärmungsgrösse in Locarno-Monti.
20 Seiten, 1968 (vergriffen)

Nr. 7 Ambrosetti Fl., Schram K. und Thams J.C., Die Intensität der direkten Sonnenstrahlung in verschiedenen Spektralbereichen in Locarno-Monti.
13 Seiten, 1968 (vergriffen)

Nr. 8 Uttinger H., Die Zahl der Tage mit Windspitzen von mindestens 20 Metern pro Sekunde in Zürich (1934–1967).
22 Seiten, 1968

Nr. 9 Mäder F., Untersuchung über die Windverhältnisse in Bodennähe bei verschiedenen Wetterlagen.
42 Seiten, 1968

Nr. 10 Schram K., Die Windverhältnisse in der bodennahen Luftschicht an einem Hang von etwa 25 Grad Neigung.
13 Seiten, 1968 (vergriffen)

Nr. 11 Schüepp M., Kalender der Wetter- und Witterungslagen von 1955 bis 1967.
44 Seiten, 1968 (vergriffen)

Nr. 12 Ackermann P., Die neue Radiosondenstation Payerne der Schweizerischen Meteorologischen Zentralanstalt.
36 Seiten, 1968 (vergriffen)

Nr. 13 Junod A., Contribution à la méthodologie granulométrique des aérosols amicroscopiques.
70 Seiten, 1969

Nr. 14 Joss J., Schram K., Thams J.C., Waldvogel A., Untersuchungen zur quantitativen Bestimmung von Niederschlagsmengen mittels Radar.
37 Seiten, 1969 (vergriffen)

Nr. 15 Courvoisier H.W., Die quantitative Niederschlagsprognose winterlicher zyklonaler Witterungslagen auf der Alpennordseite der Schweiz.
15 Seiten, 1970 (vergriffen)

Nr. 16 Schram Karin und Thams J.C., Die kurzwellige Globalstrahlung und die diffuse Himmelsstrahlung auf dem Flugplatz Zürich-Kloten. 18 Seiten, 1970

Nr. 17 Kasser P., Schram Karin und Thams J.C., Die Strahlungsverhältnisse im Gebiet der Baye de Montreux. 46 Seiten, 1970

Nr. 18 Gutermann Th., Vergleichende Untersuchungen zur Föhnhäufigkeit im Rheintal zwischen Chur und Bodensee. 68 Seiten, 1970

Nr. 19 Ginsburg Theo, Die statistische Auswertung von langjährigen Temperaturreihen. 42 Seiten, 1970

Nr. 20 Primault B., Du risque de gel et de sa prévision. 20 Seiten, 1971

Nr. 21 Piaget A., Utilisation de l'ozone atmosphérique comme traceur des échanges entre la troposphère et la stratosphère. 72 Seiten, 1971

Nr. 22 Zenone E., Die Gewitterverhältnisse in den südlichen Zentralalpen und Voralpen. 24 Seiten, 1971

Nr. 23 Kirchhofer W., Abgrenzung von Wetterlagen im zentralen Alpenraum. 72 Seiten, 1971

Nr. 24 Primault B., Le climat, élément du plan d'aménagement.
Das Klima, eine der Grundlagen der Landesplanung.
The climate as an element of the land management.
28 Seiten und eine Karte, 1971

Nr. 25 Fröhlich C. und Wierzejewski, Die verschiedenen Messverfahren zur Bestimmung der Strahlungsintensität mit dem Kompensationspyheliometer und die Entwicklung eines verbesserten Modells. 36 Seiten, 1972

Nr. 26 Bouët M., Le foehn du Valais. 12 Seiten, 1972

Nr. 27 Zenone E., Die Gewitterverhältnisse in den südlichen Zentralalpen und Voralpen 32 Seiten, 1972

Nr. 28 Catzeflis J., Primault B., Strehler H., Analyse de la pluviosité dans le Valais central. 15 Seiten, 1972

Nr. 29 Courvoisier H.W., Die Niederschlagswirksamkeit markanter, hochreichender Kaltlufteinbrüche im Sommer in der Schweiz. 11 Seiten, 1973

Nr. 30 Sevruk B., Erfahrungen mit Totalisatoren mit schiefen, geneigten und bodenebenen Auffangflächen im Einzugsgebiet der Baye de Montreux.
Einfluss der Temperatur auf die Messung des Niederschlages mit Totalisator.
44 Seiten, 1973

Nr. 31 Strehler H., Beziehung zwischen Witterung und Zuckerrübenmerkmalen im Spätsommer. 20 Seiten, 1975

Nr. 32 Courvoisier H.W., Katalog objektiv-statistischer Wetterprognosen für die Alpensüdseite und das Oberengadin. 24 Seiten, 1975

Nr. 33 Primault B., Essais d'évaluation climatologique du risque de gel. 28 Seiten, 1975

Nr. 34	Kirchhofer W.,	Stationsbezogene Wetterlagenklassifikation 50 Seiten, 1976
Nr. 35	Piaget A.,	L'évolution orageuse au nord des Alpes et la tornade du Jura vaudois du 26 août 1971 114 Seiten, 1976
Nr. 36	Bouët M.,	Contribution à l'étude de la variation diurne de pression en Suisse romande 23 Seiten, 1976
Nr. 37	Zenone E.,	Die Gewitterverhältnisse in den südlichen Zentralalpen und Voralpen 60 Seiten, 1976
Nr. 38	Primault B., Quiby J.,	Diagrammes psychrométriques différenciés en altitude 36 Seiten, 1977
Nr. 39	Courvoisier H. W.,	Katalog objektiv-statistischer Wetterprognosen für die Alpennordseite, das Wallis sowie Nord- und Mittelbünden 58 Seiten, 1978
Nr. 40	Gutermann Th., Mäder F. (Redaktion)	15. Internationale Tagung für alpine Meteorologie, Grindelwald 19.–23. September 1978, 332 Seiten, 1978 Tagungsbericht 1. Teil
Nr. 41	Gutermann Th., Mäder F. (Redaktion)	15. Internationale Tagung für alpine Meteorologie, Grindelwald 19.–23. September 1978, 1979 Tagungsbericht 2. Teil
Nr. 42	Courvoisier H.W.,	Starkniederschläge in der Schweiz in Abhängigkeit vom Druck-, Temperatur- und Feuchtefeld 59 Seiten, 1981
Nr. 43	Urfer Charlotte,	Mittlere Temperatur- und Windverteilung im Dischmatal bei Davos bei typischen sommerlichen Witterungslagen 32 Seiten, 1981
Nr. 44	J.-D. Altherr, M. Dupanloup, Y. Ganter, E. Junet,	Prévision objective des hauteurs de précipitations et de l'ensoleillement relatif au moyen de l'analyse discriminante 43 Seiten, 1982
Nr. 45	Courvoisier H. W.,	Abgeschlossene Höhentiefs und ihre Wetterauswirkungen in der Schweiz 44 Seiten, 1984
Nr. 46	Perret R.,	Une classification des situations météorologiques à l'usage de la prévision 127 Seiten, 1987
Nr. 47	Courvoisier H.W.	Regionale Wetterauswirkung und Prognose von Staulagen in der Schweiz 22 Seiten, 1988
Nr. 48	Gutermann Th., Mäder F. (Redaktion)	21. Internationale Tagung für alpine Meteorologie, Engelberg 17.–21. September 1990, 437 Seiten 1990 Tagungsbericht 1. Teil
Nr. 49	Gutermann Th., Mäder F. (Redaktion)	21. Internationale Tagung für alpine Meteorologie, Engelberg 17.–21. September 1990, 135 Seiten, 1991 Tagungsbericht 2. Teil
Nr. 50	Defila C.,	Pflanzenphänologie der Schweiz, 238 Seiten, 1991

Nr. 51 Binder P., Aspects of precipitation simulation in numerical weather prediction
Towards an operational mesoscale NWP model,
148 Seiten, 1992